MANIPULATING AND UNDERSTANDING THE CULTURED NEURONAL NETWORK THROUGH CONDUCTING POLYMERS

by

William Richard Stauffer

B.S., University of Pittsburgh, 2003

Submitted to the Graduate Faculty of

Swanson School of Engineering in partial fulfillment

of the requirements for the degree of

Doctor of Philosophy

University of Pittsburgh

2009

UNIVERSITY OF PITTSBURGH

SWANSON SCHOOL OF ENGINEERING

This dissertation was presented

by

William Richard Stauffer

It was defended on

November 19th, 2008

and approved by

Guo-qiang Bi, Associate Professor, Department of Neurobiology

Robert E. Kass, Professor, Department of Statistics, CMU

Andrew B. Schwartz, Professor, Department of Bioengineering and Neurobiology

Elizabeth Tyler-Kabara, Assistant Professor, Department of Neurological Surgery

Dissertation Director: Xinyan Tracy Cui, Assistant Professor, Department of Bioengineering

MANIPULATING AND UNDERSTANDING THE CULTURED NEURONAL NETWORK THROUGH CONDUCTING POLYMERS

William Richard Stauffer, PhD

University of Pittsburgh, 2009

Conducting polymers are class of polymer that can be synthesized directly on conductive substrates and incorporate various functional molecules into it. Its conductivity and customizability make it an ideal interface material for neuronal network research. In the first phase of this thesis, the incorporation of laminin fragments into conducting polymer films is investigated. The laminin fragments are shown to produce low impedance surfaces for neuronal recording. Furthermore, it is shown that the incorporated laminin fragments promote the adhesion of neurons to the surface. These results could provide a means for promoting a stable interface for chronic recording devices.

In the second phase of this thesis, *In vitro* multielectrode arrays provide a framework for studying polypyrrole-mediated controlled release of neurochemicals from microelectrodes, and neuronal network dynamics in a controlled setting. We have developed a technique to achieve transient and local inhibition of synaptic transmission in cultured networks. Conducting polymer films containing the glutamate receptor antagonist CNQX are synthesized directly on the microelectrodes in the recording array. Release of CNQX is achieved through a brief electrical pulse. Through single cell patch-clamp recording, the effectiveness of CNQX release on inhibiting excitatory post-synaptic currents (EPSC) is characterized as a function of distance and time from the releasing electrode, and evidence is shown supporting a diffusion-mediated process following release.

At the network level, simultaneous patch-clamp and extracellular recordings are used to characterize stimulus-evoked responses from the network. Cross correlation and a model-based variable clustering technique identify functional connectivity in a neuronal network response to electrical stimuli. Use of the controlled release of CNQX in conjunction with these techniques will allow us to examine the functional clustering of neurons in response to a given stimulation, and how a functional cluster is affected by transient, local inhibition in the network.

TABLE OF CONTENTS

LIST OF TABLES

LIST OF FIGURES

PREFACE

"To see a World in a Grain of Sand
And a Heaven in a Wild Flower,
Hold Infinity in the palm of your hand
And Eternity in an hour."
-William Blake

The above phrase perfectly captures my idea of the joy and wonder of science. That I have the opportunity to pursue a career in science is due in large part to the help and support of others. First and foremost I would like to thank my academic advisor, Dr. Tracy Cui. Dr. Cui has been a constant source of knowledge, support, encouragement and intellectual stimulus throughout my time as a graduate student. She provided guidance when it was most needed by proposing interesting experiments, while at the same time engendering the independence that I will rely on throughout my scientific and academic career. This dissertation would not have been possible without her assistance, for which I am grateful. I would also like to thank her for the monumental feat of putting up with me for almost 6 years; if there is a degree for patience she has earned it many times over.

Along with Dr. Cui, the other members of dissertation committee are Dr Guo-qiang Bi from neurobiology, Dr. Rob Kass from the statistics department at CMU, Dr. Andrew Schwartz of the departments Bioengineering and Neurobiology and Dr. Elizabeth Tyler-Kabara of the Neurosurgery and Bioengineering department. Dr. Bi did me the great kindness of making himself, as well as some space in his laboratory, available to me when I needed it. Not only did

he provide assistance and guidance in the collection and interpretation of neuronal data, but also played an active role in helping me formulate and refine the questions I attempted to address.

Dr. Rob Kass provided guidance and support (and almost infinite patience) on the complex problem of the analysis of neuronal network data. I am sure he will rejoice if he never has to explain cross-correlation again, but my work has benefited greatly from his advice. Dr. Andrew Schwartz would, from time to time, let me in on a portion of his unmatched vision. His willing participation in my graduate education and my career development has left me very grateful. Physician and scientist Dr. Tyler-Kabara I have had the pleasure of knowing as mentor and friend for more than eight years. She has provided me with constant encouragement and support. Many of our conversations regarding neuronal network function early in my career found expression in the ideas for this dissertation.

As I transition from thanking my academic mentors for their teaching, guidance and assistance to thanking my family and friends for their support and encouragement, I need to single out one individual who managed to take on both roles, Dr. Parameswar Krishnakumar. Dr kk, as I know him, has been a friend and neighbor to me for the better part of my life. When I started doctoral studies he took on the mantle of advisor. He has played a role as a sounding board for ideas, an editor, and a teacher. As one of the most capable minds I have encountered his input and guidance has played a massive role in delivering me here, to the finish line. As arguably the kindest soul, his paternal hand has made the landing soft.

Though her acknowledgement comes towards the end here, nothing can diminish the role that my mother Theresa has had in my life. From my decision to go to graduate school, to then pursue the doctoral degree and hopefully someday use my training to do some good for the world, my mother has been an inspiration. Furthermore, no son could ask for more

unconditional love and support. She is truly great. Her sister, my Aunt Alice, has proven another vital source of support. Few people have proven as willing to listen to me drone on about research. I have truly appreciated all she has done for me.

Finally, I thank my one and only partner in crime, Angela. She inspires me through love, support and example to be a good human, and though she knows it or not the best scientist I can be.

I acknowledge the financial support provided by the Department of Bioengineering (University of Pittsburgh), McGowan Institute for Regenerative Medicine, and Center for Neural Basis of Cognition, University of Pittsburgh - CMRF (Competitive Medical Research Fund), and CRDF (Central Research Development Fund), NSF grant CBET07 29869 and NSF IGERT fellowship (DGE-9987588). I also thank my many collaborators Dr. Pakming Lau, Dr. Carl Lagenaur, Dr. Simon Watkins, Dr. Donna Stolz, and Mr. Rubin (Center for Biological Imaging at U. Pitt), Dr. Jianjun Wei , Mr. Bartkovsky, Ms. Azemi, and Ms. Wadhwa for their technical help during the course of this thesis work.

1.0 INTRODUCTION

The functional cells of the brain are neurons. In order to study the function of the brain it is necessary to record the signals that arise from individual neurons as well as neural ensembles. Traditional electrical recording techniques have commonly utilized metal electrodes made of tungsten, platinum, silver, or gold to detect the changes in potential arising from neuronal activity. The central thesis of this dissertation is how conducting polymers can be used at the interface between tissue and electrode to enhance the capabilities of neurophysiologists. Conducting polymers are a class of molecules that can be synthesized directly on many conductive substrates. As their name implies they are electrically conductive and can be used for stimulation or recording purposes. The morphology is highly customizable and they can be created with a high surface area resulting in low impedance to the flow of charge. Different molecules can be incorporated into conducting polymers, including ligands that cells can recognize and interact with, enzymes that retain their bioactivity, and host of others that imbue the polymer, and hence the interface, with new functional capability. In this way they can mediate a more biocompatible interface with living tissue or act as biosensors for the detection of changes in the tissue environment. Furthermore, conducting polymers can undergo a reversible charging and discharging of their backbone, and this mechanism can mediate controlled release of charged compounds that are electrostatically associated with the polymer.

My graduate research is focused on the use of conducting polymer polypyrrole (PPy) at this physiological interface. In the first phase of this dissertation, the role that functional peptide sequences enmeshed in a PPy film have on determining the identity and number of different cell types that associate with a conductive surface is examined. In the second phase of this dissertation, the incorporation and release of neurochemicals from PPy films as well as the direct effects of released neurochemicals on cultured neurons is demonstrated. Finally, the functional clustering of neurons in an *in vitro* neuronal network is quantified through measures of correlation, and the effect of conducting polymer-mediated release of a synaptic inhibitor on functional clustering is reported.

In the following introduction, we first discuss the basic interface problem between neural tissue and electrodes. Next, an introduction to conducting polymers is provided and the literature examining the application of conducting polymers specifically to the neural interface is provided. In the third section of the introduction, a close look is taken at the reversible redox property of conducting polymers and how this has been used as a mechanism to mediate release of compounds. Finally, we will examine work done on neuronal networks using in vitro MEAs and an attempt is made to frame the basic questions motivating this dissertation.

1.1 ELECTRODE-NEURON INTERFACE

Neural electrode arrays are devices that contain a multitude of electrodes for simultaneous recording or stimulation from many neurons at once. Some electrode arrays are implantable devices for the interface with neurons in the brain, and others are dishes for the recording of explanted neural tissue. Many research activities are underway that require small

and complex neural implant devices with single neuron resolution. One of the most exciting areas is brain/machine interface study for decoding motor intent. Microelectrode arrays are placed in the motor cortex of monkey to extract motor signals that are then used to control a robotic arm or cursor in virtual space (Taylor, Tillery et al. 2002; Velliste, Perel et al. 2008). In the fullness of time, these studies will not only significantly enhance our understanding of neurophysiology of motor control, but also bring hope to approximately 250,000 patients with full or partial paralysis in the U.S.

The central paradigm of this research and treatment modality is an array of electrodes that serves as a conduit of signals from the central nervous system. For higher spatial resolution and accuracy, it is desirable to have large numbers of electrodes precisely patterned in space.

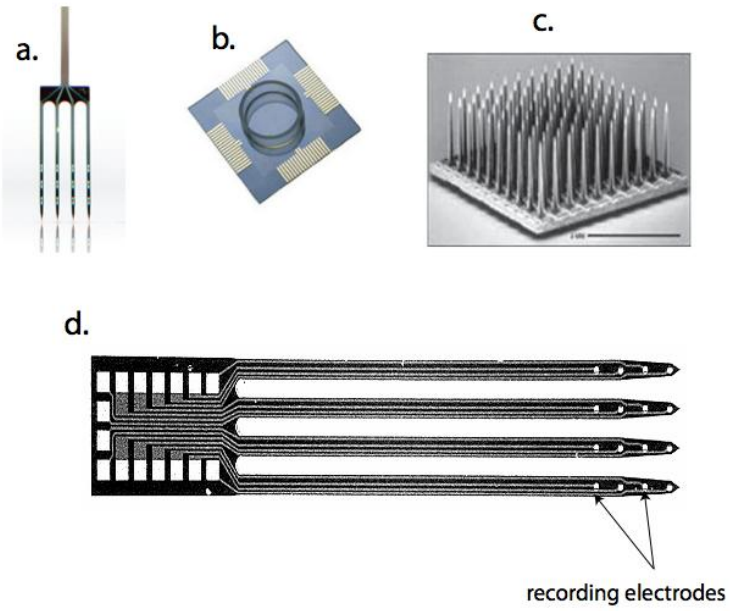

Figure 1-1 Examples of different multielectrode arrays including a) Michigan probe (NeuroNexus), b) MED64 *in vitro* recording array, c) Utah array (Cyberkinetics) and d) a blow-up of a Michigan array highlighting the recording sites.

For this purpose there exist several neural microelectrode arrays, including microwire arrays and several different types of silicon based micromachined arrays. Micro-fabrication technology has the ability to reproducibly manufacture very small and highly complicated microelectrode arrays that yield high quality multichannel single unit recording (Najafi and Wise 1986; Wise and Najafi 1991; Maynard, Nordhausen et al. 1997). Figure 1-1(a-c) shows several examples of neural electrode arrays for use *in vivo* and *in vitro*. Figure 1-1(d) highlights a Michigan probe electrode array for implant. Openings in the dielectrics at the probe tip regions define the vertical connection to stimulating or recording sites for interfacing neural tissue (Anderson, Najafi et al. 1989). These neural probes demonstrated superb ability in recording high quality neural signals.

A common problem with recording array technology is a general reduction in performance over time, leading ultimately to device failure (Helms Tillery, Taylor et al. 2003; Schwartz, Cui et al. 2006). The causes of this degeneration are still controversial, but candidate explanations include chronic micromotion of the implanted electrode, degeneration of neurons local to the electrode site and encapsulation of the recording device through reactive astrocytosis leading to a glial sheath (Turner, Shain et al. 1999; Szarowski, Andersen et al. 2003; Schwartz, Cui et al. 2006). What is known is that post-mortem neural density around the probe is greatly reduced (Biran, Martin et al. 2005).

One approach for the improvement of the microelectrode array/neural tissue interface properties is to deposit conducting polymers directly on the electrode sites (Cui, Hetke et al. 2001). These conducting polymers can be doped with different ionic species that can lower the electrical impedance, promote specific cell-type attachment, or release anti-inflammatory drugs or other molecules into the extracellular space (Cui, Hetke et al. 2001; Cui, Lee et al. 2001; Cui,

Wiler et al. 2003; Stauffer and Cui 2006; Wadhwa, Lagenaur et al. 2006; Cui and Zhou 2007). To provide for a better understanding of this research, the following section serves as an introduction to conducting polymers. To develop a framework for the research of this dissertation, special focus will be placed on conducting polymers ability to incorporate dopant molecules that promote specific cell attachment (such as neuronal attachment), and the ability to release doping molecules into the extra-electrode region.

1.2 CONDUCTING POLYMERS

Conducting polymers are polymers bearing a conjugated double bond along their backbone. This delocalized π bond provides a continuous supramolecular orbital in which electrons are free to move. When charge carriers in the form of extra electrons or holes are injected into the material through 'doping', the polymer will become electrically conductive (Wallace 1997). Synthesis pathways for conducting polymers include chemical and electrochemical pathways. For application of conducting polymers to electrode arrays, electrochemical synthesis is an ideal method as it targets conductive substrates such as the recording sites of electrode arrays. All of the research contained herein uses electrochemical synthesis and the following discussion focuses solely on conducting polymers synthesized using this method.

Electrochemical synthesis proceeds when an oxidizing potential is created in a solution containing monomers, for instance pyrrole (Py) or ethylenedioxythoiphene (EDOT), and doping molecules. Dopants are small charged molecules (normally anions) that are incorporated into the polymer during chain growth and serve to balance the charge that accumulates on the backbone.

Polymerization proceeds through an oxidation and radical coupling mechanism. For PPy, oxidation of free Py monomer in solution creates radical monomers. These monomers then form oligomers through free radical polymerization. As chain growth ensues through this mechanism, the increasing molecular weight will cause the polymer to come out of solution and deposit on the anode surface (Wallace 1997). The coupling of two radical monomers leaves a residual partial positive charge. A doping anion (A-) will be associated with the backbone whenever the monomer chain has grown sufficiently large that the total positive charge is equal in magnitude to the charge of a doping molecule. For this reason the amount of dopant incorporated will be highly dependent on the type of polymer being synthesized (Wallace 1997). The underlying principle of electropolymerization of PPy is shown in figure 1-2 (where n = the number of monomers per incorporated doping molecule).

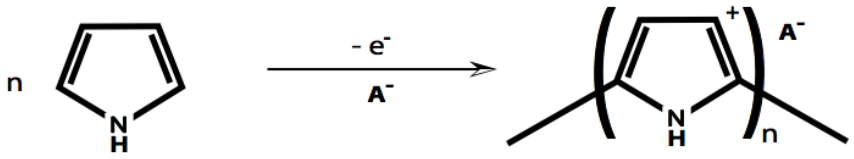

Figure 1-2 PPy synthesis

All of the research described here (with the exception of Appendix C) uses PPy, but there are other common conducting polymers with similar properties including polyaniline, polythiophene, polyacetylene and others (fig 1-3).

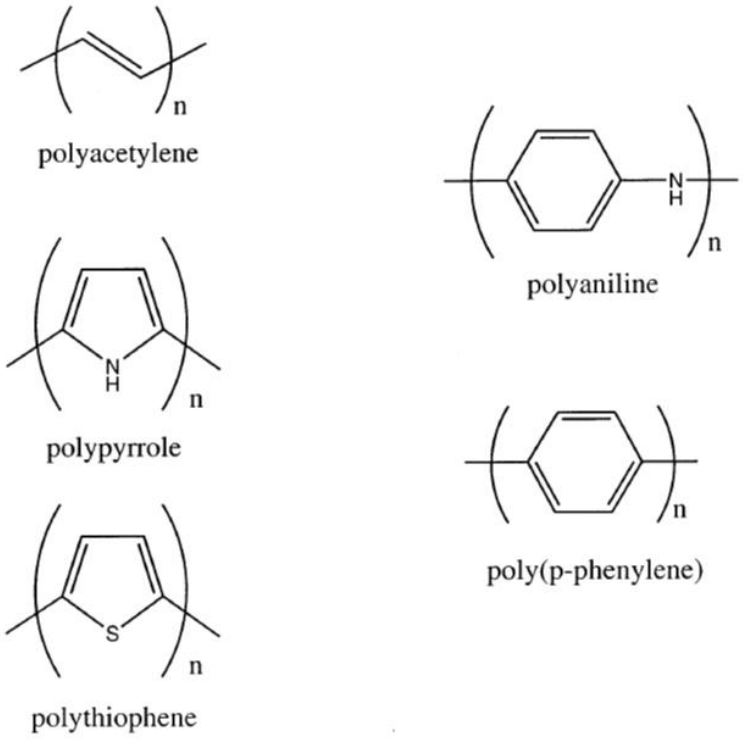

Figure 1-3 Examples of different conducting polymers (reproduced from Cosnier et. al.,1999)

A common theme in conducting polymer research is the customizability of these polymers. Several customization pathways exist, including covalent modification of the constituent monomers (Cosnier 1999) as well as the use of different doping agents. The latter of these is relatively simple and is the route used throughout the research for this dissertation. The identity of the chosen doping molecule can have a profound effect on the resulting morphology (fig 1-4), electrical properties and biocompatibility (demonstrated in Chapter 2) of the resulting polymer films. Of special interest is the notion that biomolecules, such as enzymes, antibodies, receptors and surface ligands can be incorporated in the deposited polymer film as dopants and still retain the biophysical functionality.(Cosnier 1999; Cosnier, Stoytcheva et al. 1999; Cui, Lee et al. 2001; Cosnier and Senillou 2003; Cui, Wiler et al. 2003; Stauffer and Cui 2006; Cui and

Zhou 2007; Gomez and Schmidt 2007). The first demonstrations of this for a neural recording probe by Cui et. al. showed that peptide fragments from fibronectin and laminin could be incorporated

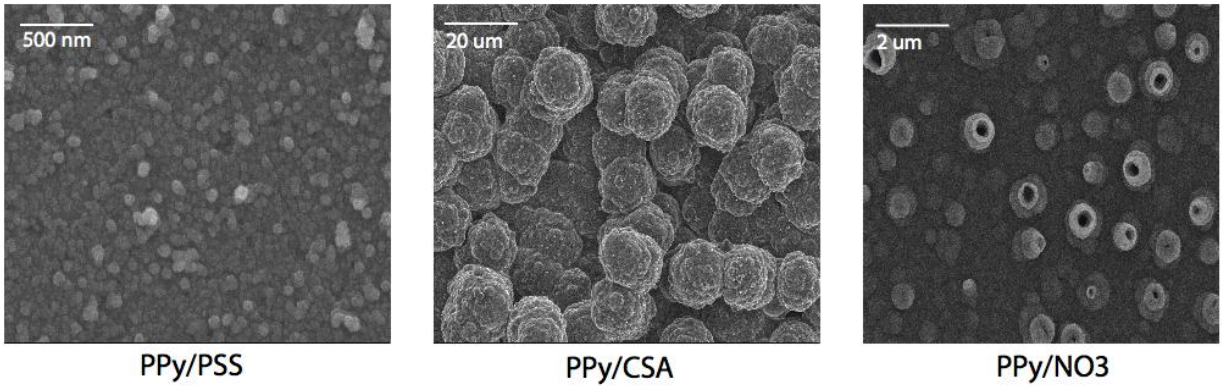

Figure 1-4 The effect of dopant on surface morphology of PPy. (PSS = polystyrenesulfonate, CSA = camphosulfonic acid, NO3 = nitrate)

into PPy films deposited on the electrodes of a Michigan array. The peptide-doped polymers had a high surface area that lowered electrochemical impedance relative to gold surfaces. Furthermore, the ability of these fragments to act as cell attachment sites was retained as glial cells showed preferential attachment to fibronectin fragment doped conducting polymers while human neuroblastoma cells showed greater attachment to PPy doped with the laminin fragment CDPGYIGSR(Cui, Lee et al. 2001). A follow up study demonstrated that when PPy-CDPGYIGSR coated arrays were implanted into guinea pig brain, stable recordings could be obtained and greater neurofilament staining was observed around explanted electrodes that had been coated(Cui, Wiler et al. 2003). A later study concerning laminin fragment immobilization, the report of which is reproduced as chapter 2 of this dissertation, different laminin fragments were shown to have different effects on neuron growth around polymer films, and furthermore

the immobilized fragments were shown to be sufficient for neuron attachment and neurite outgrowth (Stauffer and Cui 2006). In a different study nerve growth factor (NGF) was incorporated into a conducting polymer film and a 50% increase in neurite length was observed when stimulation was applied to the films (Gomez and Schmidt 2007). In light of PPy's ability to undergo a reversible switch in backbone charge under electrical stimulation, it is worthwhile to wonder whether this effect occurred through neuron recognition of surface bound NGF or whether it was released into solution and affected neurite outgrowth in a soluble form.

1.2.1 Reversible redox of conducting polymers: Electrochemical Release

In the previous section we examined conducting polymer films and how dopants are incorporated, as well as how the dopants can influence the surface properties of the films and their interactions with nearby cells. In this section the "switchability" of conducting polymers is examined. Conducting polymers can undergo reversible red-ox reactions in response to an electrical potential. The red-ox reaction involves the charging and discharging of the polymer and is also accompanied by the movement of ions(Wallace 1997) (fig 1-5).

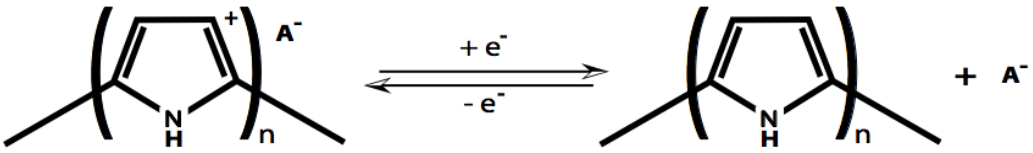

Figure 1-5 Electrochemical release of anions (A^-) from PPy

A consequence of this charging and discharging is that the electrostatic interactions between the backbone and the doping molecules can be temporarily disrupted. When this happens, the

possibility for the dopant molecule to diffuse from the polymer to the solution is created, and this forms the basis for a controlled, electrochemical release process. The basic reaction scheme is detailed in figure 1-5. The reversible nature of this process can be visualized by examining a cyclic voltammetry plot (figure 1-6). In cyclic voltammetry the potential is swept back and forth along a potential range and the resulting currents are measured. In the plot in figure 1-6 a reduction peak can be seen (where the backbone charge is neutralized and anions move out of the films) as well as an oxidation peak, where the backbone regains its positive charge (and anions move into the film).

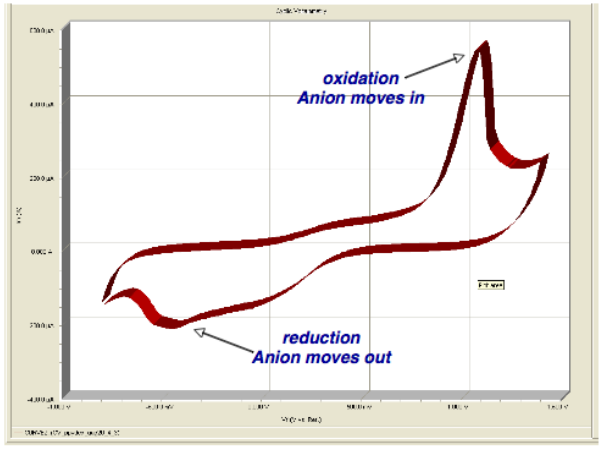

Figure 1-6 A cyclic voltammetry scan (reproduced from Wadhwa et. al. 2006)

Utilizing this property, efforts have been made to develop drug delivery systems in which the conducting polymer can release some chemical substance in response to an electrical (Wadhwa, Lagenaur et al. 2006) or chemical (Pernaut and Reynolds 2000) stimulus. The list of chemicals that have been incorporated and released from conducting polymers include dopamine (Miller, Lau et al. 1983), glutamate and ferrocyanide (Zinger and Miller 1984), salicylate and TCNQ (tetracyanoquinodimethane) (Chang and Miller 1988), naproxen and tosylate (Kontturi,

Pentti et al. 1998), ATP (Pernaut and Reynolds 2000), EHP (Massoumi and Entezami 2002), biotinylated NGF (George, LaVan et al. 2006), dexamethasone (Wadhwa, Lagenaur et al. 2006) and neurotrophin-3 (NT3) (Richardson, Thompson et al. 2007; Evans, Thompson et al. 2008). In the course of the research conducted for this dissertation that list will be expanded to include fluorescein and the glutamate receptor antagonists AP5 ((2*R*)-amino-5-phosphonopentanoate) and CNQX (6-cyano-7-nitroquinoxaline-2,3-dione).

Several studies have shown that PPy films are relatively stable through successive release cycles and that only a small fraction of the incorporated drug leaks from the film without an electrical stimulus (Kontturi, Pentti et al. 1998; Wadhwa, Lagenaur et al. 2006). Release of neurochemicals has been demonstrated under a wide variety of conditions. Studies have been performed either on glassy carbon and carbon electrodes ranging in size from 8 mm^2 to .66 cm^2 (Miller, Lau et al. 1983; Zinger and Miller 1984; Chang and Miller 1988) or on large gold electrodes ranging in size from 40 mm^2 to .7cm^2 (Kontturi, Pentti et al. 1998; Pernaut and Reynolds 2000; George, LaVan et al. 2006; Wadhwa, Lagenaur et al. 2006). Release has been evoked using both square-wave stimuli (George, LaVan et al. 2006) and with potential sweeps in cyclic voltammetry (Miller, Lau et al. 1983; Wadhwa, Lagenaur et al. 2006). The duration of the stimuli has been as short as 10 s and has lasted for up to several minutes. The detection of released chemicals has been performed with EQCM (electrochemical quartz crystal microbalance), HPLC, and UV-Vis spectroscopy. Importantly, the experiments examining release of dexamethasone and biotinylated NGF demonstrated evidence supporting the idea that released drug retains native bioactivity. The released dexamethasone was shown to have the same inhibitory effect on cultured astoglial cells as freshly added dexamethasone (Wadhwa, Lagenaur et al. 2006).

To summarize, a variety of chemicals have been released from conducting polymer films on conductive substrates using electrical command. Recent results have shown that when the drug is released from conducting polymers, it is still bioactive. However, to utilize this technology for neural recording arrays several questions remain. First, even the smallest of electrodes used in previous studies (.06 mm^2) is much larger than neural recording electrodes (generally from .001-.0025 mm^2). Secondly, to study localized effects of many neurochemicals, such as the inhibitory molecule CNQX, the release stimulus needs to be of a sufficiently short duration as to be on the same time-scale as network dynamics. Finally, the neural tissue and the release system need to reside in the same device and be directly connected so that the neural tissue can directly detect the release of the chemicals from the conducting polymer.

An ideal apparatus to address these issues is an *in vitro* multielectrode array (MEA) (figure 1-1(b)). These arrays are commercially available and permit the recording of extracellular voltage spikes (action potentials) from neurons growing in a network situated directly upon the array. Commercial MEAs normally consist of ~60 electrodes arranged in a defined spatial grid, which provides multiple electrodes upon which to test release and multiple recording sites at a variety of distances from the release site to monitor the effects. In order to utilize cultured neuronal network activity to detect and test neurochemical release, some basic foreknowledge of the field is provided in the next section.

1.3 IN VITRO MULTIELECTRODE ARRAYS

The advantage of studying groups of neurons within an intact, behaving animal is the ability to provide behavioral context and meaning to neuronal function. The obvious disadvantage of these studies is the immense complexity of even the simplest of brains as well as the limited accessibility to the cranial vault. Throughout the history of neuroscience a common simplifying step has been to remove the neurons (or, in some cases, parts of a neuron) from the brain and study its isolated physiology. Our understanding of the membrane dynamics of the resting potential as well as the active changes in conductivity underlying nerve signaling was famously described through studies of isolated *Loligo* giant axons (Hodgkin and Huxley 1952; Hodgkin and Huxley 1952; Hodgkin and Huxley 1952; Hodgkin and Huxley 1952; Hodgkin, Huxley et al. 1952). The advantage of *in vitro* studies is the unparalleled control of external sources variability, which allows very basic questions to be addressed. This benefit comes at the cost of revealing how complex interactions between neurons might contribute significantly to the function of the brain. Furthermore, from a practical perspective traditional single cell recording technologies such as patch-clamp limit the number of cells that can be simultaneously monitored. A more recent technological advance that could address some of these limitations is the *in vitro* multielectrode array (MEA). First reported in the early 1970's (Thomas, Springer et al. 1972), *in vitro* MEAs dramatically expand upon the ability to record from a number of neurons simultaneously and allow for the study of coordinated network activity. *In vitro* MEAs are devices that consist of a planar array of electrodes numbering from 8 – 256 that record the extracellular potentials from local neuronal somas or axon initial segments (Taketani and Baudry 2003; Martinoia and Massobrio 2004; Martinoia, Massobrio et al. 2004). These devises have advanced technologically and now there are several commercially available devices.

Neuronal networks cultivated and grown on MEAs form synaptically connected networks containing excitatory and inhibitory cells. Research on cultured neuronal networks (CNNs) can initially be divided into four categories: 1) CNNs as drug sensors, 2) the formation of spontaneous activity patterns and implications this has for network wiring, 3) the effect of electrical stimulation on network activity and how it can induce plastic changes across the network and 4) the use of CNNs in closed loop paradigms.

Briefly mentioning the last of these first, an intriguing subset of MEA research has been devoted to the use of dissociated neuronal cultures as a "brain" for the control of external devices to which the network output flows and from which "sensory" information is collected (Demarse, Wagenaar et al. 2001; Bakkum, Chao et al. 2007). The literature on this subfield is preliminary but the future may hold exciting applications for this technology.

1.3.1 Cultured neuronal networks as drug sensors

The use of CNNs as drug sensors has demonstrated an exquisite sensitivity to certain drugs combined with fast feedback, which can occur within milliseconds. This application is most powerful when the drug being tested is one to which network dynamics are highly labile, such as strynchnine (Gross, Rhoades et al. 1995) or glutamate receptor antagonists (Wagenaar, Pine et al. 2006). In cases like these a large dynamic range dose dependency can be observed. Toxic chemicals can also be identified through a 'paroxysmal responses indicating major, pathological membrane currents in large subpopulation of cells' (Gross, Harsch et al. 1997). A feature of network dynamics we will soon address is spontaneous coordinated firing across the network. The parameters of this firing patterns, including the interval between bursts, their duration and the percentage of spiking activity occurring within a burst have all been shown to

co-vary with the concentration of a variety of different neuroreactive chemicals, including K^+ (Rhoades and Gross 1994; Canepari, Bove et al. 1997), CNQX (Canepari, Bove et al. 1997; Wagenaar, Pine et al. 2006), AP5 (Jimbo, Kawana et al. 2000), Ca^{2+} (Canepari, Bove et al. 1997), Mg^{2+} (Jimbo, Robinson et al. 1993; Maeda, Robinson et al. 1995; Canepari, Bove et al. 1997; Jimbo, Kawana et al. 2000), cholinergic agents (Tateno, Jimbo et al. 2005),(Tateno, Jimbo et al. 2005) bicuculline (Khatami, Nam et al. 2004) and strychnine (Gross, Harsch et al. 1997). A recent study has evaluated CNNs for biosensing of botulism toxin and found that increases in firing and network-burst rate increased with toxin application (Scarlatos, Cadotte et al. 2008). As we employ CNNs as detectors for the release of tiny amounts of CNQX and AP5 this dose dependency will become an important aspect to examine.

1.3.2 Spontaneous network bursting

Probably the most striking feature of the data recorded from dissociated cultures is the presence of brief, semi-periodic, array-wide, synchronous neural discharges (Bove, Grattarola et al. 1997; Bove, Martinoia et al. 1998; Jimbo and Robinson 2000; Wagenaar, Madhavan et al. 2005; Wagenaar, Nadasdy et al. 2006; Wagenaar, Pine et al. 2006). The development, etiology, and persistence of network up-states, as well as their physiological significance, have been the subject of continuous study for the past ten years. A central question that these up-states engender is whether one or several cells in the network act as ‘pacemakers’ for the network. Results suggest this is not the case. An early study attempt to address this question applied patch-clamp to neurons in a bursting network and used the patch to stimulate different neurons to fire. While bursts could be evoked in these patched networks through extracellular stimulation (which supposedly excited a group of cells), bursts could not be elicited through stimulation of

individual cells (Jimbo, Robinson et al. 1993). Furthermore, examination of the neuronal order of onset during individual up-states suggests a random burst initiation at many different neurons. When laser ablation was used to section a mature network into four quadrants, the four quadrants expressed up-state, or network bursting, behavior independently of one another (Maeda, Robinson et al. 1995) . More recently, a study has divided recorded neurons into two functional groups, those that fire predominantly during network up-states, and those whose spike times are more uniformly distributed. It was found that these so called 'highly active (HA)' neurons were most easily evoked with electrical stimulation and HA spiking tended to precede network up-states, but the evidence did not support an initiator role (Shein, Volman et al. 2008).

The random nature of up-state initiation leaves open the possibility that the observed activity pattern is the result of a correlated noise input, as opposed to the case where these up-states are synaptically mediated. However, numerous studies have shown that application of specific glutamate synaptic transmission inhibitors CNQX and AP5 reduces or completely abolishes the presence of up-states (Kamioka, Maeda et al. 1996; Wagenaar, Pine et al. 2006; Shein, Volman et al. 2008).

A hypothesized physiological role for network bursting is the formation of network structure during a critical development period. Several studies have shown a high degree of variability in the firing patterns of young (1-2 week) cultures (Jimbo, Robinson et al. 1993; Kamioka, Maeda et al. 1996). The patterns of activity seemed to normalize as cultures grew older (Jimbo and Robinson 2000; Wagenaar, Nadasdy et al. 2006). This finding is supported by reports examining the correlation space of spontaneous firing patterns of neuron pairs. Within young cultures the correlation between pairs of neurons changes rapidly, after 25 DIV the correlations become more stable (le Feber, Rutten et al. 2007). However, a more exhaustive

survey demonstrated that there was a great deal of culture-to-culture variability and that the randomness of the activity pattern did not resolve in any predictable fashion (Wagenaar, Pine et al. 2006). Also providing evidence that these network bursts are not a physiological development mechanism are experiments done in cortical slice culture where the same phenomenon is observed (Jimbo and Robinson 2000). In slice culture most synapses would have been preserved during harvest, and one would not expect major synaptic restructuring to occur. Currently, the most promising explanation for this network-bursting phenomenon is the lack of external input into the network. It has been shown that providing random background electrical stimuli to the network reduces the instances of bursts (Wagenaar, Madhavan et al. 2005). Furthermore, through reduced effectiveness of bicuculline it is thought that inhibitory circuits deteriorate over time, further reinforcing the excitatory bursting nature of CNNs (Li, Zhou et al. 2007).

1.3.3 Evoked network activation

Along with the broad network activation observed during spontaneous bursting events, the networks can also be activated through electrical stimulation from substrate electrodes. Electrical stimulation of cultured neuronal networks through substrate electrodes results in the firing of action potentials from neurons located all over the electrode array (Gross, Rhoades et al. 1993; Jimbo, Tateno et al. 1999; Jimbo, Kawana et al. 2000; Jimbo, Kasai et al. 2003; Wagenaar, Pine et al. 2004). In at least one study there was a network refractory period of 3 s and an interval greater than 15 s between stimuli would allow spontaneous bursts to occur (Jimbo, Robinson et al. 1993). Central to understanding evoked responses is answering whether this broad evoked response is due to local stimulation that spreads physiologically or is it the effect of a generated

electrical field that directly stimulates cells distributed across the dish. UV laser ablation to isolate a small neural network around an individual electrode showed that electrical stimulation of that electrode did not evoke APs outside the region isolated by the ablation (Maeda, Robinson et al. 1995). However, several studies have observed that increasing the magnitude of the stimulation voltage increases the radius within which cells fire APs during a critical time window thought to delineate direct electrical stimulation from more prolonged recurrent network activation (Pinato, Parodi et al. 1999; Jimbo, Kasai et al. 2003). The true answer to this question will probably be some combination of direct stimulation of local and distant cells due to how closely and tightly neurons are associated with a stimulating electrode. This feature, the so-called 'sealing resistance' will effect how strongly local cells are activated by a given stimulus as well as how an electrical field will spread from the source (Martinoia and Massobrio 2004; Martinoia, Massobrio et al. 2004). A possible approach to normalizing this parameter is through the use of patterned surfaces where neuron attachment is directed by different substrate molecules (Nam, Chang et al. 2004).

Whatever the mechanism is for spatially broad activation, a network response is initiated. The time varying firing rates of neurons in the network increase rapidly following stimulation and fall off gradually. Using electrical stimuli that essentially control the time at which a burst occurs (Jimbo, Robinson et al. 1993) has allowed for studies to begin addressing the role of network activity in activity dependent plasticity. High frequency, high voltage stimuli (2-3 V, 100 μs, 20 Hz) given for brief (1 s) periods of time at multiple electrode simultaneously was found to increase the number of spontaneous bursts as well as increasing the probability that a single electrical stimulus would evoke a network response (Maeda, Kuroda et al. 1998). A more detailed study of this phenomenon combined the use of extracellular recordings with patch-

clamp of individual neurons. The changes in network activity were correlated with changes in the late phase of excitatory post-synaptic potentials (EPSPs) (Jimbo, Robinson et al. 1998). This late phase of EPSC has been shown to be inhibited by AP5 (Jimbo, Kawana et al. 2000) so this provides indirect evidence that the NMDA receptor (which is inhibited by AP5) may underlie the plastic changes observed in the studies. Examination of the correlation space between neurons demonstrated that the initial relative timing of spikes determined the effect of tetanic stimulation. Tetanic activation of highly correlated groups of neurons would result in potentiation, while similar activation of uncorrelated groups would result in depression (Jimbo, Tateno et al. 1999). A similar yet slightly different group of experiments has attempted to induce and measure plasticity through changes in a stimulus-response (SR) relationship (Shahaf and Marom 2001; le Feber, Stegenga et al. 2008; Stegenga, le Feber et al. 2008). In these experiments a low frequency stimulus is applied to the network until a predefined response appears. This process is repeated until the number of stimuli needed to evoke the response decreases.

1.3.4 Glutamatergic synaptic transmission

For the studies that follow we are particularly interested in the role that different glutamate receptors play in network activation. Glutamate is the major excitatory neurotransmitter in the brain (Kandel, Schwartz et al. 2000) as well as in the *in vitro* MEA (Taketani and Baudry 2003). A family of ionotropic and metabotropic receptors mediates glutamate neural transmission. In the vertebrate central nervous system, ionotropic glutamate receptors always mediate an excitatory response. Ionotropic glutamate receptors are classified as either NMDA or non-NMDA receptors. The nomenclature is derived from the ability of N-methyl-D-aspartic acid (NMDA) to precipitate opening of the associated ion channels. Non-

NMDA receptors are further divided into the AMPA and kainate receptor subtypes (also described by the functional responses to α-amino-3-hydroxyl-5-methyl-4-isoxazole-propionate (AMPA) and kainate, respectively). Binding of glutamate to the non-NMDA class of receptors directly opens ion channels permeable to Na^+ and K^+. The reversal potential of these receptor is around 0 mV. NMDA receptors are permeable to Na^+ and K^+, as well as Ca^{2+}(Kandel, Schwartz et al. 2000).

Functionally, the activities of the two classes of receptors have differing impacts on the postsynaptic cell. The AMPA and kainate receptors are purely ligand-gated channels that open in the presence of glutamate. These channels mediate the early-phase of the EPSPs observed in post-synaptic neurons. NMDA receptors are voltage and ligand-gated ion channels. In the resting state NMDA receptor ion channels are blocked by the presence of a Mg^{2+} ion that resides in the channel pore through electrostatic attraction to the electronegative interior side of the membrane. When a neuron is depolarized (normally through the activity of AMPA and kainate receptors) the electrostatic attraction of the Mg^{2+} ion is removed and the channel can then open (provided glutamate is present). The NMDA receptor thus prolongs the EPSP and may play a role in extended bursting events (Kandel, Schwartz et al. 2000). The NMDA receptor plays a central role in activity dependent plasticity (Kleinschmidt, Bear et al. 1987; Bi and Poo 1998).

A developing body of research is beginning to highlight how these two excitatory channels affect network activity. The activities of the two classes of ionotropic glutamate receptors can be separated through the use of selective pharmacological blockers. Non-NMDA receptors are inhibited by CNQX (6-cyano-7-nitroquinoxaline-2,3-dione), which does not effect NMDA receptors (Blake, Brown et al. 1988; McBain, Boden et al. 1988). Conversely, NMDA receptors can be inhibited with AP5 ((2*R*)-amino-5-phosphonopentanoate). Together with the

late role for NMDA and early role for AMPA in a synaptic response, research suggests that they play very different roles in mediating precise spike timing. Using a dynamic clamp paradigm, it was demonstrated that AMPA like currents injected into neurons produce precisely timed and repeatable spiking while NMDA-like currents introduced a great deal of variability into spike timing(Robinson and Harsch 2002). This fact will have a significant contribution to the interpretation of the results provided in the final chapter of this paper, when network responses are examined in correlation space.

Previous research on the role of AMPA and NMDA currents utilizing *in vitro* MEAs used bath addition of CNQX or AP5 to modulate the entire network on a broad time scale. A more precise description of a network's functional structure and generation of dynamic activity patterns could be obtained with a technique to deliver chemicals to precise locations with greater timing precision. Several technologies have been developed for the local delivery of chemicals, including pressure injection (Gerhardt and Palmer 1987; Barker, Billups et al. 2008), microiontophoresis (Hicks 1984; Gerhardt and Palmer 1987; Haidarliu, Shulz et al. 1995), caged compounds (Ellis-Davies 2007) and microfluidics (Kaji, Nishizawa et al. 2003; Mourzina, Kaliaguine et al. 2006). Through the use of these techniques focal chemical perturbations of individual cells or regions of the brain have become an important approach in investigating mechanisms of neural processing and intervening disease conditions (Kandler, Katz et al. 1998; Maalouf, Dykes et al. 1998; Lesniak, Upadhyay et al. 2005). However, all of these techniques require additional hardware to be introduced (aside from microfluidic channels in the probe itself, but these can complicated design and fabrication greatly). *In vitro*, introduction of iontophoretic pipettes increases the likelihood of infection and can decrease the lifespan of the network under study. *In vivo*, this methodology causes further injury to the brain. Using

photo-uncaging techniques easily causes photo-toxicity to cultured neurons while the depth the laser can penetrate limits studies in the brain. Here we propose a new technique for local, precisely timed release of neurochemicals: the incorporation and release of pharmacological agents from conducting polymer films deposited directly on recording microelectrodes. The system can be easily integrated into pre-existing MEAs without complex microfabrication or the need to implant extra hardware for recording. Flexibility can be achieved through dopant selection and pattern creation on the existing electrode grid.

As we proceed through this dissertation, we will look at the *in vitro* MEA paradigm as a two-way street. In the initial phase we wish to develop and characterize the conducting polymer mediated release of neurochemicals that inhibit synaptic transmission. On the scale at which this system will be implemented (microelectrode arrays), the polymer film will be limited in size by the microelectrode dimensions and the release amounts of neurochemicals far below the detection limit of conventional analytical techniques. The CNNs however will act as highly sensitive and fast detectors of changes in the local chemical environment. In this way the CNN will inform our studies of neurochemical release. In the second phase, having a well characterized local release system that can chemically perturb small regions of the CNN, the release system can be used to investigate the role of local synaptic transmission on the interdependencies within the network activity. From an organizational perspective, chapter 3 will travel in one direction on this highway while chapter 4 will travel in the opposite way.

1.4 OUTLINE OF THESIS

Chapter two of this dissertation focuses on the customizability of PPy surfaces for specific neuronal growth. Chapter three utilizes the reversible redox properties of these films to develop a release system capable of locally delivering neurochemicals to an in vitro neuronal network. In the final chapter, cross-correlation and a model-based variable clustering technique developed by Wang (Wang 2005) is implemented for data collected from an *in vitro* multi-electrode array using the local release system. The functional connectivity that is described by this technique is investigated as well as changes in the correlation structure described by the differing time scales the techniques operate on. What follows is a brief description of the rational and summary of the conclusions from the three proceeding data chapters.

Chapter two presents an extension of earlier work by Cui et.al., demonstrating that peptide sequences can be incorporated in conducting polymers as dopants and that they are recognized by neurons and other cells(Cui, Lee et al. 2001; Cui, Wiler et al. 2003). These studies had shown that the laminin fragment CDPGYIGSR (p31) could be incorporated into the conducting polymer polypyrrole (PPy) and that PPy-p31 surfaces were more attractive to human neuroblastoma cells than were PPy surfaces that had incorporated a non-biological dopant PSS. In this thesis the laminin fragments p31 and RNIAEIIKDI (p20) are used as dopants in electropolymerization of the conducting polymer PPy. The electrical properties of the resulting films are analyzed by impedance spectroscopy and cyclic voltammetry and compared to gold. PPy/p20 surfaces consistently demonstrate the lowest impedance and largest charge capacity for a given deposition charge. Next, *in vitro* studies using primary neurons cultured in a defined media and primary astrocytes in a serum containing media were performed; neuron density and neurite length, as well as astrocyte density, were quantified. Surfaces doped with a combination

of the two peptides (PPy/p20-p31) consistently supported the highest neuronal density. It is shown that surfaces doped with the laminin fragment p20 had significantly longer primary neurites than either the p31 doped or PSS doped PPy surfaces. Finally, the astrocyte studies demonstrate that PPy surfaces have significantly less astrocyte attachment in culture than the common electrode material, gold, suggesting that modified surfaces might reduce glial cell adhesion that leads to electrode encapsulation. In conclusion, polypyrrole doped with laminin peptide p20 and p31 provides a better interface to neural tissue.

Chapter three develops a PPy-mediated local release system for the glutamate synaptic transmission inhibitor CNQX and implements the system on *in vitro* MEAs. In this report, the anionic dye fluorescein is used as a dopant in PPy synthesis. The PPy-fluorescein films are deposited on microelectrodes in an MEA. Time-lapse fluorescence microscopy is used to monitor the release of fluorescein from the microelectrodes in response to electrical stimuli of varying magnitude. A positive correlation is found between the amount of release and the magnitude of the release signal. The release parameters defined by this study are used to release CNQX from PPy-CNQX films synthesized on MEAs which neuronal networks have been cultured on. Neurons at various distances from releasing electrodes are patch-clamped and the effect of CNQX and control substance release is monitored at various time points. With the time, distance, and inhibition data evidence is presented that the effect of released CNQX concur with a common diffusion model.

In chapter four, initial results demonstrating the use of electrochemical release of CNQX in studying functional network structure. Two methods for describing the functional correlation structure of the network will be employed. Cross-correlation using 1 ms time bins will demonstrate the statistical dependency between neurons on the scale of spike-timing

predictability. Clustering based on the correlation of firing rates from trial to trial will be performed using a model-based clustering algorithm. This technique will quantify the statistical dependency of the neurons on a much broader time scale than cross-correlation does. These techniques will demonstrate evidence for a stimulus specific network response. Finally, results will be presented showing that local release of CNQX from the microelectrode arrays transiently reduces network firing rates and interferes with the correlation between neurons. In one network we will demonstrate that CNQX release from different electrodes produces different effects on the correlation structure of the network. This result distinguishes these results from cases where CNQX is added directly to the bath and produces uniform inhibition across the dish. That correlations are disrupted while firing rate modulation remains suggests that the AMPA inhibition resulting from CNQX release is sufficient to disrupt spike timing (and would interfere with coincidence detection) but that enough network drive (possibly due to unaffected NMDA currents) remains intact for broad fluctuations in firing rate.

Taken together, this thesis demonstrated different ways by which the conducting polymer can be used to affect neuronal growth and activity. Such manipulations may enable us to better study the nervous system *in vitro* and *in vivo*.

2.0 POLYPYRROLE DOPED WITH 2 PEPTIDE SEQUENCES FROM LAMININ

2.1 ABSTRACT

In the field of neural tissue engineering, electrically conducting, biocompatible surfaces are of great interest. Over the past several decades conducting polymers have been studied as candidate surfaces because they fit these criteria. Several attempts have been made to combine the conductivity and biocompatibility of conducting polymers with biomolecules that could promote specific cell attachment and growth. In this report the laminin fragments CDPGYIGSR (p31) and RNIAEIIKDI (p20) are used as dopants in electropolymerization of the conducting polymer polypyrrole (PPy). The electrical properties of the resulting films are analyzed by impedance spectroscopy and cyclic voltammetry and compared to gold. PPy/p20 surfaces consistently demonstrate the lowest impedance and largest charge capacity for a given deposition charge. Next, in vitro studies using primary neurons cultured in a defined media and primary astrocytes in a serum containing media were performed; neuron density and neurite length, as well as astrocyte density, were quantified. Surfaces doped with a combination of the two peptides (PPy/p20-p31) consistently supported the highest neuronal density. It is shown that surfaces doped with the laminin fragment p20 had significantly longer primary neurites than either the p31 doped or poly(styrenesulfonate) doped PPy surfaces. Finally, the astrocyte studies

demonstrate that PPy surfaces have significantly less astrocyte adhesion in culture than the common electrode material, gold.

2.2 INTRODUCTION

Polypyrrole (PPy) is a biocompatible, electrically active, and conductive material (Diaz, Castillo et al. 1981; Wong, Langer et al. 1994; Schmidt, Shastri et al. 1997; Collier, Camp et al. 2000; Cui, Lee et al. 2001; Cui, Wiler et al. 2003; Cui and Martin 2003; Cui and Martin 2003; Wallace 2003). This makes it an ideal candidate for electrodes used in neural prostheses and guidance channels for nerve regeneration where electrical signal conduction is the implicit function. Previous research has examined neurite outgrowth on PPy films both with and without electrical stimulation and found that neurite extension was enhanced on PPy films when an electrical current was passed through the films (Schmidt, Shastri et al. 1997). Using the Michigan recording probes, Cui et al (Cui, Lee et al. 2001; Cui, Wiler et al. 2003; Cui and Martin 2003) showed that PPy coatings on the surface of the electrodes dramatically reduced electrical impedance and improved signal conduction.

Along with the electrical properties exhibited by PPy, another feature that can be exploited for regenerative medicine purposes is the dopant selection. Electropolymerization of conducting polymers incorporates counter ions in solution, referred to as dopants, to balance charge (Wallace 1997). A common non-bioactive dopant used in many studies is the anionic poly(styrenesulfonate) (PSS) (Wong, Langer et al. 1994; Schmidt, Shastri et al. 1997; Collier, Camp et al. 2000; Webb, Hlady et al. 2000; Cui, Lee et al. 2001; Kotwal and Schmidt 2001; Cui and Martin 2003; Wallace 2003; George, Lyckman et al. 2005). However, of great interest is the

use of biological agents as dopants. These biological agents are immobilized on the PPy surface and are able to interact locally with cells. In one study, the proteoglycan, hyaluronic acid, was used as a dopant during electropolymerization. The resulting surfaces promoted vascularization *in vivo* but did not promote PC-12 cell attachment *in vitro* (Collier, Camp et al. 2000). In a separate study, the laminin fragment CDPGYIGSR was used as a dopant in the surface modification of Michigan recording electrodes. *In vitro* studies showed that neuroblastoma cells grew preferentially on and around electrodes coated with PPy/CDPGYIGSR compared to PPy/CH_3COO^- films (Cui, Lee et al. 2001). Furthermore, in vivo studies demonstrated that electrodes surface modified with PPy/CDPGYIGSR showed a significant increase in local neurofilament staining 1 week after implantation (Cui, Wiler et al. 2003).

The goal of this work was to design an electrically conductive surface that is not merely biocompatible but actively promotes the growth and differentiation of desired cells types *in vitro*. Previous *in vitro* studies have used neuroblastoma or PC-12 cells cultured in a serum based media with or without Nerve Growth Factor (NGF) (Wong, Langer et al. 1994; Schmidt, Shastri et al. 1997; Collier, Camp et al. 2000; Cui, Lee et al. 2001; Kotwal and Schmidt 2001) or primary neurons in a serum based media (George, Lyckman et al. 2005). Serum based media contains an unknown mixture of proteins which adsorb onto the surface to facilitate cell attachment and growth, thereby diminishing the effect of any surface immobilized biomolecule. Furthermore, neuron-like cell lines such as PC-12 and neuroblastoma cells are excellent means of establishing preliminary data. However, these cell lines lack key neuronal features such as polarity of markers, and the ability to form synaptic connections (neuroblastoma cells can be forced to form connections by over expression of synapsin IIB) that makes them fundamentally different from primary neurons (Craig and Banker 1994). In this work we examine the effects of

PPy surfaces doped with laminin fragments on primary neuronal culture in a defined media with no added growth factors.

Laminin is a multifunctional extracellular matrix (ECM) protein and basement membrane component associated with several cell types. As such, different peptide sequences within laminin are responsible for its various functions (Graf, Iwamoto et al. 1987; Ard and Bunge 1988; Liesi, Narvanen et al. 1989). Two well characterized cell binding domains are p31 (CDPGYIGSR) and p20 (RNIAEIIKDI). It has been shown that p31 plays a role in the binding of many different cell types including neurons and astrocytes (Graf, Iwamoto et al. 1987). Furthermore, as indicated earlier, p31 has been utilized as a dopant in electropolymerization of PPy and the growth of glial and neuroblastoma cells were quantified on the surface. The *in vivo* neuronal tissue response to PPy/p31 coated electrodes has also been assessed (Cui, Lee et al. 2001; Cui, Wiler et al. 2003). Conversely, previous literature has suggested that p20 is a neurite outgrowth promoting domain of laminin (Liesi, Narvanen et al. 1989). To the best of our knowledge, p20 has never been utilized as a dopant in the electropolymerization of conducting polymers.

In this work, the electrical properties of the different PPy surfaces were tested and compared for enhanced transmission of electrical signals. It is demonstrated that the chosen biomolecular dopants have a significant effect on neuron attachment and neurite extension. The work shows that the effect on neuron growth occurs specifically through the bioactive species immobilized on the surface. Finally, astrocyte growth on the different surfaces was examined and it is shown that fewer cells attached and grew on PPy surfaces than on gold after 3 days in culture.

2.3 MATERIALS AND METHODS

2.3.1 Substrate Preparation

Gold coated plastic coverslips (Fisher) were used as a model system for the electrochemical deposition of polymer and as cell culture substrates. In order to ensure constant current density and provide suitable sized surfaces to fit in tissue culture wells, the coverslips were cut to a uniform dimension of 7 mm x 22 mm. The coverslips were cleaned with 8 N HNO_3 for 30 min followed by two washes in deionized H_2O and stored in ethanol until gold deposition.

To create a conductive surface for electrochemical deposition, the cut, cleaned coverslips were sputter coated with a layer of gold using a Cressington Sputter Coater (Cressington Scientific Instruments, Inc.) with thickness control. The thickness of the gold layer was approximately 40 nm. The coated coverslips were stored in a dessicator until used.

2.3.2 Electrochemical Deposition

The peptides DCDPGYIGSR (p31) and DRNIAEIIKDIC (p20) were synthesized at the Peptide Synthesis Facility at the University of Pittsburgh. An aspartic acid (D) was added on the N terminal of each peptide to increase the negative charge for more efficient dopant incorporation. A cysteine (C) was added to the C terminal of p20 for additional coupling capability. Two types of electrodes were used for deposition of PPy/peptide film, gold electrode sites (1.25×10^{-5} cm^2) of a Michigan Probe (NeuroNexus), and gold-coated coverslips (0.7 cm^2).

The films on the electrode sites of the Michigan probe were grown under an anodic current density of 0.5 mA/cm^2. The electrochemical cell was a 2 ml glass cuvette with a platinum plate as the counter electrode. The monomer solution contained 0.5 M pyrrole (Sigma) and 5 mg/ml of peptide. Thickness of the films was controlled by time of deposition. On gold coated coverslips, PPy/peptide films were grown galvanostatically under varying anodic current density for electrochemical studies and for use as cell culture substrates. The dopants used were the laminin fragments p31 and p20, both at 5 mg/ml, a mixture (50:50) of the two peptides at a total peptide concentration of 5 mg/ml, and the non-bioactive dopant poly(styrenesulfonate) (PSS) at 0.1 M. To analyze the electrochemical properties and to optimize the thickness for cell growth, five different deposition charges (1.25 – 25 μC) were used during electropolymerization.

2.3.3 Surface Characterization

2.3.3.1 Thickness Measurement

The PPy film thickness was measured with a Gaertner L-117 Null ellipsometer (Gaertner Scientific Corporation). A linearly polarized He-Ne laser with wavelength 632.8 nm was used in the measurement at incident angle 70º. The analyzer (A) can detect the change in the phase angle (Δ) and the amplitude change (Ψ) of the light after reflection from the sample. Refractive indices of n1=1 for air, n2=1.45 for the organic molecular monolayer, and n3=0.166+3.22i for gold were used to calculate the thickness of films. The measurements were performed four times at different locations for each sample, and the results are reported as an average of the measurements.

2.3.3.2 Scanning Electron Microscopy

Surface morphology was analyzed by Scanning Electron Microscopy (SEM). Specimens were synthesized according to the method described above, and then a 3.5 nm coating of Au/Pd was sputtered on the surface. Imaging was done in a JEOL 9335 Field Emission Gun SEM (Jeol USA) at 5 KV. Cells growing on the different surfaces were analyzed by SEM also. Biological samples were prepared with 2.5% gluteraldehyde and 1% osmium-tetroxide, both for 1 h, followed by dehydration and critical point drying.

2.3.3.3 Fourier Transformed Infrared Spectroscopy

To characterize the chemical composition of the polypyrrole/biomolecule coatings, reflective Fourier transform infrared (FTIR) spectroscopy was performed using a Thermo-Nicolette Magna-IR 560 Spectrometer attached to a Continuum microscope equipped with a liquid nitrogen-cooled MCT detector (Thermo Electron Corporation). The microscope accessory enabled the focusing of the IR beam on a small area of the sample. The microscope aperture was used to adjust the infrared light spot area. The background signal was collected from a gold mirror. The samples were scanned 100 times in the range of 4000 to 650 cm^{-1}. OMNIC software was used to generate the FTIR spectrum.

2.3.4 Electrochemical Impedance Spectroscopy and Cyclic Voltammetry

Electrochemical impedance spectroscopy was performed using a Gamry Potentiostat, FAS2/Femostat (Gamry Instruments), under the control of the Gamry Framework software. A solution of 0.1 M PBS buffer (pH = 7.0) was used as the electrolyte in a three-electrode cell. A

platinum foil was used as the counter electrode, a saturated calomel electrode (SCE) was employed as the reference electrode, and the electrode (gold coated coverslip or microelectrode sites on the Michigan probe) with or without polymer coatings, was used as the working electrode. An AC sinusoid of 5 mV amplitude was applied as the input signal with the DC potential set to 0 V. The value of the impedance was determined at four discrete frequencies per decade over the range of 10 to 10^5 Hz.

Cyclic voltammetry (CV) was performed using the same electrochemical setup as described above. The voltage was swept from -0.6 V to +0.8 V versus SCE and the scan rate was set to 50 mV/s for 4 cycles.

2.3.5 Cell Culture

Surface modified plastic coverslips were affixed to the bottom of cell culture wells in 24 well tissue culture plates (Corning Costar) using Kwik-Sil (World Precision Instruments, Inc.). Following placement of the coverslips in the tissue culture plates, the entire plate was exposed to UV light under a laminar flow hood for 30 min to sterilize the samples. Following sterilization, the culture wells containing the samples were washed 3 times with sterile PBS.

E18 Sprague Dawley (SD) rat cortices were purchased from BrainBits, LLC. Cell culture was performed according to Brewer et al. (Brewer and Price 1996). Briefly, rat cortices were triturated with a 1 ml pipette and removed from Hibernate Media™ by centrifugation at 800 x *g*. The cells were re-suspended in 1 ml Neurobasal media (Gibco, 21103-049) containing B27 (Gibco, 17504-044), 0.5 mM glutamine (Sigma), and 25 μM glutamate (Sigma). Cell counts

were performed using trypan blue and cells were plated at a density of 1.5 x 10^5 cells/cm^2. Cells were grown in culture for three and eight days at 37^o in 5% CO_2. Media changes were performed every four days as needed.

Astrocytes were isolated by enzymatic digestion with trypsin of a murine cortex. The resulting suspension was plated on uncoated TCPS and grown in DMEM with 10% fetal calf serum (FCS) (Hyclone, SH30071.04). Astrocytes were passaged once a week, up to four weeks. For experiments, astrocytes were digested with 0.25% trypsin, and plated at 1.5 x 10^5 cells/cm^2 in DMEM /10% FCS on the PPy surfaces. They were allowed to grow for three days.

2.3.6 Immunohistochemistry

Cells were fixed in 4% paraformaldehyde for 10 minutes. Immunochemical labeling was done using antibodies against a neuronal marker, class III β-tubulin (Covance), and the astrocyte-specific marker glial fibrillary acidic protein (GFAP; Dako). Nonspecific binding was blocked by incubation with 2% goat serum. Primary antibodies were diluted 1:500 in PBS containing 2% goat serum and incubation was performed for 1 hour at room temperature. Following PBS washes, an Alexa 488 goat anti-mouse secondary (Molecular Probes) was diluted 1:1000 in PBS containing 2% goat serum and incubated for 1 hour at room temperature. Cells were counterstained using the nuclear dye Hoechst 33258 (Sigma) at a concentration of 2 mg/ml in PBS.

2.3.7 Data Collection and Statistical Analysis

Cell counts on the β-tubulin and GFAP images were obtained manually by looking for co-localization of the respective marker with a DAPI stained nuclei. Ten random images from each coverslip were counted in this manner and the total number summed. The summed values were then averaged across all the coverslips in a particular group. This value was then used to statistically evaluate the different conditions. Neurite measurement was performed with the program ImageJ and the plug-in NeuronJ. On ten random images from each condition, the primary axon of each cell was measured with the tracing algorithm contained in Neuron J (figure 11). Statistical Analysis was performed in SPSS. For experiments that involved the comparison of two groups (such as the inhibition studies) the standard student's t-test was performed. For comparisons involving multiple groups, ANOVA followed by Bonferroni's post-hoc analysis was used.

2.4 RESULTS

2.4.1 Chemical and Electrochemical Characterization

The deposited film was characterized qualitatively by FTIR spectroscopy shown in figure 2-1. From 1800 to 4000 cm^{-1}, the spectrum showed a continuous increase in absorption. This is the tail of the ~1 eV (~8066 cm^{-1}) bipolaron absorption band, which is the signature for electrical conductivity of conducting polymers (Allen, Murray et al. 1997; Cui, Wiler et al. 2003).

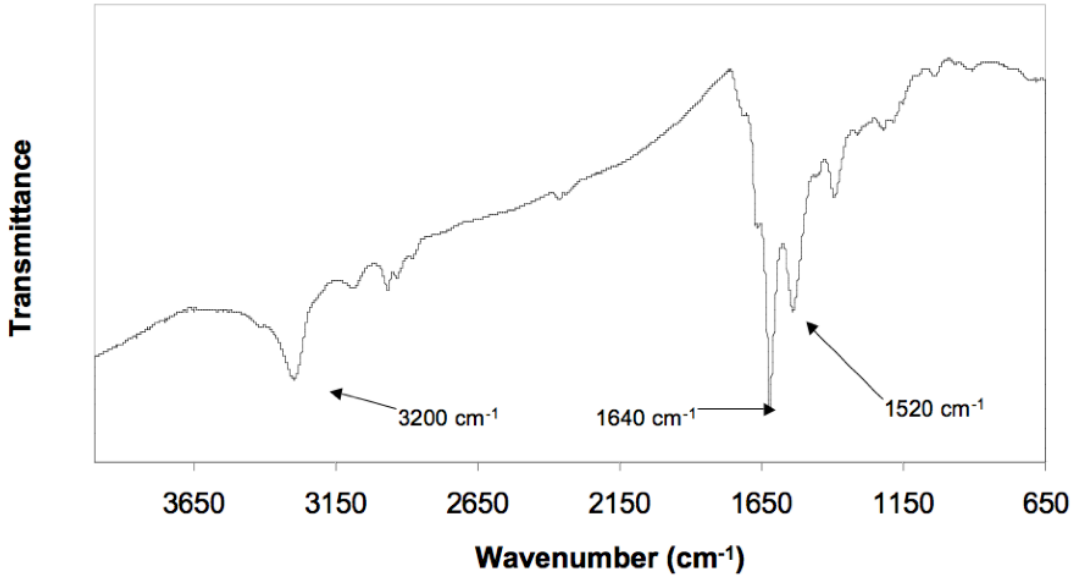

Figure 2-1 FTIR spectrum of PPy/peptide film. The peaks at 1640 and 1520 are indicative of amide I and II, the peak at 3200 is indicative of pyrolle.

The first requirement of a biomedical surface intended to communicate with the nervous system is that it be electrically conductive. We used electrochemical impedance spectroscopy and cyclic voltammetry to assess the conductive nature of the surfaces.

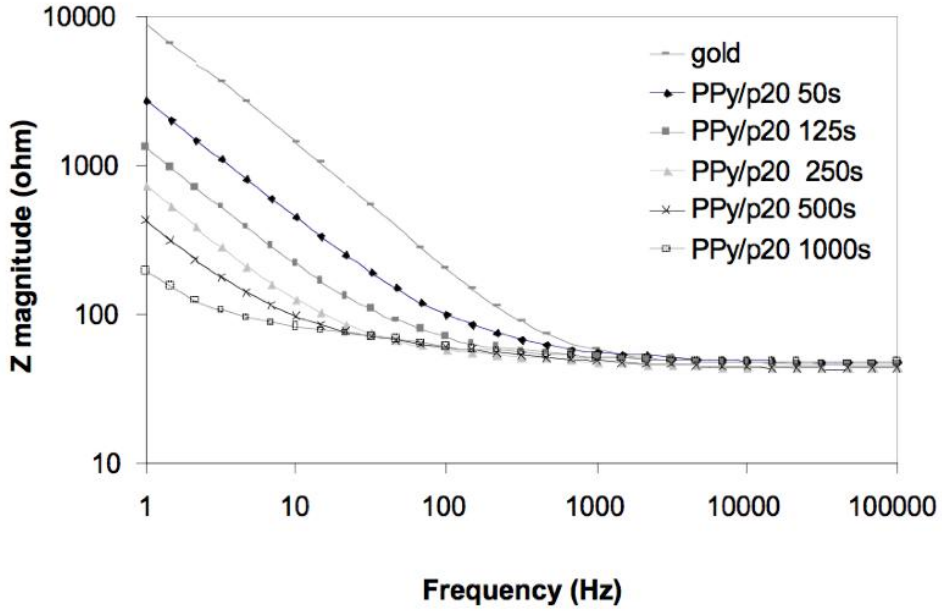

Figure 2-2 Bode plot of impedance spectroscopy of PPy/p20 coatings on gold coverslips deposited at different charge densities (current density of 36 μA/cm^2 for 50, 125, 250, 500, and 1000 s).

Figure 2-2 shows the impedance spectrum of a gold-coated coverslip and five PPy/p20 coatings of different thicknesses on gold coverslips. As can be seen from the graph, impedance drops as the coating time increases, this is probably due to the increase in surface area as the coating gets thicker and rougher. Figure 2-3 compares the impedance behavior of the three different bioactive coatings on gold coverslips using a nyquist plot, a graph of the imaginary versus real parts of the impedance at different frequencies. In order to further analyze the differences in impedance behavior based on coating thickness and dopant choice, equivalent

circuit models were built using the Gamry software Electrochemical Analyst. For the PPy/p20 coating, a simple model of solution resistance (Ru) in series with a Constant Phase Element (CPE) produced a good fit (Figure 2-4). The same model was used to describe gold electrode in (Cui and Martin 2003). Capacitors in electrochemical impedance spectroscopy (EIS) experiments often do not behave ideally. Instead they act like a CPE (MacDonald 1987). The impedance of a CPE has the form of $Z = (1/Y_0)(j\omega)^{-n}$. Y_0 is a constant that describes the admittance at ω = 1 rad/s. When n = 1, Y_0 is equal to capacitance C. The exponent n is an empirical constant with a value less than one for a rough electrode. When n is close to 1, as in the case of our model, Y_0 approximates the

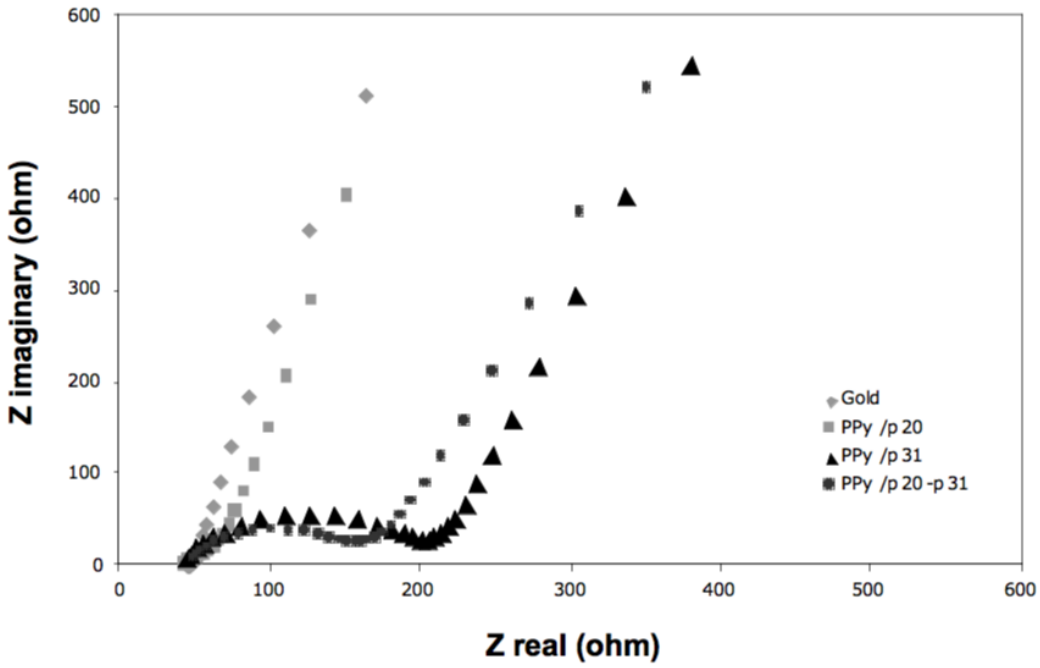

Figure 2-3 Nyquist plots of impedance spectroscopy comparing several PPy/peptide surfaces with a bare gold coverslip.

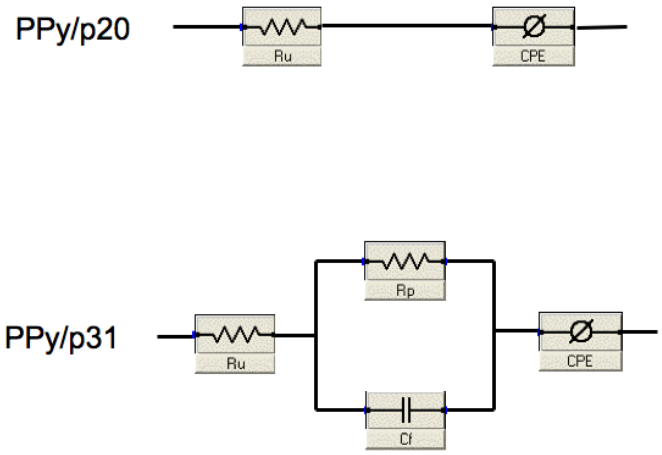

Figure 2-4 Equivalent circuit model of the PPy/p20 and PPy/p31 films. Ru = solution resistance, CPE = constant phase element, Rp and Cf in parallel = Randles element, Rp = polarization resistance and Cf = double layer capacitance.

capacitance of the electrode. By definition, the capacitance is proportional to the surface area of the electrode; therefore Y_0 can be used to compare the surface area. The calculated circuit parameters of PPy/p20 coating deposited at different charge density is listed in Table 2-1A. It can be clearly seen that the solution resistance (Ru) value is independent of the samples, as expected since the solution resistance should be constant under the same electrochemical set up. The Y_0 value increases as the film grows, which is an indication of increasing effective surface area for interfacial charge transport. As addressed in (Cui, Hetke et al. 2001; Cui and Martin 2003), the effective surface area is length scale dependent. At very low frequencies such as 1 rad/s at which Y_0 is defined, the appropriate characteristic length scale to measure the surface area is the size of the hydrated ions.

When PPy is doped with p31, the previous model does not fit the data. The interfacial charge transport may be more complicated, and a less conductive component seems to exist that impede the process. The nyquist plot revealed a semicircle in the higher frequency region,

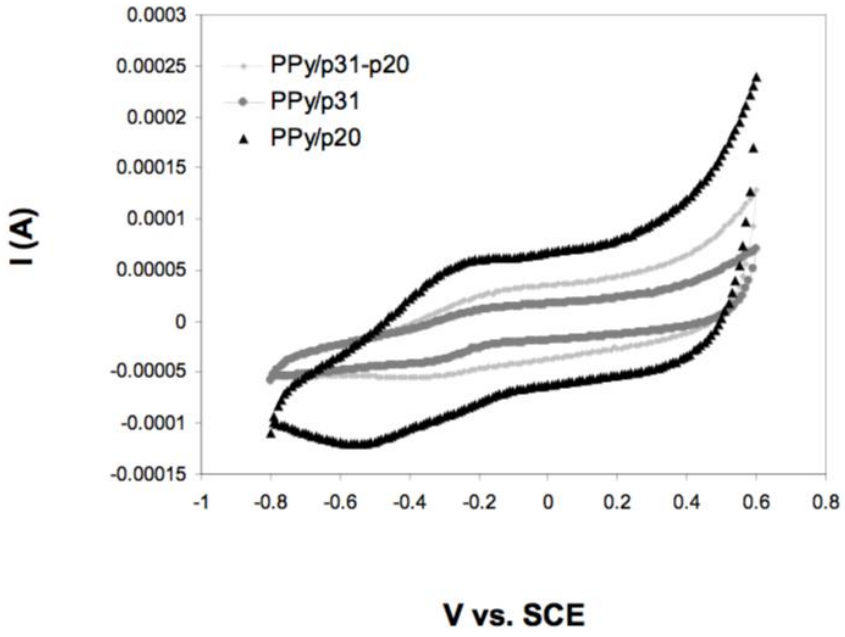

Figure 2-5 Cyclic voltammetry scans of three different PPy/peptide surfaces. The scan rate is 50 mV/s.

suggesting that a Randles element, consisting of a polarizing resistance (Rp) and double layer capacitance (Cf) in parallel, may be appropriate. Adding a Randles element in the PPy/p20 model in series indeed produced good fit for PPy/p31 coatings (model shown in Figure 2-4). Table 2-1B lists the calculated circuit element values for the PPy/p31 coatings. Again, the solution resistance value is independent of the film deposition charges, and is even similar to the value obtained from the PPy/p20 circuit. This further validates both circuit models.

Table 2-1 Calculated circuit elements for PPy-p20 (A) and PPy- p31 (B)

A

PPy/p20 Coating Charge Density	Ru (ohms)	Y_0 (uS)
0 (bare gold)	46	23
1.8 mC/cm^2	50	89
4.5 mC/cm^2	49	188
9 mC/cm^2	46	342
17.9 mC/cm^2	47	679
35.7 mc/cm^2	50	1991

B

PPy/p31 Coating Charge Density	Ru (ohms)	Y_0 (µS)	Rp (ohms)	Cf (nF)
1.8 mC/cm^2	50	459	104	233
4.5 mC/cm^2	50	334	135	269
9 mC/cm^2	50	209	66	571
17.9 mC/cm^2	40	155	26	1924
35.7 mc/cm^2	53	78	23	7499

Table 2-2 Charge capacity as a function of deposition charge

Charge Density	PPy/p31	PPy/p31-p20	PPy/p20
1.8 mC/cm^2	422 µC	482 µC	614 µC
4.5 mC/cm^2	374 µC	457 µC	621 µC
9 mC/cm^2	417 µC	458 µC	621 µC
17.9 mC/cm^2	387 µC	545 µC	1089 µC
35.7 mc/cm^2	443 µC	763 µC	1528 µC

A second assessment of the electronic properties of the PPy coatings is through cyclic voltammetry (CV). In this procedure the potential is swept through a defined range and the resulting current is recorded. Figure 2-5 shows the CV curves for PPy/p20, PPy/p31, and PPy/p31-p20.

The charge capacity, Q, can be obtained from integrating the current passed for half a cycle. The charge capacities for different thickness films with different dopants can be found in

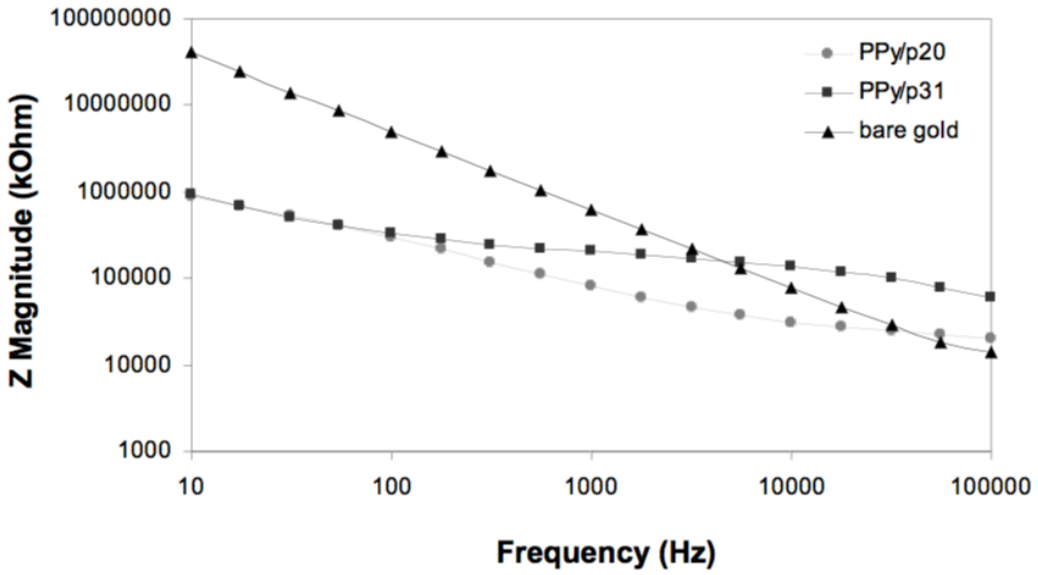

Figure 2-6 Impedance spectra of coated and uncoated Michigan probe recording electrodes.

Table 2-2. Note that for PPy/p20 coatings, the charge capacity increases as the deposition charge increases, the same trend found in Y_0. This is not surprising given the fact that charge capacity is related to the electrode capacitance.

To test the electrical property of the coatings on actual neural electrodes, PPy/p31 and PPy/p20 coatings were grown galvanostatically on the electrodes of Michigan Probes. Figure 2--6 shows the impedance spectrum of a bare gold electrode, an electrode with a PPy/p31 coating, and an electrode with a PPy/p20 coating. At the biological relevant frequency of 1 kHz(Kuffler 1976), both PPy/p31 and PPy/p20 showed lower impedance than the bare gold electrode. Lower impedance is beneficial in recording minute extracellular neural signal. In this respect, PPy/p20 showed superior electrical property than PPy/p31.

2.4.2 Bioactivity Test

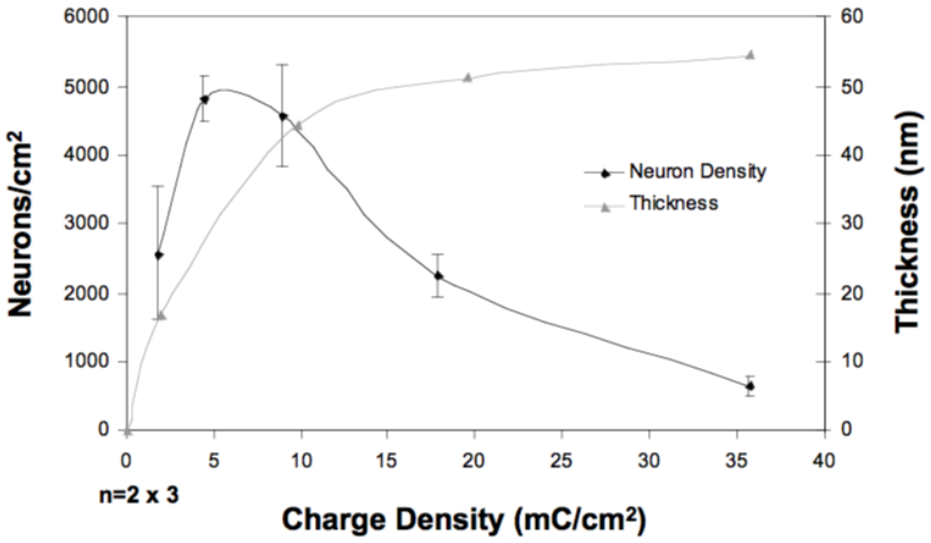

Figure 2-7 Neuron density as a function of charge density. Thickness increased with increasing charge density as seen on the Y_2 axis. A significantly higher neuron density was found on surfaces with charge density between 4.5 and 9 mC/cm^2 ($p < .02$).

As indicated earlier, laminin is a multifunctional ECM protein that associates with several cell types. As such, different peptide sequences within Laminin are responsible for its different functions (Graf, Iwamoto et al. 1987; Liesi, Narvanen et al. 1989). Research has demonstrated that p31 is an effective dopant for PPy and produces a rough surface with low impedance that enhances the attachment of neuroblastoma cells relative to PPy/CH3COO$^-$ films, as well as promoting neuronal binding *in vivo*(Cui, Lee et al. 2001; Cui, Wiler et al. 2003). One

of our goals was to extend this research by using primary neurons instead of neuroblastoma or PC-12 cells, and a defined culture media to better isolate surface effects. A second goal was to investigate other short peptide fragments that could be utilized as dopants and have positive

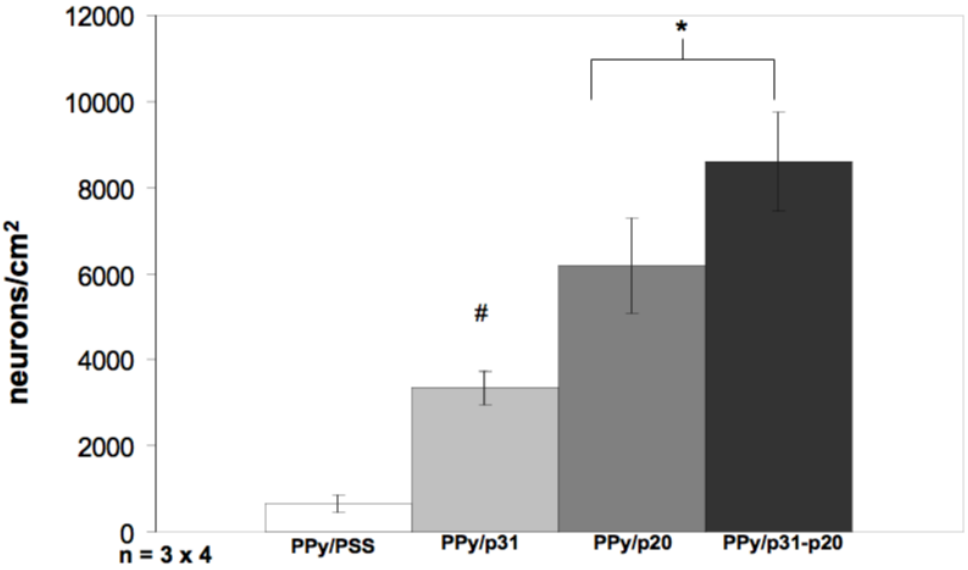

Figure 2-8 Neuron density on PPy surfaces. (#, $p < .002$) (*, $p < .03$).

effects on neuronal growth. Given the previous literature showing that p20 plays an important role in neurite extension (Liesi, Narvanen et al. 1989), it was an ideal candidate for investigation.

Primary neurons obtained from the cortices of E18 SD rats were cultured in a defined media containing Neurobasal, B27, glutamine, and glutamate. Early observations of primary neuronal growth on relatively thick PPy/p31 surfaces (thickness was set with charge density of 17.9 mC/cm^2) showed a very heterogeneous cell density. Assuming that film thickness variation within a relatively thick sample could account for differences in cell growth, films with different thickness as controlled by total charge density and verified by ellipsometry, were synthesized as

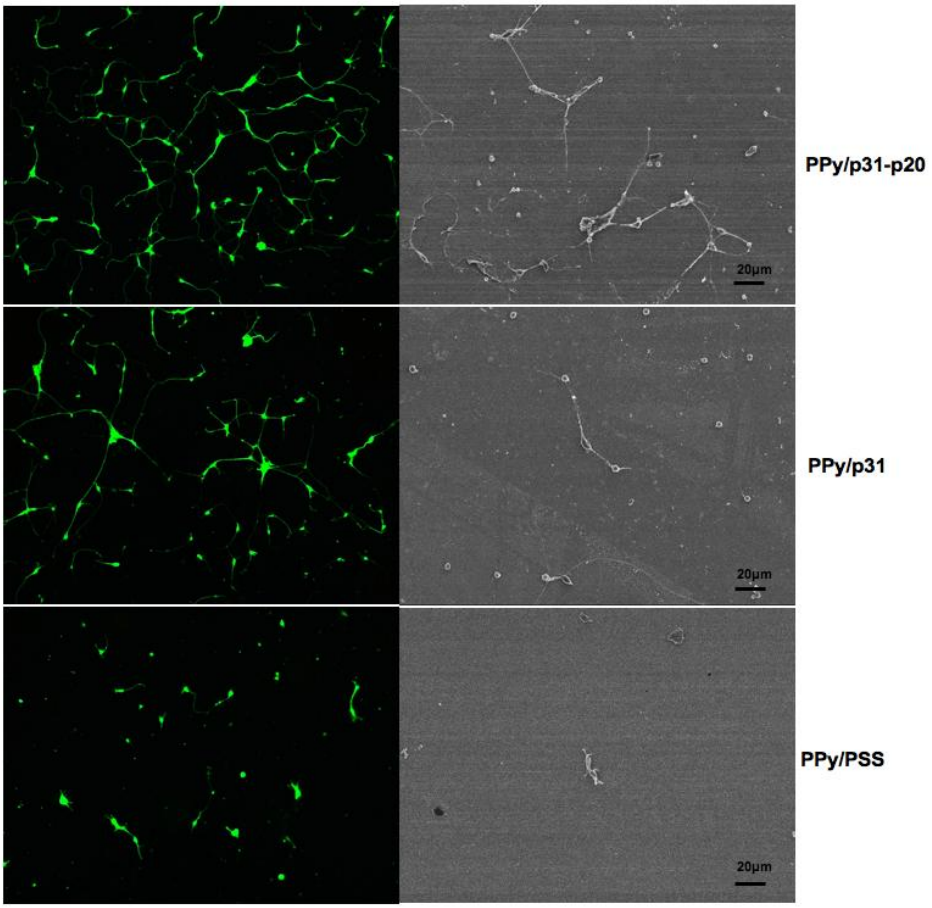

Figure 2-9 Immunfluorescent and SEM images of neurons on conductive substrates showing increased neuronal growth on biological dopants (green is β-III tubulin staining).

substrates for cell growth. Films with charge density of 1.8, 4.5, 9.0, 17.9, and 35.7 mC/cm^2 were synthesized. Figure 2-7 shows the resulting thickness versus charge density curve. For the PPy/p31 coated coverslips, optimal cell growth (highest cell density) tended to occur on thinner, rather than thicker samples. Surfaces having charge densities between 4.5 and 9.0 mC/cm^2 were found to have a significantly higher average cell density than for surfaces with charge density of 17.9 mC/cm^2 and higher ($p < .02$), see figure 2-7. Coatings with charge density of 4.5 mC/cm^2 are therefore used as the optimized surface for the bioactivity test.

PPy doped with PSS was used as the control PPy surfaces and the positive control was laminin adsorbed surfaces. The bioactive surfaces that we tested were PPy/p31, PPy/p20, and PPy/p31-p20. Significantly higher cell densities were found using Bonferroni post-hoc analysis on all bioactive surfaces relative to the PPy/PSS surface. Furthermore, the PPy/p20 and

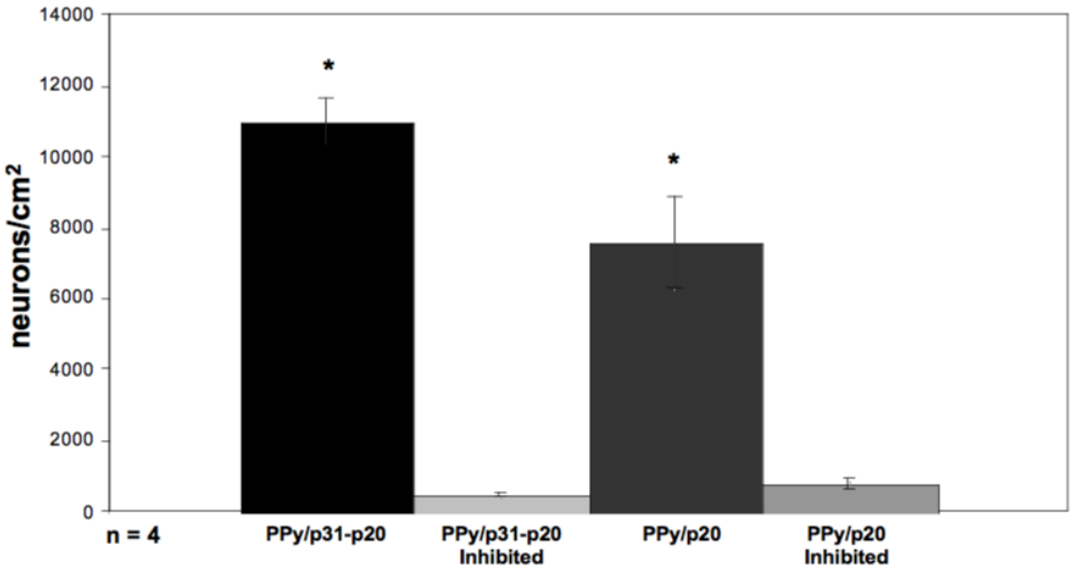

Figure 2-10 Neuron density with and without the presence of soluble peptide on PPy/peptide surfaces ($p < .001$).

PPy/p31-p20 showed significantly higher neuron densities than the PPy/p31 ($p < .03$). Figure 2-8 shows a graph of cell density versus peptide after 3 DIV. Neuron density on the laminin control was found to be approximately 3 fold greater than the best PPy/peptide surface. Cellular growth can be qualitatively appreciated by referring to figure 2-9 which shows fluorescent and SEM images of neurons on PPy/p31-p20, PPy/p31, and PPy/PSS after 3 DIV.

During electropolymerization, the choice of the dopant can have a significant affect on the final morphology of the PPy film (Cui, Lee et al. 2001; Cui, Wiler et al. 2003). Since

different peptides were used as the dopants to create the different surfaces, it was important to verify that the differences in cell density were due specifically to the immobilized peptide and not an effect of a secondary consequence such as differences in film morphology, i.e. roughness. This was accomplished through inhibition studies. In the inhibition studies, prior to plating the

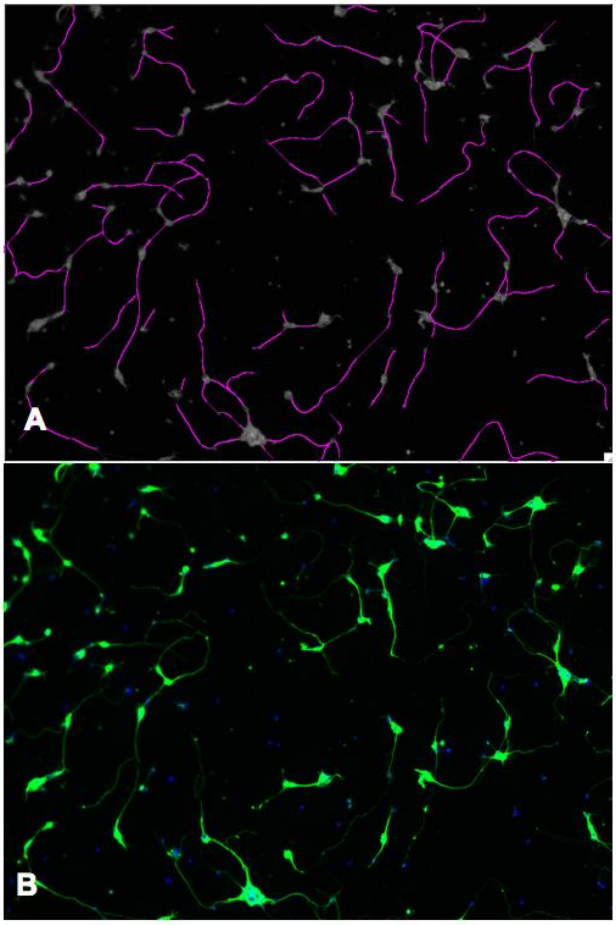

Figure 2-11 Tracing results for neurite length measurement using the ImageJ plug-in NeuronJ.

cells on the surface, p20 was dissolved into the cell suspension (0.2 mM) and then added into the culture plates containing PPy/p20 coated coverslips. Similarly p31 was added into the plates containing PPy/p31 surfaces and 1:1 mixture of p20 and p31 was added into the plates of PPy/p20-p31. The rational for these inhibition studies is that if the cell attachment is being mediated by the surface immobilized peptides, then cell attachment should be inhibited when

peptide receptors are blocked by the corresponding peptides in soluble form. Figure 2-10 shows the cell density on PPy/p20 and PPy/p20-p31 surfaces with and without soluble peptide after 3 DIV. In both cases a near total inhibition of cell growth was observed ($p < .001$). As a control, cells with solubilized peptide in suspension were plated on polylysine coated TCPS dishes and no significant difference in cell growth was observed (not shown). This result clearly indicates that cell attachment is being mediated through the peptides immobilized in the polypyrrole surface.

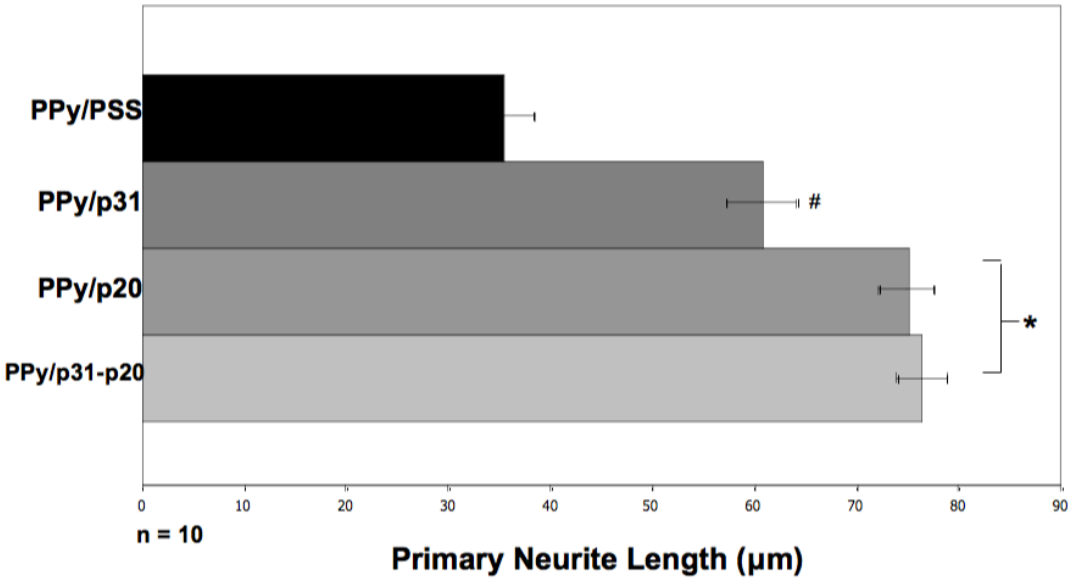

Figure 2-12 Average primary neuron length on the different PPy surfaces. All bioactive surfaces had significantly longer primary neurites than the non-bioactive PPy/PSS ($p < .001$) Surfaces with immobilized p20 had significantly longer primary neurites than surfaces without ($p < .003$).

Finally, primary neurite (axon) length was examined (figure 2-11) to see if the different surfaces would affect neurite outgrowth. Neurons on all three bioactive surfaces had significantly longer axons than those on the non-bioactive surface ($p < .001$). In Figure 2-12, the differential

effect on primary neurite outgrowth found among the bioactive surfaces is shown. Surfaces that have p20 immobilized (both the PPy/p20 and PPy/p31-p20) had neurons with significantly longer primary neurites than neurons on the PPy/p31surfaces after 3 DIV ($p < .005$). As stated above, previous literature has shown that p20 plays an important role in promoting neurite outgrowth while p31 only has effect on cell attachment (Liesi, Narvanen et al. 1989). The results of this study show similar findings indicating the bioactivity of the peptides were well preserved in the PPy film.

While one of the main objectives of this study was to optimize neuronal growth and

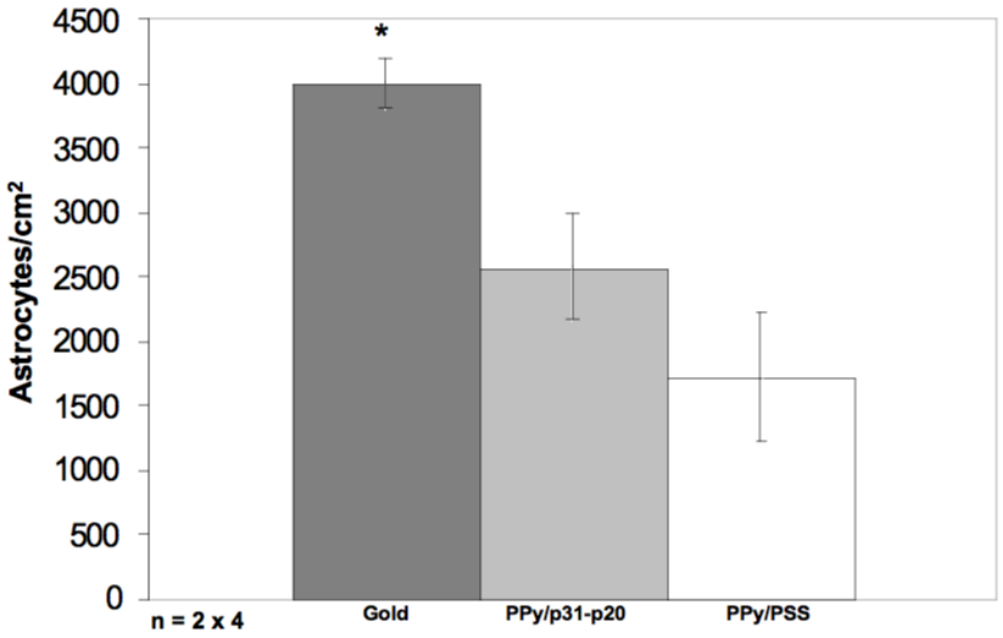

Figure 2-13 Astrocyte density on gold and bioactive and non-bioactive PPy surfaces. A significantly higher number of astrocytes was found on gold coverslips 3 days after plating ($p < .01$).

attachment on a material that could be used to modify brain recording electrodes, it was recognized that the brain consists not only of neurons but other cell types as well and the immobilized peptides could have a deleterious effect if it were to promote other cellular in-

growth, such as that of astrocytes. To account for this possible phenomenon, the same surfaces, as well as bare gold coverslips, were used as a substrate for astrocyte culture. A significantly higher number ($p < .01$) of astrocytes were found on the gold surfaces than on any PPy surface (figure 2-13). There was a trend towards PPy/p31 having significantly higher astrocyte attachment than PPy/p20. If a less stringent post-hoc analysis than Bonferroni's correction is used, such as a least-square difference method, then $p < .05$. While it would be unsafe to draw conclusions from this, the result highlights the need for further study of the effect of biomolecules on astrocyte attachment to PPy surfaces.

2.5 DISCUSSION

In the field of biomaterials, the design of bioactive surfaces is of particular interest since biological systems interact with biomaterials via the interface. A variety of surface modification and immobilization methods have been developed to create surfaces having bioactive ligands to interact with biomolecules and cells. Conducting polymer materials bring an extra dimension to surface control by adding electrical conductivity and electrochemical switchability. The electrochemical switchability means that the surface characteristics can be switched from hydrophobic to hydrophilic, from conductive to resistive, by simply applying electrical potential stimuli to trigger the redox reaction of the polymer. This feature makes conducting polymers a promising candidate for constructing dynamic biosurfaces for *in vitro* study of cell behavior. The conductivity feature is especially attractive for electrically excitable cells such as neurons and cardiac cells and biosensors that use electrical signal detection. Many aspects of conducting polymers, from their synthesis and especially their customizability, to their electrical properties,

make them ideal candidates for neural interface surface modification. That is, they can be synthesized directly at the electrode site, they can be customized through dopant selection to promote the growth of specific cell types (Cui, Lee et al. 2001), and their unique electrical properties allow them to mediate the difference between the ionically conductive brain and electrically conductive electrodes (Cui, Lee et al. 2001; Cui, Wiler et al. 2003).

In this paper we have focused on optimizing PPy surfaces for *in vitro* growth of primary neurons. We have demonstrated a PPy/peptide surface that actively participates in neuron attachment and neurite extension. Such a surface can be used to study the effect of surface electrical stimulation on primary neurons, which otherwise won't attach and grow well on the non bioactive conductive polymer surface. This surface design can also be applied on the neural electrode for improving the long-term structural and functional connection with the host neurons.

As suggested above, the first requirement of these surfaces is that they should be conductive. The conductivity of PPy/p31 and PPy/p20 surfaces was confirmed through electrochemical impedance spectroscopy. PPy/p20 surfaces showed consistently lower impedance values than PPy/p31 surfaces. This would be particularly important for extracellular recording applications where the neural signals are on the microvolt range.

One of the most interesting results of the EIS and CV experiments is the observation that they may provide a means to assess the nature of the mixture of the two peptides. Close examination of both the CV sweeps and the nyquist plot of the impedance, along with analysis of the charge capacity, reveals that the PPy surface doped with the peptide mixture, PPy/p31-p20, always shows intermediate characteristics between PPy/p20 and PPy/p31. This indicates that when PPy was grown out of the mixed solution of p20 and p31, both peptides were truly incorporated and the final coating inherits the electrochemical characteristics of both peptides.

This is especially exciting given that there are few analytical means to asses the amounts of the two individual peptides in the coatings.

In bioactivity studies, PPy film deposition charge was found to have a significant effect on neuronal cell density. The underlying cause of this difference has yet to be fully elucidated, but several hypotheses exist. While quantitative analysis of surface roughness, such as AFM has yet to be performed, qualitative surface analysis by SEM has shown a different surface morphology between thin and thick samples. The EIS and CV also indirectly demonstrated a surface area increase (at the length scale of ions) as the film grows thicker. Our results show that the thinner, qualitatively smoother surfaces, support a higher cell density. Confounding factors, however, make it impossible to conclude that surface roughness was responsible for the differences. A likely alternative hypothesis is that during polymerization of the films, there is a mass transfer problem of peptides to the surface. At the start of the polymerization the solution contains a homogenous mix of monomer and dopant (peptide) which are deposited on the surface, but due to the larger size of the dopant, local concentrations fall, and as the films thicken, less bioactive dopant is presented at the surface thereby rendering it useless. The plateau of the film thickness versus deposition charge curve showed a slow down of film growth and suggested the insufficient dopant supply as deposition time increases. Future studies examining surface roughness and peptide concentration in a quantitative manner along with a modification to the polymerization process should shed more light on the process.

The presence as well as the choice of bioactive peptides in the surface was found to have a significant effect on neuron growth and neurite extension. The non-bioactive surface used as a control in these experiments was PPy/PSS. The bioactive surfaces that we measured were PPy/p31, PPy/p20, and PPy/p31-p20. The results were consistent with what one would expect

given previous literature on the nature of the bioactive species p20 and p31 (Graf, Iwamoto et al. 1987; Liesi, Narvanen et al. 1989). The p20 surface showed a significantly higher number of neurons than the p31 surfaces and axons were significantly longer. Furthermore, through inhibition studies, we demonstrated that the effective difference seen in neuron density was in fact due to the immobilized peptide and not some secondary factor such as morphology differences in the film due to different dopants.

The nervous system consists not only of neurons but also other cells such as astrocytes and microglia; the bioactivity of the surfaces could be viewed negatively if they bind greater numbers of the other cell types also. Our research demonstrates that PPy surfaces in general support adhesion of fewer astrocytes than the common electrode material gold. Further work is necessary to conclude whether one specific bioactive dopant is better than others (that is, supports less astrocyte adhesion). Again, previous research suggests p31 plays a broader role in cell adhesion than p20, whose activities seem more specific to neurite out growth(Graf, Iwamoto et al. 1987; Liesi, Narvanen et al. 1989). We hypothesize that a PPy/p20 surface will support fewer astrocytes than a PPy/p31. If this hypothesis were supported then it would point to PPy/p20 being an optimal surface for applications where direct neuron attachment and intimate connections are vital to the desired function. The results in this paper however showed no significant difference between any of the polypyrrole surfaces (including the non-bioactive PPy/PSS) when astrocytes are cultured on them. Nevertheless, the experiments were done in a serum based media; therefore the difference in surface composition could be masked by the adsorbed serum proteins. It has been shown that when cultured in serum containing media, astrocytes are relatively insensitive to differences in surface chemistries as long as the proteins necessary for cellular attachment are capable of adsorbing to the material to some extent(Biran,

Noble et al. 1999). Ongoing work is being conducted to establish a serum free astrocyte culture system to better isolate the effects of surface biomolecules.

This work compares the efficacy of two different laminin fragments as dopants in conducting polymer surfaces. The electrical as well as the biological properties of the resulting surfaces are reported. It is found that polypyrrole surfaces containing bioactive peptides are better at supporting neuronal growth and neurite extension than non-bioactive surfaces. Furthermore, it is shown that the choice of bioactive molecule has a significant effect on both the electrical and biological properties of the resulting surface. Polypyrrole surfaces using p20 as the dopant were found to support a higher density of neurons and promote longer axon growth than surfaces doped with p31. A surface with the combination of the two laminin fragment dopants was discovered to support a higher neuronal density than surfaces containing either of the dopants individually. Finally, it was observed that astrocytes were less prone to attachment on polypyrrole surfaces compared to the common electrode material gold. These surfaces exhibit low electrical impedance and high charge capacity relative to conventional conductive substrates, such as metals. Such a material has the potential to make a positive impact on the field of neural tissue engineering and neural prosthetic devices.

3.0 CONTROLLED DRUG RELEASE FROM POLYMER-COATED ELECTRODES FOR RAPID MODULATION OF LOCAL NEURAL ACTIVITY

3.1 ABSTRACT

We present a method for spatially targeted modulation of neuronal activity with controlled release of neurochemicals from the conducting polymer polypyrrole (PPy). The PPy films are coated on in vitro recording array electrodes through individually controlled electro-chemical deposition. The recording capabilities of PPy electrodes are quantified and shown to be equivalent to platinum black electrodes. Release of charged molecules including fluorescent dyes or AMPA glutamate receptor antagonist CNQX is achieved by delivery of a brief voltage pulse. Inhibition of evoked synaptic currents in neurons within 200 μm of the electrode is observed within 100 ms of the release of CNQX, but not control ions. In neuronal networks grown on CNQX-PPy-coated multi-electrode arrays, spiking activity of neurons recorded with the releasing electrode is shown to transiently disappear following the release stimulus and to be local to that electrode. This method is applicable to many neuro-modulatory chemicals and various recording electrodes including implantable chronic arrays. It is an inexpensive technique capable of precisely controlled chemical perturbation of target neurons without implantation of any devices secondary to the recording array. With the use of multielectrode arrays and different

releasing molecules, it is feasible to achieve sophisticated patterned chemical stimulation for the modulation of neuronal circuits in vitro and in vivo.

3.2 INTRODUCTION

Fundamental brain functions such as cognition, learning, and memory are carried out by the coordinated activity of many neurons that form intricate circuits(Abeles 1991; Salinas and Sejnowski 2001). Technological advances in multielectrode array development and recording now permit the study of this ensemble activity both *in vitro* and *in vivo*. Combined with pharmacological perturbations that specifically alter the dynamics of network activity, the role of different excitatory and inhibitory mechanism in neural ensemble behavior can be elucidated. Conventionally, global perfusion, systematic administration and intra-cortical injection have been the most commonly used methods of drug delivery *in vitro* and *in vivo* for studies that require low spatial and temporal resolution. Alternatively, focal chemical perturbations of individual cells or regions of the brain have become an important approach in investigating mechanisms of neural processing and intervening disease conditions (Kandler, Katz et al. 1998; Maalouf, Dykes et al. 1998; Lesniak, Upadhyay et al. 2005). Current techniques which provide active control over the drug delivery process include microiontophoresis(Hicks 1984; Gerhardt and Palmer 1987), pressure injection(Gerhardt and Palmer 1987; Barker, Billups et al. 2008), and the photolysis of caged compounds(Ellis-Davies 2007). These methods are generally limited to a few target sites. Recently efforts have been made to fabricate microelectrodes with fluid channels(Kaji, Nishizawa et al. 2003; Mourzina, Kaliaguine et al. 2006). This integration

eliminates the requirement of extra positioning devices and improves the spatial resolution of local delivery. However, the addition of channels, pumps and valves for active delivery control complicates device fabrication, and can lead to lower yield, higher cost and higher failure rate. Furthermore, the size of the device will be increased, which is undesired for minimizing insertion injury and host tissue reaction for *in vivo* applications.

Described here is a different approach to drug delivery with high spatiotemporal control through the incorporation and release of pharmacological agents from conducting polymer films deposited directly on recording electrodes. Conductive polymers require ionic dopants in order to conduct electric currents(Wallace 1997). Previous work with large surface-area electrodes has shown that dopant species can be exchanged with solution ions in resonse to electrical stimulation of the conducting polymer films(Miller, Lau et al. 1983; Zinger and Miller 1984; Kontturi, Pentti et al. 1998; George, LaVan et al. 2006; Wadhwa, Lagenaur et al. 2006). Based on these drug releasing properties of conducting polymers, we display a new system of individually addressable polypyrrole (PPy) films capable of targeted delivery of small amount of neurochemicals in real time. The system can be easily integrated into pre-existing MEAs without complex microfabrication or the need to implant extra hardware for recording.

AP5 and CNQX inhibit glutamatergic synaptic transmission at the NMDA and non-NMDA receptors, respectively(Alford and Grillner 1990). In this study, CNQX and AP5 are shown to retain their native bioactivity when released from the conducting polymer PPy. Proof of the concept of real-time chemical perturbation from prefabricated MEAs, as well as estimation of the necessary parameters, is proffered through the incorporation and release of the easily detectable fluorescein molecule. PPy-CNQX films are synthesized on the electrodes of MEAs and the resulting impedance and signal-to-noise ratio are shown to be comparable to standard

platinum black electrodes. Neuronal networks are cultivated on MEAs whose electrodes have been modified with PPy-CNQX and PPy-C (C = Control and indicates the ions incorporated into the PPy films synthesized in PBS, the majority of which are Cl^- and PO_4^-). Individual neurons are patch-clamped at various distances from releasing electrodes and transient inhibition is demonstrated to be a function of CNQX and its diffusion following release. Finally, the local-network consequences of PPy-mediated CNQX release are shown through extracellular recordings from the overlying network.

3.3 METHODS

3.3.1 Polypyrrole Synthesis and Release

Individual MED64 arrays (Panasonic) were exposed to pure oxygen plasma for 8 seconds and then stored in sterile PBS until electrochemical deposition. Pyrrole (Sigma 131709) was vacuum distilled and stored frozen. Dopants for this study are CNQX disodium salt (Sigma C239), AP5 (Sigma A5282), fluorescein disodium salt (need catalog info), and the ions found in PBS (Sigma P7059). Films were synthesized directly on the electrodes of the MED array (2.5×10^{-5} cm^2). The monomer solutions consisted of 0.5 M Py and either 7.5 mg/ml CNQX, 10 mM Fluorescein, or the ions contained in PBS. A Platinum foil counter electrode and a Ag/AgCl reference electrode were used for the electropolymerization. For PPy-CNQX and PPy-Fluorescein coatings, 800 mV was applied for 100 s. For PPy-PBS coatings, 700 mV was applied for 20 s. To determine appropriate release parameters, the duration of the release pulse was varied from 200 ms to 4 seconds. The magnitude of the voltage was varied from 1.0-5.0 mV.

The Conductor software (MED64, Panasonic) was programmed to control all other hardware including a 16-bit EM-CCD camera (Cascade 512B; Roper Scientific) and an illumination source (Lambda DG4, Sutter Instruments). The camera attached to a PC took images at 10 Hz and the exposure time was set to 100 ms.

3.3.2 Neuronal culture and electrophysiology

PPy coating synthesis was done on the day prior to cell culture. Under laminar flow, the chambers were washed once with ultrapure H_20, then UV exposed for 30 min for sterilization. Following sterilization, the chambers were washed five times with ultrapure H_20 to remove any remaining monomer solution. The surfaces of the chips were then treated according to the protocol found in (Wagenaar 2005). Briefly, 0.05% polyethyleneimine (PEI, Sigma P3143) was incubated at room temperature for 1 h followed by 4 washes with ultrapure H_20. A solution containing 20 μg/ml of laminin (Sigma L2020) in DMEM (Invitrogen 11960) was added after the final wash and incubated overnight. On the day of culture the MEAS were removed from the incubator and washed 5 times with ultrapure H_20 ,Following the final wash, all of the solution was removed from the chamber and the surface was allowed to dry until cells were plated.

Low-density cultures of dissociated embryonic rat hippocampal neurons were prepared as described previously(Lau and Bi 2005). Hippocampi were removed from embryonic day 18–20 (E18–20) rats and treated with trypsin for 15 min at 37°C, followed by washing and gentle trituration. The 2-4 μl drops of dissociated cells were plated at a density of 15,000 - 20,000 cells/ml on PEI and laminin treated MED64 arrays. The plating medium was DMEM

(BioWhittaker 12-614f w/o HEPES) supplemented with 2% heat-inactivated fetal bovine serum (Hyclone), 8% bovine calf serum, 10% Ham's F12 with glutamine (BioWhittaker), 25 mM HEPES buffer, B27, and 50 U/ml penicillin–streptomycin (Sigma). Twenty-four hours after plating, the culture medium was changed to the above medium containing 20 mM KCl. Cytosine arabinoside (Sigma) was added to the culture dish (final concentration, 5 μM) around 7–10 DIV to prevent overgrowth of glial cells. Both glial and neuronal cell types are present under these culture conditions. Cells were used for electrophysiological recordings after 8–14 d in culture. For high-density cultures the protocol for culture was derived from (Wagenaar 2005). As a source of cortical neurons, E18 cortex pairs were purchased from Brainbits LLc. (cx1) and the supplied dissociation protocol was followed.

Extracellular recordings and whole-cell perforated-patch recordings from one to two hippocampal neurons were performed simultaneously, using amphotericin B (Sigma) for perforation. For perforated-patch recordings, the micropipettes were made from borosilicate glass capillaries (Kimax), with a resistance in the range of 2–4 MΩ. The pipettes were tip-filled with internal solution and then backfilled with internal solution containing amphotericin B. The pipette solution contained 136.5 mM potassium gluconate, 17.5 mM KCl, 9 mM NaCl, 1 mM MgCl2, 10 mM Hepes, 0.2 mM EGTA, and 200 μg/ml amphotericin B (pH 7.3). The external bath solution was a Hepes-buffered saline (HBS) containing 150 mM NaCl, 3 mM KCl, 3 mM $CaCl_2$, 2 mM $MgCl_2$, 10 mM Hepes, and 5 mM glucose (pH 7.3). The bath was intermittently perfused (perfusion interfered with extracellular recordings so the network was perfused between trials) with fresh recording medium at a slow rate throughout the recording, and all experiments were performed at room temperature. The neurons were visualized by phase-contrast microscopy with an inverted microscope (Leica DMIRB). Recordings were performed with one or two patch

clamp amplifiers (Axopatch 200B; Axon Instruments). Signals filtered at 2 kHz were acquired at a sampling rate of 11.1 kHz by using a 16-bit digitizing board (DigiData 3200, Axon Instruments) and processed with the PCLAMP software (Axon Instruments). For assaying network structure, each electrode was stimulated with by 1V for 100 μs, and the responses from the neurons were recorded.

3.3.3 Data analysis

The signal to noise ratio for an electrode was computed in the following way:

$$snr = 20 * \log_{10}\left(\frac{rms(waveform)}{rms(rawdata)}\right)^2$$

where *waveform* is the peak-to-peak heights of the extracted waveforms while *rawdata* is simply the entire recording from which the waveforms were extracted. A *t* statistic was used to compare the log of signal to noise ratios for two groups of electrodes, platinum and conducting polymer.

To control for short-term synaptic effects, control trials with no release stimuli were performed. The short-term adjustment factor was the ratio of the peak current deflection after neural stimulation and the baseline peak current deflection. Each current trace was then multiplied by the adjustment ratio arising from a neural stimulation at the corresponding time point.

To assess the role of diffusion in mediating the effect of release, a quantity *k* was derived from Fick's diffusion equation

$$c(x,t) = \frac{Q}{2\sqrt{\pi D t}} \exp\left(-\frac{x^2}{4Dt}\right)$$

where *c* is concentration as a function of distance (*x*) and time (*t*), Q is the amount of substance released at a point source, and D is diffusion constant in water (10^{-5} cm^2/s). In the case of our experiments, the amount released is unknown. *k* was derived by factoring *Q* from the above relationship.

$$c(k) = Q * k$$

$$k = \frac{1}{2\sqrt{\pi D t}} \exp\left(-\frac{x^2}{4Dt}\right)$$

The degree of inhibition was plotted as a function of *k* and a linear regression was performed for each release trial. A meta-analysis of the p-values from the independent trials was performed using Fisher's method for combining probabilities (Fisher 1948):

$$X_{2k}^2 = -2\sum_{i=1}^{k} \log_e(p_i)$$

3.4 RESULTS

3.4.1 Bioactivity of released CNQX and AP5

CNQX (6-cyano-7-nitroquinoxaline-2,3-dione) and AP5 (2-amino-5-phosphonopentanoate) are incorporated into the polymer as dopants during electrochemical synthesis and balance the *n* positive charges that accumulate on the backbone during chain growth (figure 3-1a) PPy undergos a reversible redox reaction in response to electrical

stimulation whereby discharging and recharging of the backbone is accompanied by the movement of hydrated ions (figure 3-1b) CNQX and AP5 released from macroelectrodes retained their native

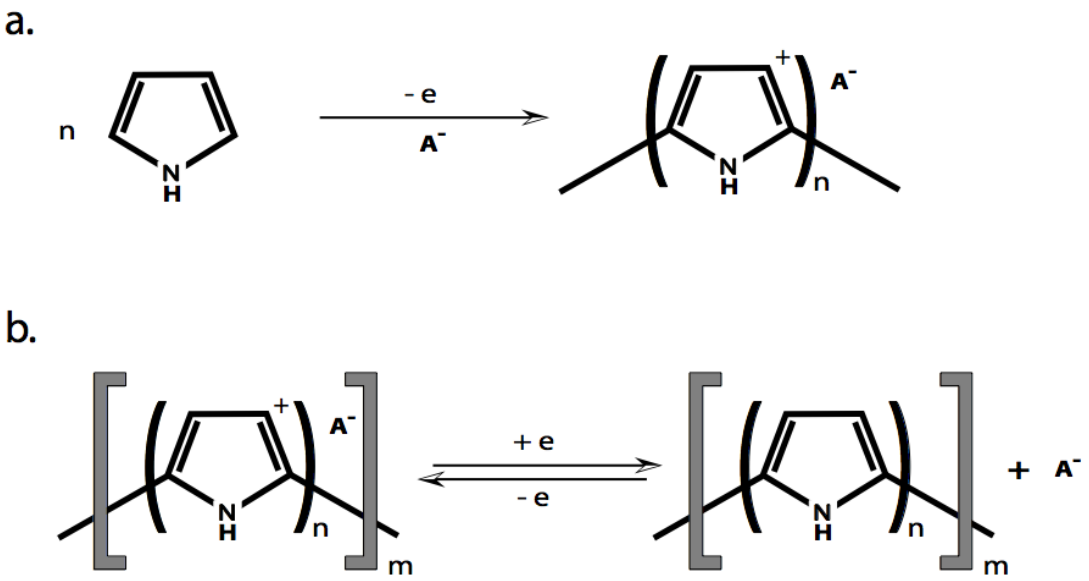

Figure 3-1 a) synthesis reaction for PPy and b) anionic release reaction for PPy

bioactivity when applied to the bath of cultured neurons (figure 3-2). We hypothesized that on the smaller scale of release from microelectrodes in the MEA, the effect of CNQX would be easier to detect than AP5 since much of the fast, excitatory transmission leading to spiking is mediated by the AMPA receptor (McBain, Boden et al. 1988). Therefore all subsequent experiments focus on CNQX release.

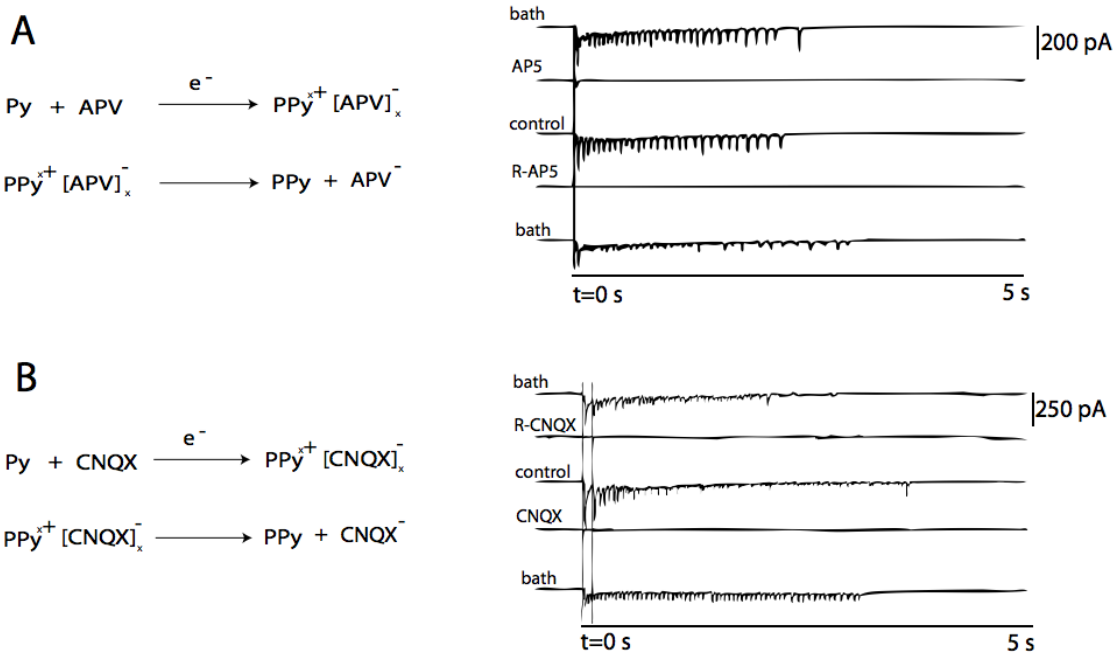

Figure 3-2 Release of AP5 (a) and CNQX (b) from macroelectrodes. Release solution was bath applied to a network when an individual neuron was under voltage clamp.

3.4.2 Controlled release from microelectrodes

To determine the appropriate electrical stimulus for release and visualize the release dynamics, PPy films doped with fluorescein were synthesized on MEA electrodes. Fluorescein and CNQX have similar molecular weights and both molecules carry two negative charges. Unlike CNQX, release of fluorescein can be easily detected using fluorescent microscopy. Using an inverted microscope attached to a CCD camera, time-lapse images of the MEA were taken after application of a square wave pulse of various potential magnitudes and duration of 200 ms to the fluorescein loaded microelectrode(figure 3-3a). A real-time movie of the release

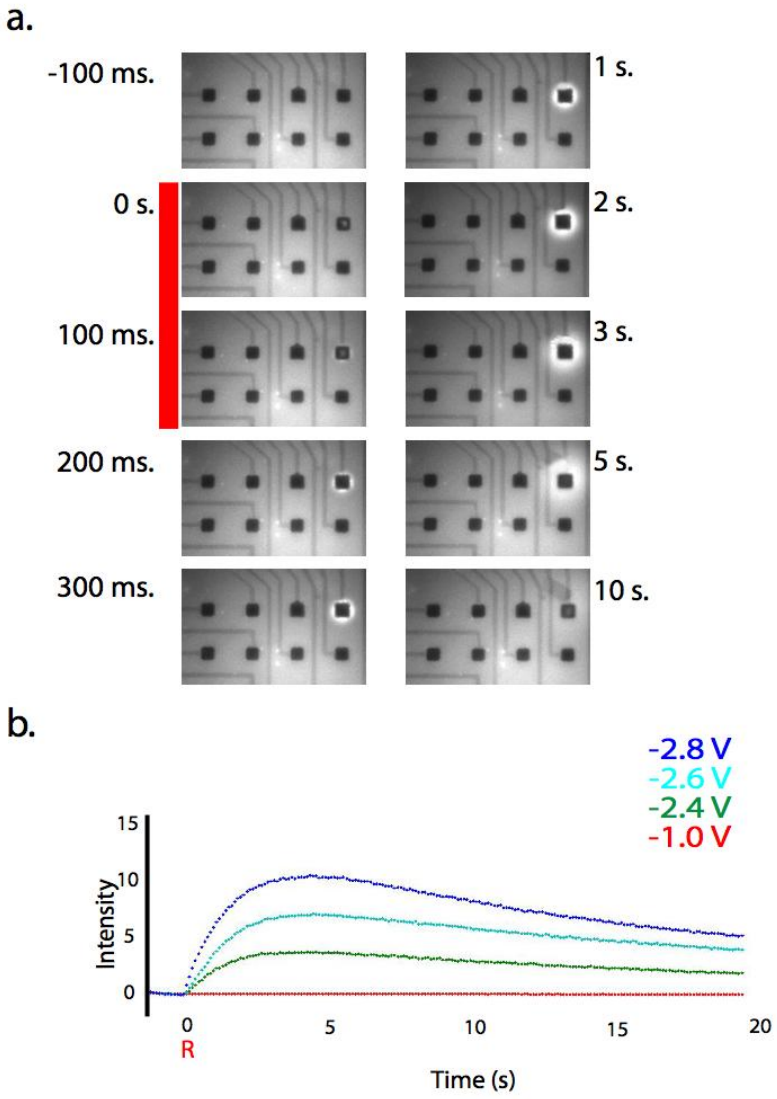

Figure 3-3 Release of fluorescein from MEA electrodes and the effect of voltage magnitude. a) Time-lapse microscopy showing different time points after release and b) the effect of release voltage on intensity as a function of time.

process can be found in the supplementary information. It was found that a magnitude of 1 V vs. Ag/AgCl never resulted in fluorescein release that was detectable with the 200 ms duration. The magnitude was increased in small increments to find the voltage necessary for release as well as examine the relationship between magnitude and release amount (intensity). Across n = 11

electrodes, the magnitude necessary to detect release ranged from -1.7 V to -2.3 V. Individual time-series were normalized by subtracting the mean intensity of the ROI in the first ten frames (prior to fluorescein release) from each subsequent frame of the series. On every electrode tested, a positive relationship between the stimulus magnitude and the intensity was discovered(figure 3-3b). To test whether the high magnitude drug releasing stimulus damaged the electrodes, impedance spectroscopy was utilized. No apparent change in the physiologically relevant 1 kHz impedance was measured after applying the release stimulus (figure 3-4).

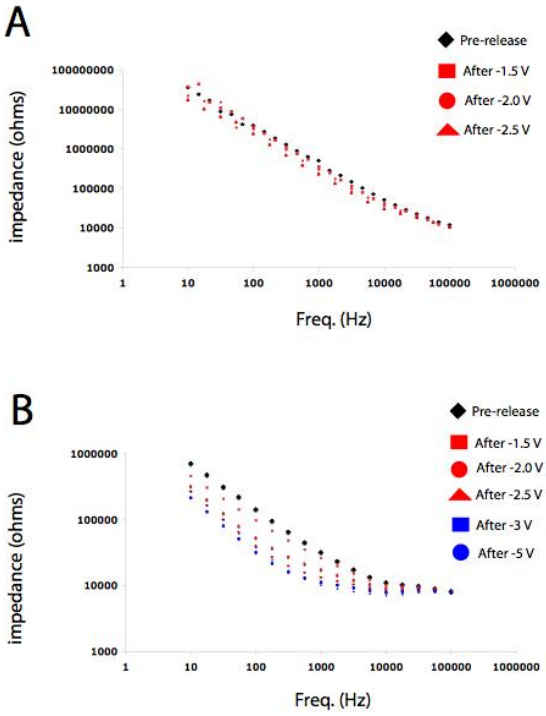

Figure 3-4 Impedance spectroscopy of PPy-coated (A) and uncoated (B) electrodes subject to high voltage release stimuli

3.4.3 Electrophysiological effect of local CNQX Release on single neurons

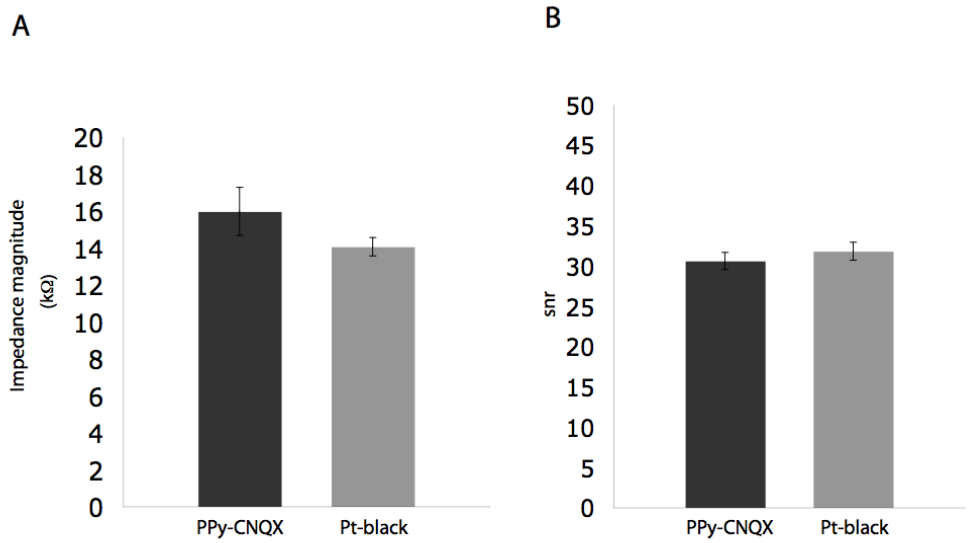

Figure 3-5 A) average 1 kHz impedance and B) *snr* of PPy and uncoated electrodes

PPy-CNQX films synthesized on MEA electrodes maintained the electrical properties of the pt-black electrodes (figure 3-5). CNQX competitively blocks glutamate binding to non-NMDA receptors (Alford and Grillner 1990). To directly monitor the effect of CNQX release from electrodes, patches were made on individual neurons at various locations in the dish (figure 3-6a). The evoked responses of the patched neuron were mapped by providing a brief neural stimulation (1 V, 100 μs) at each of the 64 extracellular electrodes. Reliable monosynaptic currents could be evoked by stimulation of multiple electrodes (figure 3-6b). These responses provided a baseline from which inhibition could be observed. A single trial was defined by a series of 8-15 sequential neural stimulations (ns) spaced equally in time from an electrode found to elicit a reliable monosynaptic trace (figure. 3-7a). The inter-stimulus interval was constant within a trial but varied from 1 s – 6 s on different trials. Three types of trials were performed:

baseline control, release control and CNQX. In baseline control trials, the -2.5 V release stimulus was not given. The purpose was to account for short-term synaptic effects. In the release control trials, a

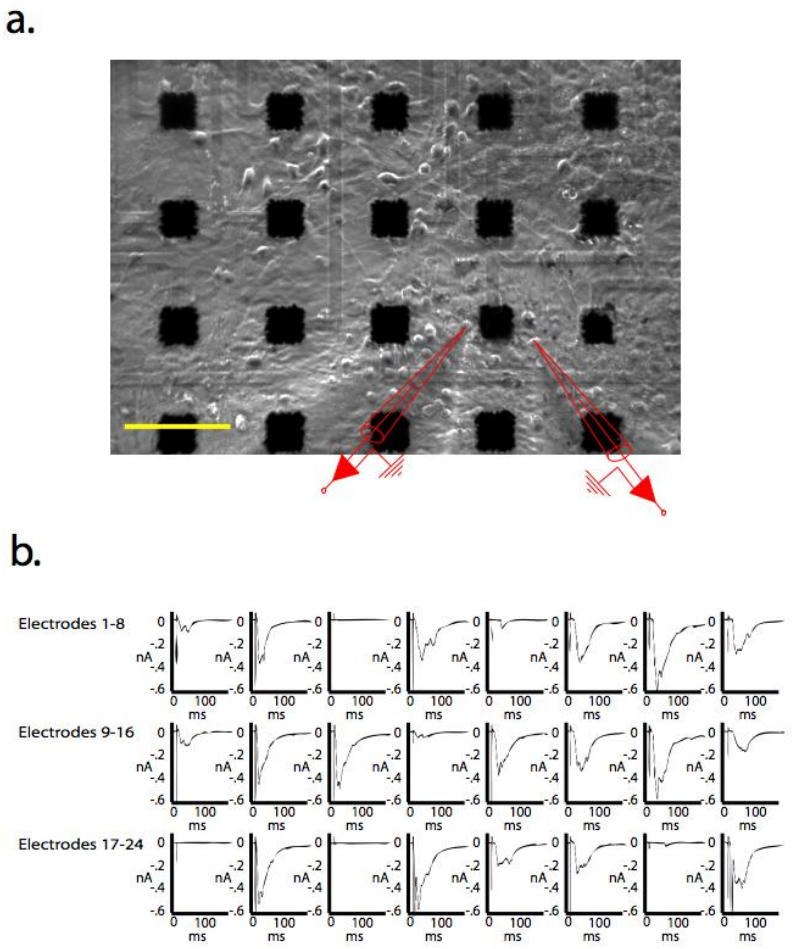

Figure 3-6 a) Individual neurons are patch clamped and b) reliable currents can be evoked from electrical stimulation at multiple sites in the network.

-2.5 V, 200 ms release stimulus was applied to PPy electrodes that had been synthesized in a phosphate buffer saline that does not contain CNQX. The purpose was to isolate the effect of CNQX release from any effect the electrical stimulus itself provided. In CNQX trials the -2.5 V, 200 ms pulse was applied to PPy electrodes doped with CNQX. Figure 3-7b illustrates the

example current traces recorded from one neuron after release from 2 different releasing electrodes, one coated with control doping solution only and the other doped with CNQX. For each electrode, a trial without any drug release stimuli was first recorded as a baseline response

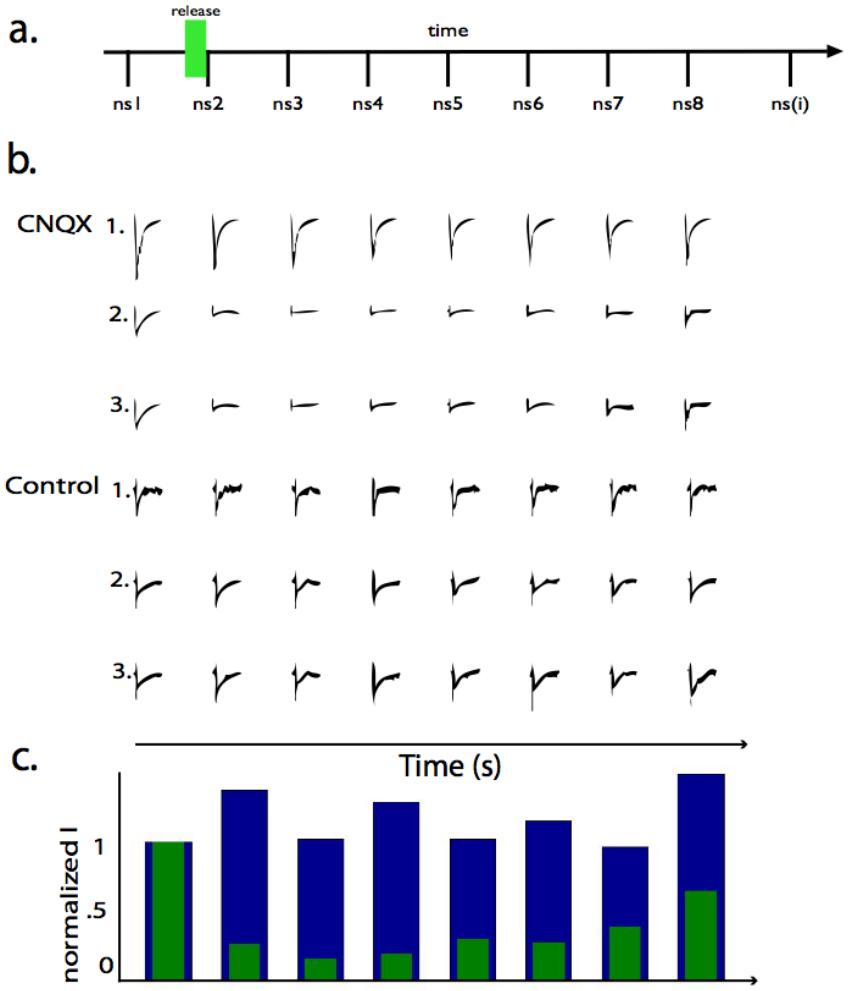

Figure 3-7 a) Schematic of the experimental paradigm (ns = neural stimulation) b) Currents recorded from a neuron prior to CNQX release (CNQX 1) and during a CNQX release trial (CNQX 2), CNQX 3 are currents recalibrated to correct for short term synaptic effects. The same procedure is followed for the control. c) The peak value of the current for CNQX 3 (green) and Control 3 (blue) as a function of stimulus.

of the neuron. The peak current values following each neural stimulus (ns) were calibrated to compensate for short-term synaptic effects (see methods). A clear reduction in the magnitude of the current can be observed following CNQX release. No such reduction occurs in either the baseline control or control release case. The CNQX response includes an initial depression of current magnitude followed by a recovery (figure 3-7c).

A patch was made on 18 different neurons at varying distances from releasing electrodes. A total of 25 different electrodes, in 6 different arrays, were tested. Reliable inhibition can be obtained when the electrode to cell distance is within ~200 um. No inhibition is found when electrode is ≥400 um from the patched neuron (figure. 3-8a). The current magnitude recovered in time as can be seen in figure 3-7c. Furthermore, multiple trials were performed with each neuron and the baseline current flow recovered by the subsequent trial. Examining the relationship between inhibition and time among many different neurons is complicated by a strong dependence on distance; the time of peak inhibition will vary greatly with distance. To combat this, a function *k* is derived from Fick's model of diffusion (see methods). Data points from CNQX trials are represented in red, and data points from release control trials are represented in black (figure 3-8b). Figure 3-8c plots 9 CNQX trials over a broad range of k. A linear regression is performed on each trial and a statistical analysis of the slopes resulted in $p <$ .025 (see methods). This result confirms that diffusion plays a role in mediating this process, as well as a providing a method to analyze the temporal characteristics of release across neurons at various distances (since in every trial distance is constant and k varies with time).

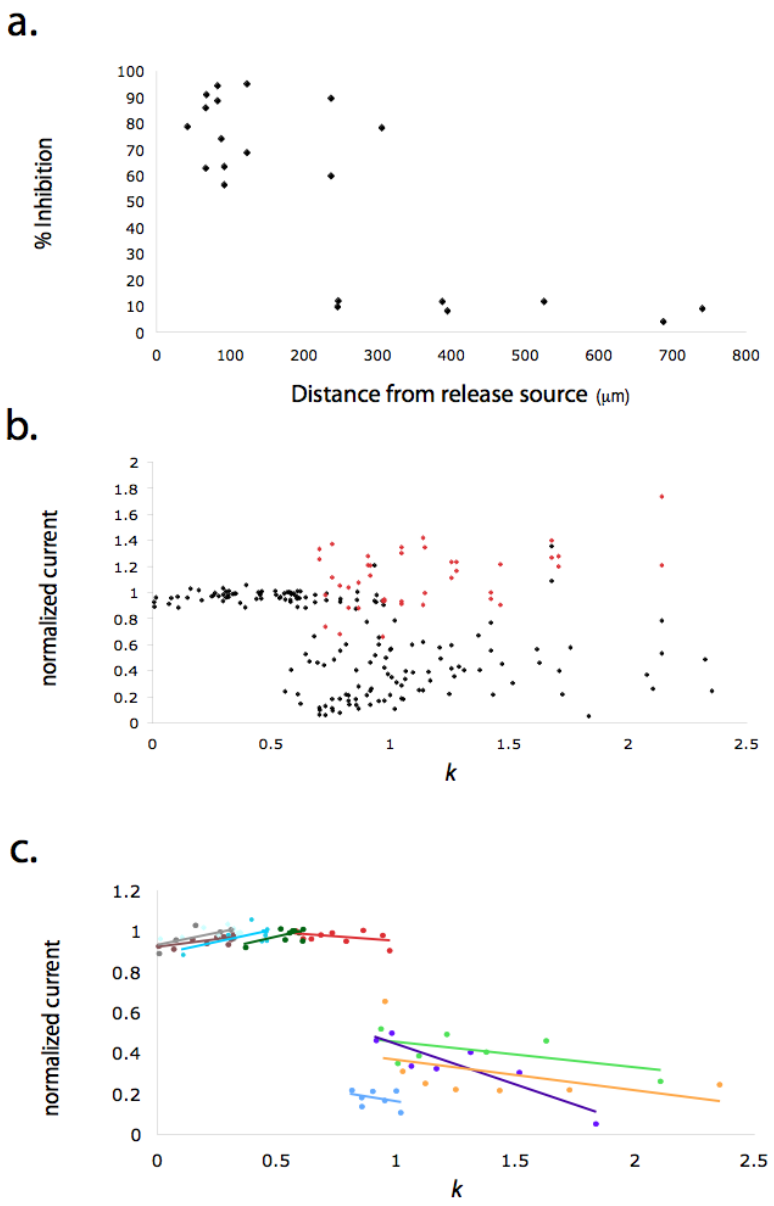

Figure 3-8 a) Maximum inhibition as a function of the distance between a neuron and the releasing electrode and b) normalized current as a function of *k* (red dots represent control trials, black dots CNQX trials. c) normalized current as a function of *k* for 9 (color-coded) trials.

3.4.4 Local Network effects of CNQX release

To examine the effects of CNQX on network activity recorded on extracellular electrodes high-density neural cultures are used. The advantage of high-density cultures is the increased amount of spontaneous activity relative to sparse cultures (Wagenaar, Pine et al. 2006). This simplifies the experimental paradigm by removing the need for neural stimulation. Spontaneous activity arose after 4-7 days in dense cultures. Prior to release, electrodes were identified that were recording high levels of spontaneous activity. Baseline recordings were taken prior to release of CNQX (using a 4 s potential with a magnitude of 1 V) and for up to 100 s after release. The voltage artifact and the switch from stimulation to recording obscure the two seconds immediately following release. Figure 3-9a shows seven subsequent 40 s segments of raw data demonstrating the complete abolition and recovery of spiking activity. The red box on the release trials indicates the time of release. The inset shows the extracted waveforms from various recovery trials. From a different electrode, ten 100 s trials were obtained showing the inhibition and recovery of firing (figure. 3-9b). The red box indicates the time obscured by artifact.

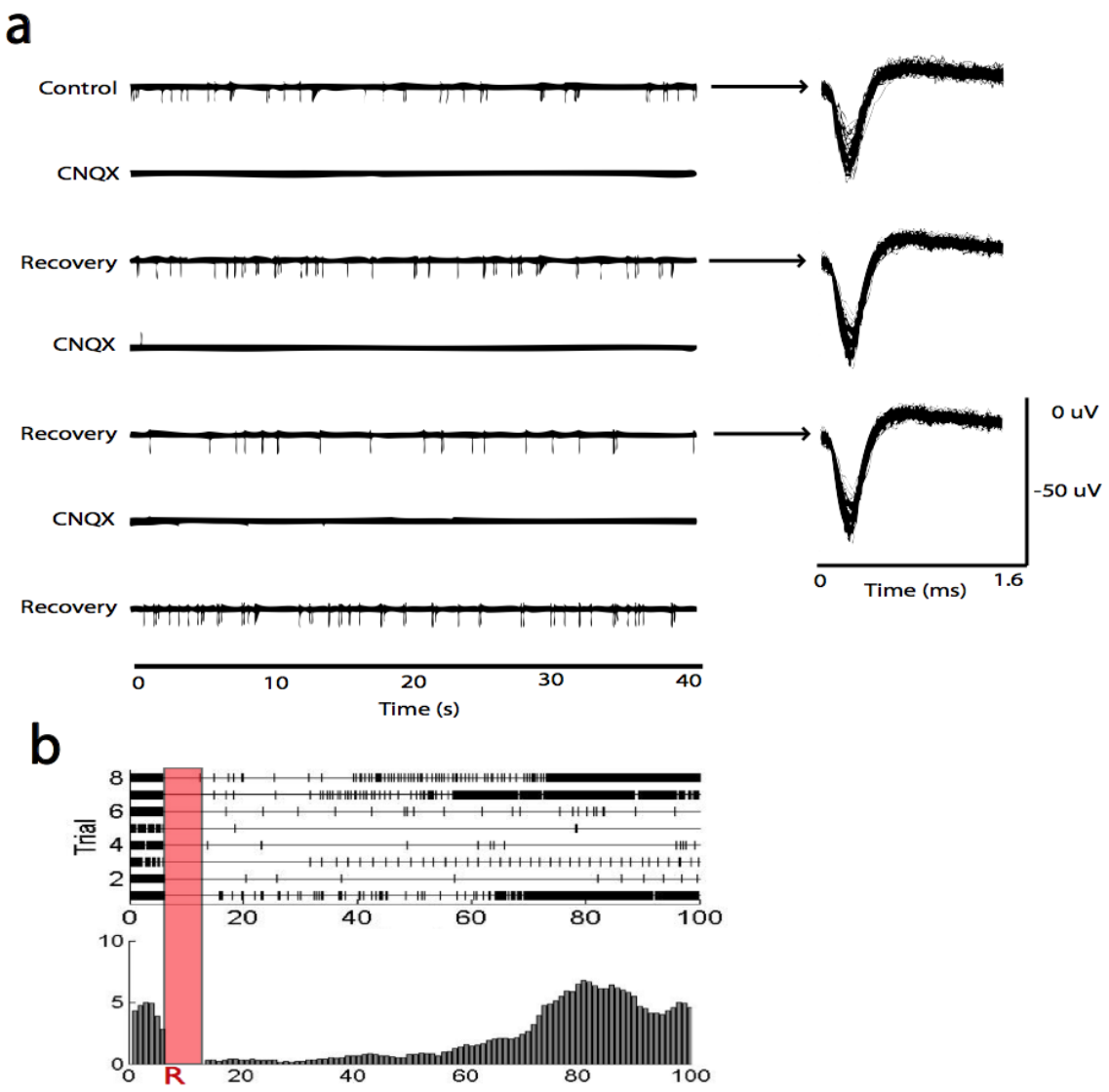

Figure 3-9 Inhibition and recovery of spontaneous activity a) CNQX released at the beginning of each CNQX trial, the inset shows the waveform shapes extracted from the baseline recording as well as the first two recovery trials. b) 8 trials of release and recovery, red box indicates the time of release as well as the time period obscured by the artifact

To examine the network effects under the same conditions as the patch recordings were studied, electrical stimuli was used to evoke network activation. Network activity could be repeatedly evoked by short (100 μs) electrical stimuli (1.2 V) delivered through the substrate electrodes, and this evoked activity could be inhibited by release of CNQX (same conditions as patch clamp experiments, -2.5 V for 200 ms) from local electrodes (figure 3-10a). Release of CNQX from electrodes near (200 μm) the response preceded a transient inhibition lasting approximately 10 seconds. As the distance between release and recording site was increased, the effect of CNQX diminished. (figure 3-10b)

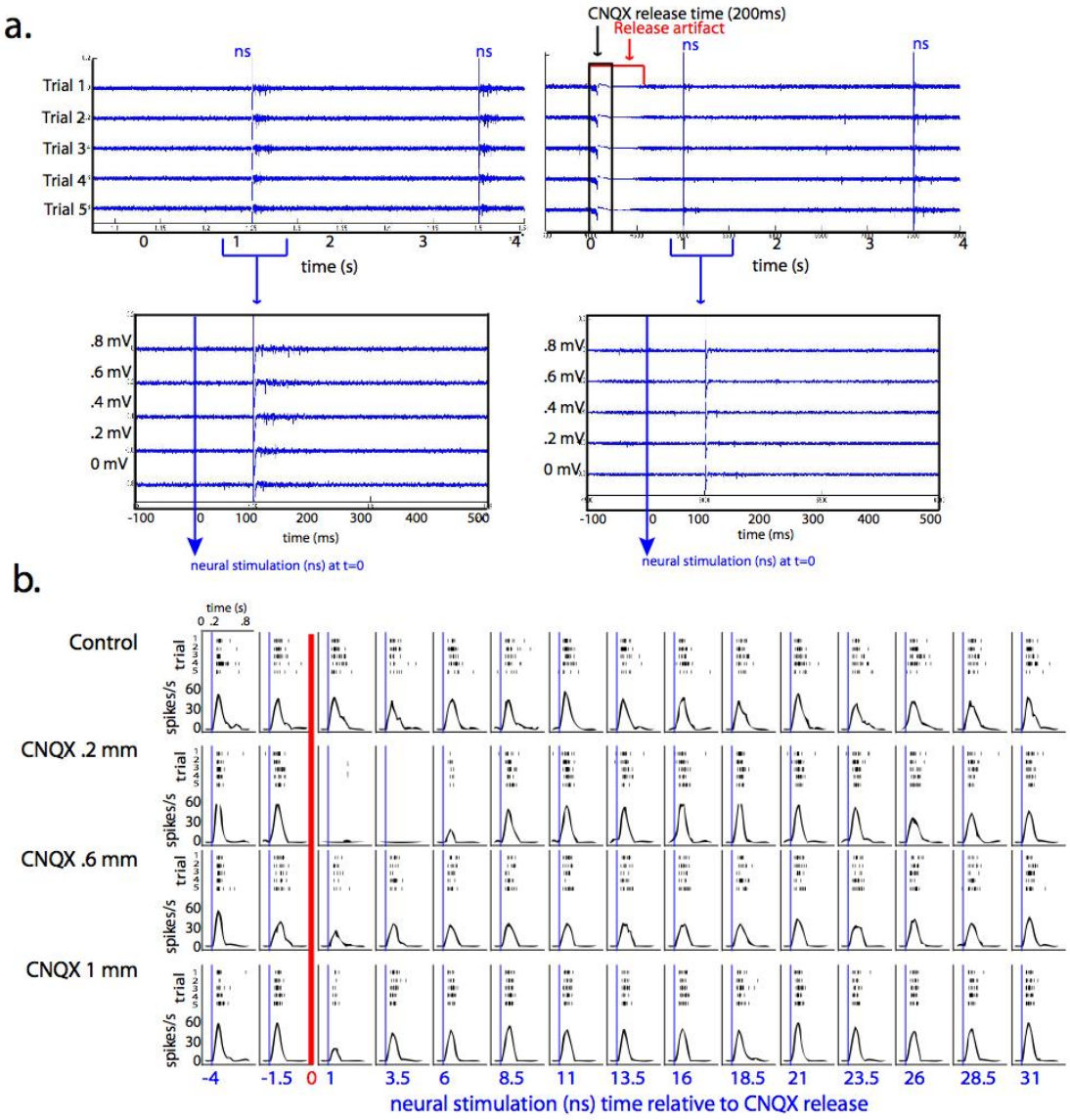

Figure 3-10 a) Raw data recordings of the same electrode, over five trials showing the response to stimulation (ns) and the inhibition due to CNQX release. b) Raster plots and PSTH for the multiunit data from a single electrode. Release of CNQX was performed at electrodes of various distances.

3.5 DISCUSSION

A deeper understanding of brain function will require the ability to monitor electrical activity of many neurons simultaneously, and the ability to introduce systematic perturbations in a highly controlled fashion. The method presented in this paper builds upon commonly used, commercially available existing technologies in a unique manner that enables customization in experimental planning and execution. For the research being conducted, PPy films mediate release of CNQX and inhibit neurons within a tight radius of the recording electrode. Of major benefit to this research is the ability to record from the array of 64 electrodes and detect highly correlated neuronal activity, then use that information to direct the location of perturbation. This ability highlights a unique power of the technique.

Prior methodologies for the local perturbation of neural tissue include microiontophoresis, pressure injection, photolysis of caged compounds and most recently, the expression of light sensitive ion channels (Chambers and Kramer 2008). All of these techniques have advantages and drawbacks. For spatial acuity, photolysis of caged compounds and activation of light sensitive ion channels reign supreme. The area that is perturbed will be clearly demarcated by the width of the excitation beam; consequently these techniques have been used to study the molecular cascades that occur in individual spines (Scheuss, Yasuda et al. 2007). A necessary drawback of techniques that rely on laser beams is that the depth of the tissue that can be studied is limited to the depth into which the light can penetrate, several hundred microns when two-photon laser beams are used. All of the techniques listed suffer from the common drawback that extra hardware needs to be placed into the brain, either to introduce compounds or to record from the neurons. With the described method, the mechanism to perturb units is a functional part of the implanted recording electrode. The decision of when and from

what electrode to release the agents can be made in real-time and be informed by the activity being recorded; and it is entirely possible to close the loop between recording and release so that agents can be disseminated in response to particular dynamic patterns. The release of the agents is through ionic diffusion and so volume displacement of the tissue does not occur, this prevents unnecessary injury.

A case can be made for the generalization of this technique in two directions: towards implementation on an implantable array and with the use of different dopant molecules. Electroactive conducting polymer films have been successfully grown on the electrodes of implantable neural electrode arrays and offer superior or equivalent recording and stimulation properties. The films also survived insertion and withdrawal from murine (Cui, Hetke et al. 2001; Cui, Lee et al. 2001) and primate (unpublished result) brains. Therefore it is highly feasible to translate the release system reported here onto *in vivo* electrode arrays. Furthermore, the electrochemically-controlled release is not limited to polypyrrole or CNQX. Other types of electroactive conductive polymers may also be applied. More importantly, the system is capable of releasing many kinds of charged molecules. Previous research has shown that dexamethasone(Wadhwa, Lagenaur et al. 2006), dopamine(Miller, Lau et al. 1983), glutamate(Zinger and Miller 1984), biotin(George, LaVan et al. 2006), salicate, naproxen and tosylate(Kontturi, Pentti et al. 1998), and ATP(Pernaut and Reynolds 2000) can be incorporated and released from conducting polymer films. Along with the advances presented here, including the miniaturization to electrodes capable of recording neural signals, the real-time interface with live cells and physiological consequences of release and the incorporation and release of CNQX, conducting polymer controlled release has the potential to serve as an important research tool in dynamic biological systems. Of particular interest for future studies is dopamine. The release

mechanism described here might be a good model of the volume transmission pathway utilized by catecholamines (Zoli, Torri et al. 1998).

The limitations include the fact that the amount of dopant present will limit the total amount that can be released. In the research performed here, the number of releases that could be achieved was highly variable. Our lab has begun to explore means to increase the drug load and release efficiency by creating nanostructured polymer film. Nanoporous polypyrrole has shown to have a 10 fold increase in drug release than the conventional film (Luo and Cui 2008). Much of the trial-to-trial variability had to do with simple voltage control of release. Release is a function of charge and so tailoring the voltage according to the resistance of the electrode provides a more exacting method of release. An alternative method would be to use current control for release, which would allow for the charge to be specified. However, a major drawback of using current control is the possibility of setting up very large potentials which can damage the electrodes and kill neurons.

Another point of discussion is the magnitude of the voltage necessary to release. In the fluorescein release studies it was shown that a voltage of -2.5 V for 200 ms was sufficient and this voltage was used for the patch clamp studies. In the extracellular analysis of the effect of release, a lower voltage of -1 V for 4 s was used. Release occurs as a function of the charge that is deposited on the polymer backbone. While it is convenient to think of the polymer existing in a charged or neutral state, charging and discharging are continuous processes that probably begin at the surface of the polymer and move inward as the charge increases. Since the current and duration will determine the amount of charge, it is natural to suspect that shorter duration stimuli will require a greater potential difference, resulting in higher current and more charge. This

relationship between duration, charge and amount released also offers another level of customizability in the system.

4.0 EVOKED NETWORK ACTIVATION AND LOCAL CNQX RELEASE

4.1 INTRODUCTION

In an intact and behaving animal, specific groups of neurons are activated by certain stimuli and it is hypothesized that some information may be contained in the correlation among the activated groups (Salinas and Sejnowski 2001). In at least one study performed in the primary auditory cortex, the relative spike timing of neurons was shown to be sufficient for feature representation even in the absence of changes in firing rate (deCharms and Merzenich 1996). In this way we can say that correlations amongst neurons are stimulus dependent. Functional groups can also be activated within *in vitro* neuronal networks through the use of electrical stimulation. Electrical stimulation of a single electrode underlying a network of neurons can cause firing of many neurons (Wagenaar, Pine et al. 2004). This paradigm, which has been extensively used to study the role of network activation in activity dependent plasticity (Jimbo, Robinson et al. 1998; Maeda, Kuroda et al. 1998; le Feber, Stegenga et al. 2008; Stegenga, le Feber et al. 2008), may also be a good model to study the mechanisms of functional clustering.

In this report, an attempt is made to classify the functional clustering of neurons in a cultured neuronal network (CNN) to an electrical stimulus. We examine whether the same group of neurons is excited by all stimuli or whether stimulus dependencies. The results will be

divided into two sections; the first section will examine the response to electrical stimulation from different electrodes. We will demonstrate that some neurons respond in a stimulus specific manner. Amongst a group of neurons activated by all three stimuli, we will show that the correlation amongst neurons is also stimulus specific. In the second section we will examine the network responses to local release of CNQX and the effect it has on cross correlation of spike-timing as well as correlation of broad firing rate fluctuations.

The methods for creation of the PPy/CNQX electrode coatings, electrochemical release, neuron culture, and electrophysiology are identical to those used in Chapter 3, the following section will only describe the analytical and statistical methodologies utilized.

4.2 ANALYSIS METHODS

4.2.1 Spike Extraction and Sorting

Continuous data was sampled at 20 kHz and the data was high-pass filtered at 100 Hz. A linear threshold set at a negative six standard deviations from the mean voltage detected spikes. Common-mode noise was rejected if it appeared on 70% of channels simultaneously (defined with a100 μs window), this removed stimulus artifacts and other common-mode noises. Extracted spikes were sorted in two steps. Initial clustering was performed using a valley-seeking algorithm that builds clusters based on Euclidean distance in PCA space (Fukunaga 1972). This was followed by manual clustering on a channel basis by waveform crossing in Offline Sorter (Plexon, Inc.). Finally, before further analysis, any unit with less than 50 spikes per 50 second recording was discarded.

4.2.2 Peri-Stimulus Time Histograms

To estimate the time varying firing rate of individual neurons, a peri-stimulus time histogram (PSTH) was computed for each neuron. The spike times were counted across trials in 5 ms bins. To correct for sampling errors, the resulting histogram was smoothed using Bayesian Adaptive Regression Splines (BARS) (DiMatteo, Genovese et al. 2001).

4.2.3 Cross-Correlation analysis

To detect short-time scale dependencies between neurons, cross-correlation analysis was used. To obtain the cross-correlogram, a joint peri-stimulus time histogram (JPSTH) was first constructed utilizing the counting procedure described by Aertsen et. al. (Aertsen, Gerstein et al. 1989) on spike time data that had been placed in 5 ms bins. The main diagonal of the raw JPSTH provided the time-varying coincident firing of the two neurons. To control for correlations induced by fluctuations in the firing rate, the diagonal of the raw JPSTH was smoothed using BARS; then this curve was normalized by the product of the square root of the PSTH of the component neurons. A time average of this corrected curve provided estimation of the correlation.

We wish to test the significance of these correlation values without making assumptions about the underlying distribution of spike times. This was accomplished through the use of a permutation test. The null hypothesis for this test was that the spike times of the two neurons were independent. Through the permutation test a distribution of correlation values generated under the condition of guaranteed independence was obtained. To do this, the order of the 25 trials was randomly permuted for both cells, independently. The procedure described above for

estimation of the correlation was performed for the permuted data. This process was repeated 1000 times, for every iteration the trial order was randomly permuted. The estimated correlation was compared to the distribution obtained from the permutation test. The number of points in the distribution that were larger than the estimated correlation was divided by the number of iterations (1000) to provide final *p*-values for the estimates. This process is illustrated for one neuron pair in figure 4-1.

4.2.4 Cluster Analysis

To define groups of cells (functional clusters) whose firing rates are correlated we will utilize the model-based clustering algorithm that puts variables into groups based on trial-to-trial variability in firing rate. The model of clustering used is was developed by Liuxia Wang in her doctoral dissertation (Wang 2005)

$$y_{ij} = \mu_i + w_i \gamma_{c(i)j} + \varepsilon_{ij}$$

$$\gamma_{kj} \sim N(0,1)$$

$$\varepsilon_{ij} \sim N(0,\sigma_k^2)$$

Appendix B gives the full details of the clustering procedure, including priors and posteriors. The firing rate of the data in the 1 s following stimuli was calculated for all stimulation trials. Initial cluster number (K) was inferred using Bayes Information Criterion (BIC), which determines the model that best explains the variability in the data while penalizing free parameters. The clustering algorithm was implemented using an MCMC simulation that was run for 4000 iterations with a burn-in of 500. During each iteration, the algorithm places each

variable in one of k=1…K clusters. The posterior probability of cluster membership is calculated for each k, and cluster membership is assigned when the posterior probability ≥ .9. Independent cells were discarded and the clustering procedure (determination of cluster number as well as clustering) was repeated until no independent cells remained. After clustering, a correlation matrix was calculated for the original firing rate data and compared to the clustering result for verification.

.

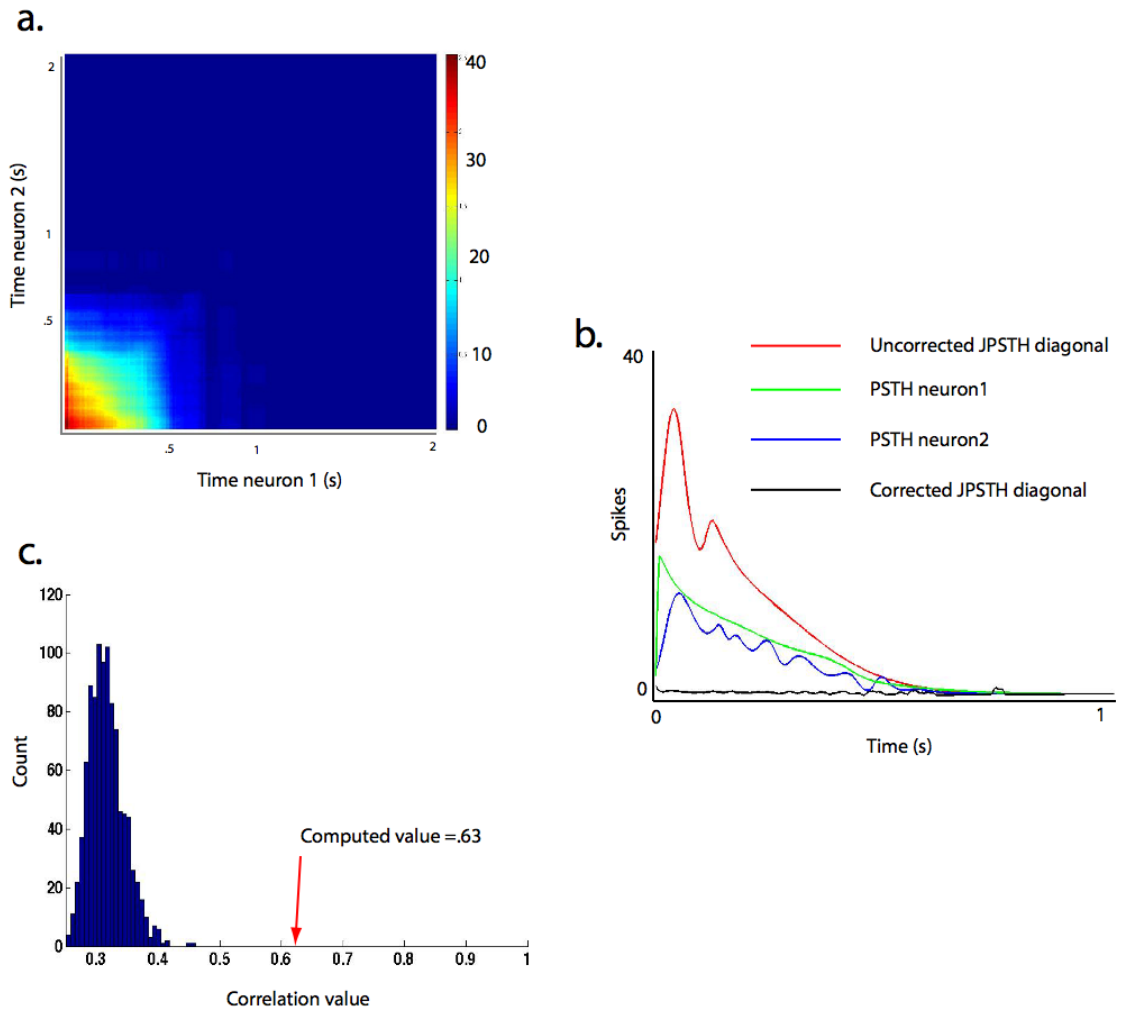

Figure 4-1 a) Raw JPSTH for 2 neurons arrived at by counting coincident spikes and b) the diagonal of the JPSTH matrix is represented in red while the PSTHs of the two individual neurons are shown in green and blue, respectively. The corrected diagonal (black) is arrived at by normalizing it by the product of the square roots of the individual PSTHs. c.) The simulated distribution of correlation values under independence is shown relative to the actual value of the correlation

4.3 RESULTS

Early experimentation with MEA recordings showed that high-density networks cultured on MEAs were able to produce the general dynamical patterns that have been often reported(Wagenaar, Pine et al. 2006). Cortical neurons were plated on MEA surfaces treated with PEI and laminin at a high-density. Between 3-4 μl of a 10^4 cells/μl suspension were plated in a drop centered on the electrode array. Figure 4-2 (A) displays a phase micrograph of these high-density networks. Spontaneous activity appeared as early as day 4. Coordinated network firing arose between days 7-10. Figure 4-2 (B) displays a raster plot of spontaneous activity from a three-week old culture. As has been reported elsewhere, the frequency and pattern of this network action was variable between networks and changed with the age of the network.

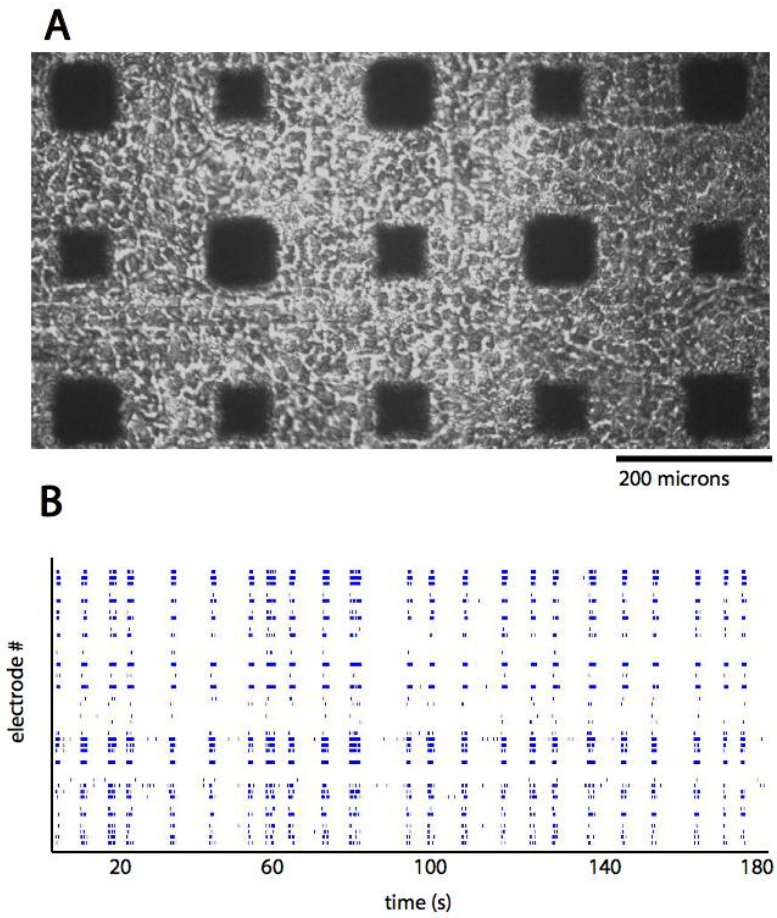

Figure 4-2 A) Phase micrograph of high density neural cultures on MED64 electrode array and B) raster plot of spontaneous spike activity. Each hash mark represents the time of an action potential and each row represents the activity recorded from a single electrode.

4.3.1 Stimulus Specific Specificity

Brief electrical stimuli (1.2 V, 100 μs) were repeatedly given at three different electrodes (numbers 5, 19, and 22) on individual trials. The sites for stimulation were chosen using a previously described protocol that defined stimulus locations based on which electrodes had

spontaneous activity(Wagenaar, Pine et al. 2004). Twenty-five trials were performed for each stimulus. After recording, neurons were sorted into single units. In order to compare the responses to different electrical stimuli, waveforms were overlaid and manually inspected to locate units that fired in response to the different stimuli. Figure 4-3 displays the common waveforms from a single network given two spatially distinct stimuli. The waveforms are plotted spatially to demonstrate the electrode they were recorded from.

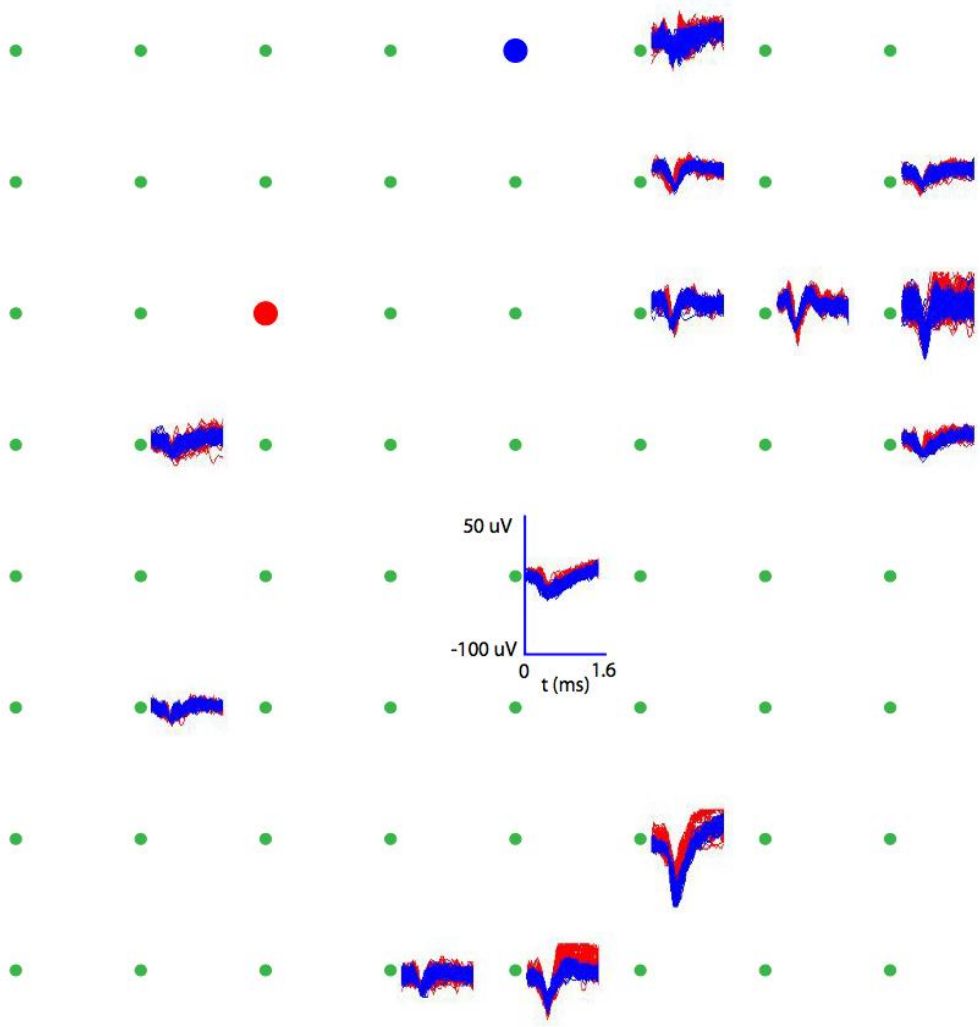

Figure 4-3 Waveform Display demonstrating signals recorded following two spatially distinct stimuli (indicated by the colored circles, all axes are the same)

Across three different stimuli, 26 different neurons fired. Of these 26 neurons, 11 responded regardless of the stimuli location.

The time varying firing rate was computed by calculating a histogram from 25 trials following presentation of the same stimulus. Figure 4-4 shows the temporal evolution of the responses to stimulation at three different electrodes.

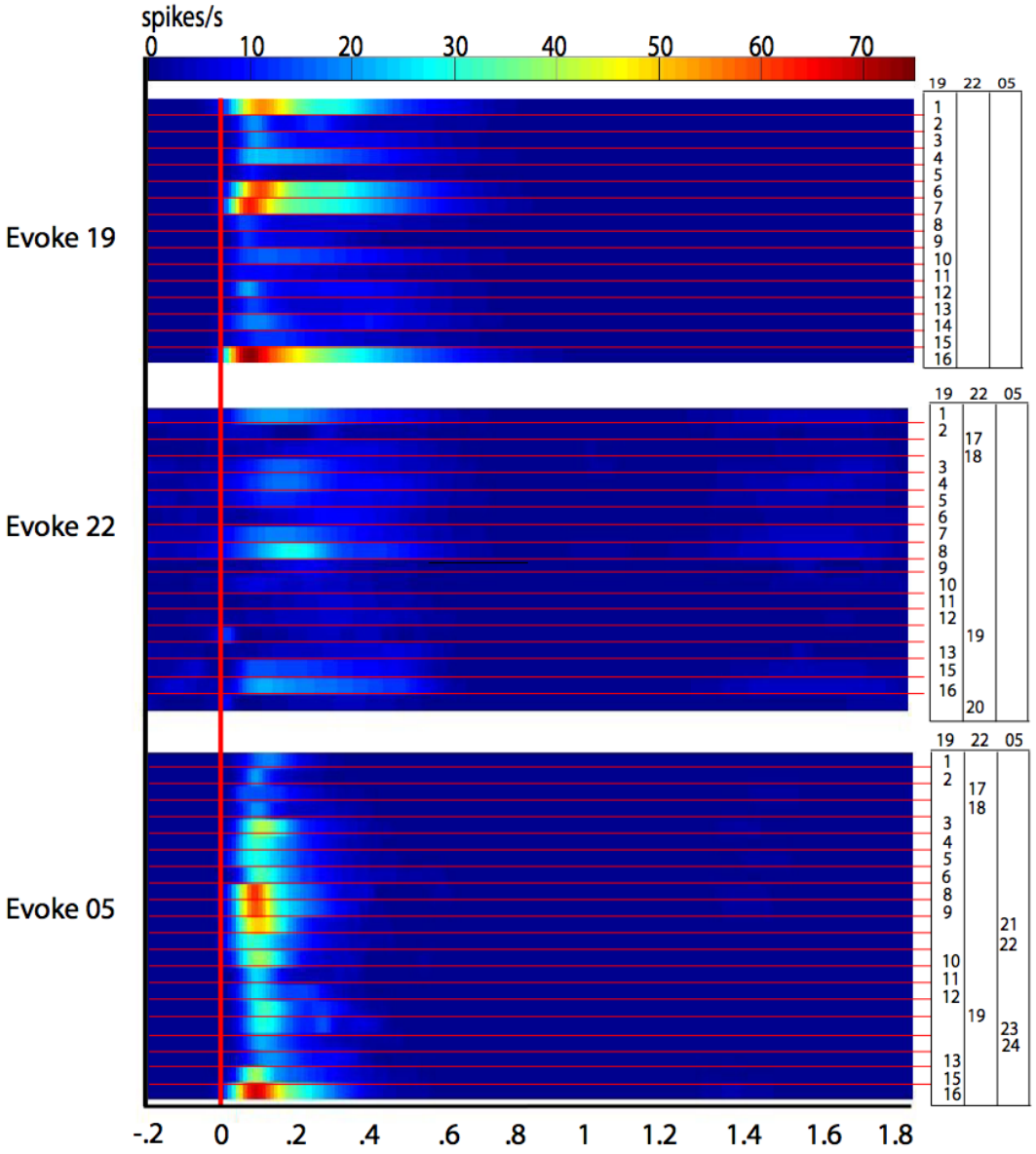

Figure 4-4 Temporal distribution of evoked responses from stimulation at electrode 19 (top), 22 (middle) and 5 (bottom). The columns on the right normalize cell identity across conditions.

The spatial distribution of the network response was plotted as a function of the location of the recording electrode, only neurons that fired more than 50 spikes were considered for this assessment. (Figure 4-5).

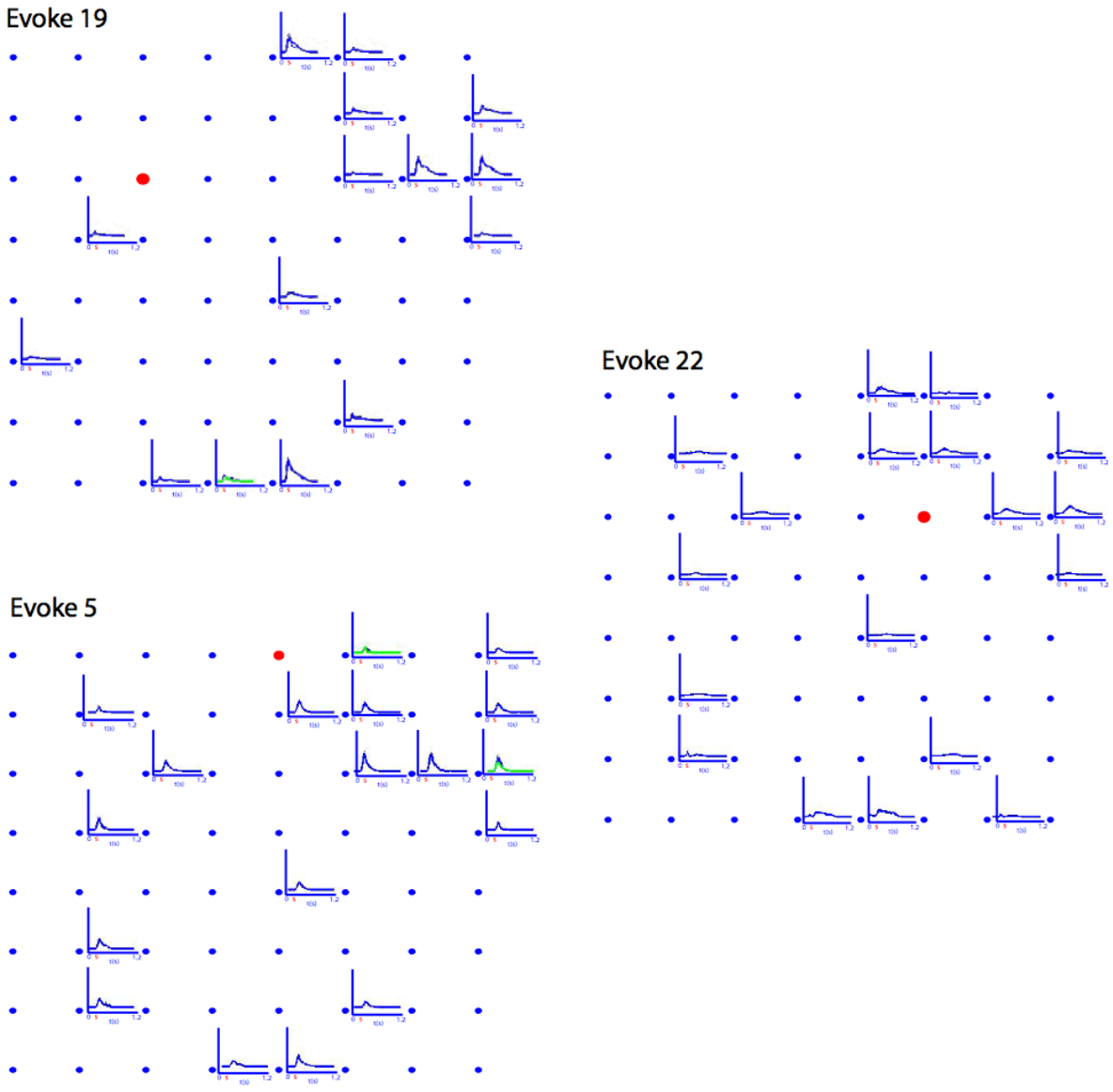

Figure 4-5 Spatial distribution of evoked responses across three different stimuli (PSTH was plotted in different colors if more than one neuron was isolated on a given electrode)

From these figures it is clear that for each condition there is at least one neuron uniquely activated by that stimulus. The implication of this is that location of the stimulus could be inferred from examination of the network output and could be a model to study information representation in an abstract yet well-controlled environment. To look for neuronal pairs that change their relationships in a stimulus dependent manner, we want to examine the correlation between neurons in the network. We will pay special attention to neurons that respond under all conditions to see if there exist stimulus specific relationships between neurons.

The pair-wise cross-correlation of the network was investigated as described above (see methods). Tables 4-1, 4-2 and 4-3 show the correlation matrix for the network data following electrical stimulation at site 19, 22 and 5, respectively. The 26 neurons were labeled arbitrarily but the labels are constant across the trials. If a cell did not fire under a given stimulus, all matrix locations associated with that cell are colored grey.

Table 4-1 Correlation matrix for neuronal activity following stimulation at electrode 19. Grey boxes represent neurons that were not modulated by this stimulus. Yellow boxes identify significant correlations (p < .001) above .5.

	1	2	3	4	5	6	7	8	9	10	11	12	13	14	15	16	17	18	19	20	21	22	23	24	25
2	0.29																								
3																									
4																									
5																									
6																									
7	0.27	0.09																							
8	0.52	0.11					0.22																		
9																									
10	0.19	0.09					0.11	0.12																	
11	0.75	0.29					0.25	0.54		0.21															
12	0.70	0.28					0.25	0.58		0.21	0.83														
13																									
14	0.06	-0.04					-0.06	-0.02		-0.10	0.06	0.03													
15	0.10	-0.02					-0.02	0.06		-0.07	0.13	0.08		-0.07											
16																									
17	0.23	-0.05					0.00	0.10		0.00	0.15	0.26		0.10	-0.01										
18	0.10	-0.06					-0.07	0.01		-0.05	0.12	0.09		0.01	-0.07		0.23								
19																									
20																									
21	0.19	-0.04					-0.02	0.01		-0.08	0.16	0.21		0.12	-0.01		0.51	0.19							
22	0.08	-0.04					-0.03	0.00		-0.09	0.10	0.10		-0.08	-0.08		0.00	-0.04			-0.04				
23	0.18	-0.06					-0.06	0.08		-0.09	0.23	0.23		-0.01	-0.03		0.06	0.06			0.15	-0.03			
24	0.16	-0.03					-0.01	0.01		0.00	0.17	0.17		-0.05	-0.06		0.07	0.05			0.10	-0.09	-0.02		
25	0.63	0.25					0.21	0.47		0.22	0.73	0.69		0.05	0.12		0.67	0.12			0.63	0.27	0.29	0.34	
26																									

Table 4-2 Correlation matrix for neuronal activity following stimulation at electrode 22. Grey boxes represent neurons that were not modulated by this stimulus. Yellow boxes identify significant correlations ($p < .001$) above .5.

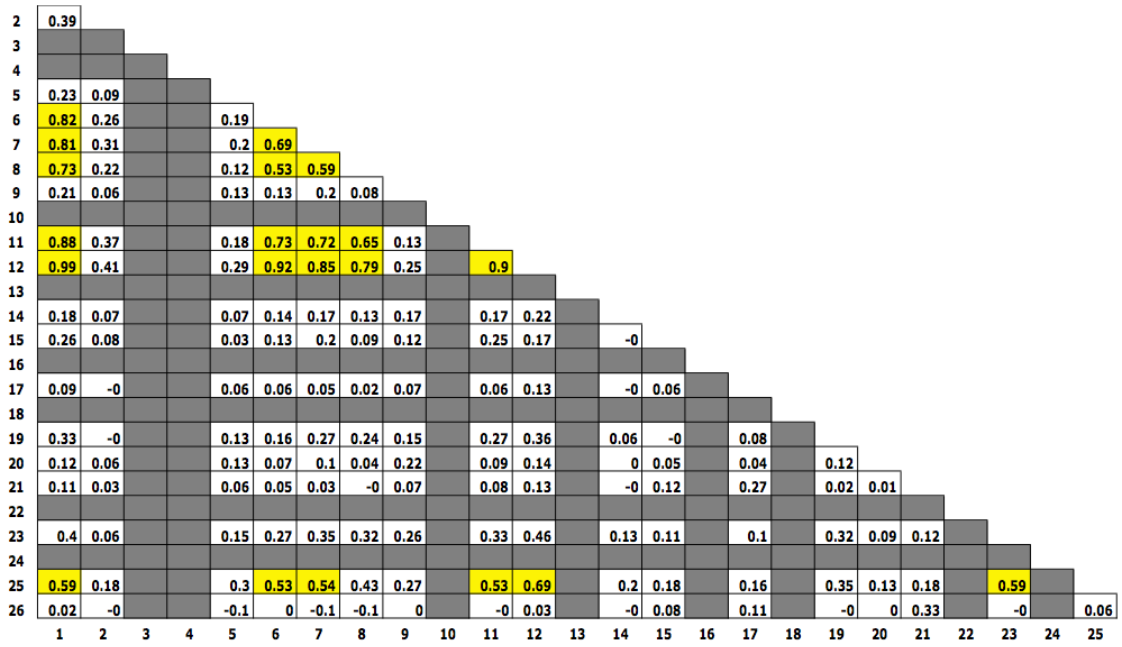

	1	2	3	4	5	6	7	8	9	10	11	12	13	14	15	16	17	18	19	20	21	22	23	24	25
2	0.39																								
3																									
4																									
5	0.23	0.09																							
6	0.82	0.26			0.19																				
7	0.81	0.31			0.2	0.69																			
8	0.73	0.22			0.12	0.53	0.59																		
9	0.21	0.06			0.13	0.13	0.2	0.08																	
10																									
11	0.88	0.37			0.18	0.73	0.72	0.65	0.13																
12	0.99	0.41			0.29	0.92	0.85	0.79	0.25		0.9														
13																									
14	0.18	0.07			0.07	0.14	0.17	0.13	0.17		0.17	0.22													
15	0.26	0.08			0.03	0.13	0.2	0.09	0.12		0.25	0.17		-0											
16																									
17	0.09	-0			0.06	0.06	0.05	0.02	0.07		0.06	0.13		-0	0.06										
18																									
19	0.33	-0			0.13	0.16	0.27	0.24	0.15		0.27	0.36		0.06	-0		0.08								
20	0.12	0.06			0.13	0.07	0.1	0.04	0.22		0.09	0.14		0	0.05		0.04		0.12						
21	0.11	0.03			0.06	0.05	0.03	-0	0.07		0.08	0.13		-0	0.12		0.27		0.02	0.01					
22																									
23	0.4	0.06			0.15	0.27	0.35	0.32	0.26		0.33	0.46		0.13	0.11		0.1		0.32	0.09	0.12				
24																									
25	0.59	0.18			0.3	0.53	0.54	0.43	0.27		0.53	0.69		0.2	0.18		0.16		0.35	0.13	0.18		0.59		
26	0.02	-0			-0.1	0	-0.1	-0.1	0		-0	0.03		-0	0.08		0.11		-0	0	0.33		-0		0.06

Table 4-3 Correlation matrix for neuronal activity following stimulation at electrode 5. Grey boxes represent neurons that were not modulated by this stimulus. Yellow boxes identify significant correlations ($p < .001$) above .5.

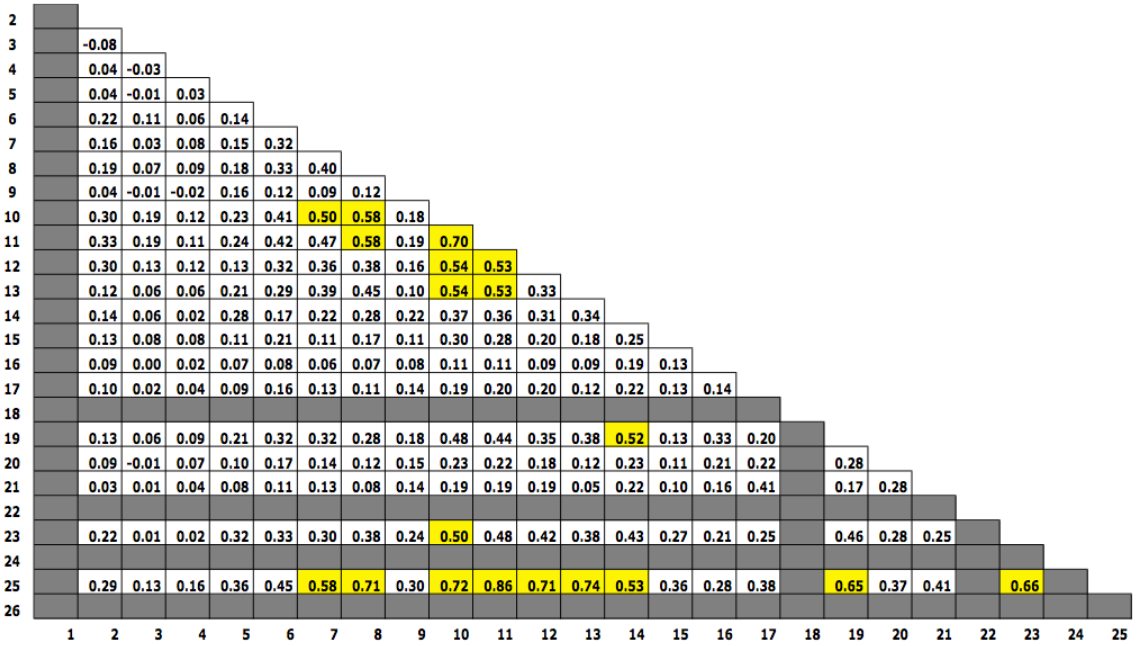

	1	2	3	4	5	6	7	8	9	10	11	12	13	14	15	16	17	18	19	20	21	22	23	24	25
2																									
3	-0.08																								
4	0.04	-0.03																							
5	0.04	-0.01	0.03																						
6	0.22	0.11	0.06	0.14																					
7	0.16	0.03	0.08	0.15	0.32																				
8	0.19	0.07	0.09	0.18	0.33	0.40																			
9	0.04	-0.01	-0.02	0.16	0.12	0.09	0.12																		
10	0.30	0.19	0.12	0.23	0.41	0.50	0.58	0.18																	
11	0.33	0.19	0.11	0.24	0.42	0.47	0.58	0.19	0.70																
12	0.30	0.13	0.12	0.13	0.32	0.36	0.38	0.16	0.54	0.53															
13	0.12	0.06	0.06	0.21	0.29	0.39	0.45	0.10	0.54	0.53	0.33														
14	0.14	0.06	0.02	0.28	0.17	0.22	0.28	0.22	0.37	0.36	0.31	0.34													
15	0.13	0.08	0.08	0.11	0.21	0.11	0.17	0.11	0.30	0.28	0.20	0.18	0.25												
16	0.09	0.00	0.02	0.07	0.08	0.06	0.07	0.08	0.11	0.11	0.09	0.09	0.19	0.13											
17	0.10	0.02	0.04	0.09	0.16	0.13	0.11	0.14	0.19	0.20	0.20	0.12	0.22	0.13	0.14										
18																									
19	0.13	0.06	0.09	0.21	0.32	0.32	0.28	0.18	0.48	0.44	0.35	0.38	0.52	0.13	0.33	0.20									
20	0.09	-0.01	0.07	0.10	0.17	0.14	0.12	0.15	0.23	0.22	0.18	0.12	0.23	0.11	0.21	0.22		0.28							
21	0.03	0.01	0.04	0.08	0.11	0.13	0.08	0.14	0.19	0.19	0.19	0.05	0.22	0.10	0.16	0.41		0.17	0.28						
22																									
23	0.22	0.01	0.02	0.32	0.33	0.30	0.38	0.24	0.50	0.48	0.42	0.38	0.43	0.27	0.21	0.25		0.46	0.28	0.25					
24																									
25	0.29	0.13	0.16	0.36	0.45	0.58	0.71	0.30	0.72	0.86	0.71	0.74	0.53	0.36	0.28	0.38		0.65	0.37	0.41		0.66			
26																									

Examination of the pattern of significant correlations shown within these tables reveals that numerous relationships are stimulus dependent, even when both cells are modulated under all conditions. This result further implies that cultured neuronal networks could provide a viable model to study stimulus-dependent clustering mechanisms.

4.3.2 Changes in network response following local CNQX release

A significant unanswered question in neuronal network science is how activity moves through the network. Basic statistical procedures such as the ones used here can identify relationships between neurons, but are able to provide less information about the nature of the relationship. One of the motivations for developing the local release system for inhibitory neurochemicals was to make an attempt to further describe the relationship between two neurons. For instance given a correlated pair, inhibiting one neuron while examining the change in activity of another could begin to address whether the correlation arises from a common input or whether a direct relationship between the pair exists. Furthermore, by combining intracellular recording with the network data (Appendix B) and local release, direct convergence of the network activity upon individual cells could be better described. Defining the functional structure of neuronal networks could greatly further the search for understanding of how the brain functions at a mechanistic network level.

With these motivations in mind the following section will examine an initial experiment with one network and the local release of CNQX. We would like to inhibit AMPA synaptic transmission in spatially restricted regions by release of CNQX from individual electrodes. A drug release stimulus with magnitude of 1 V and duration of 4 s was used to release CNQX. CNQX release preceded a general reduction in firing rate that was observed across the entire network. Figure 4-

6 displays the PSTH for neurons prior to release and afterwards. Twenty-five stimuli are delivered prior to release and 25 stimuli are delivered after release. In order to demonstrate that the responses are stable, the first grid (a) of PSTHs represents the first ten trials with no CNQX release while the second grid (b) represents a different ten trials. Likewise, the third grid (c) displays the first ten trials after CNQX release and the final grid (d) displays a subsequent ten. The firing rate of the neurons recovered after the release trial. Figure 4-7 demonstrates the PSTHs from the same trials conditions after recovery.

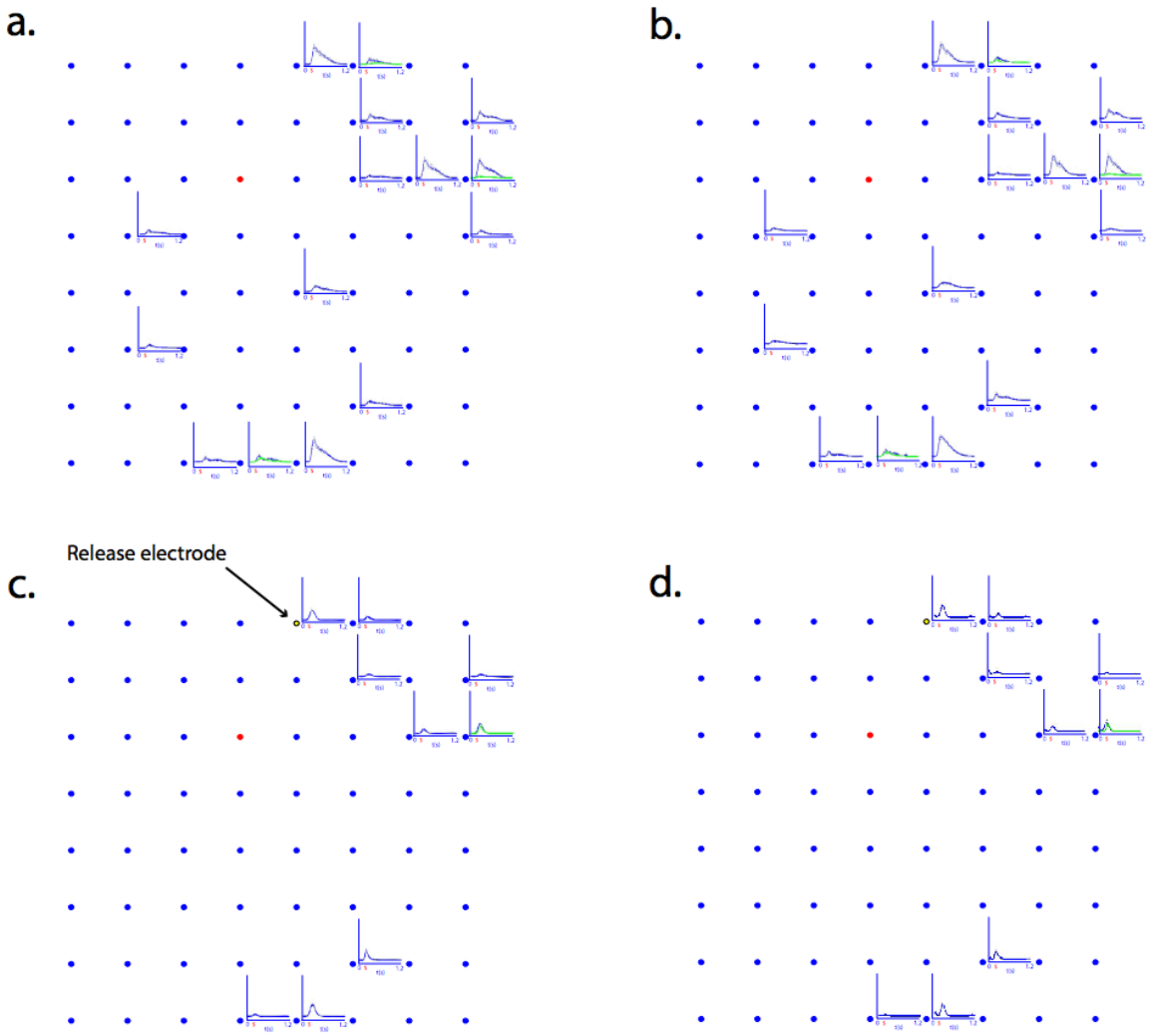

Figure 4-6 Network effect before (a and b) and after (c and d) release of CNQX. The two phases (before and after) comprising 25 trials are each broken into two sub-phases (comprising ten trials each) to demonstrate the stability of the response.

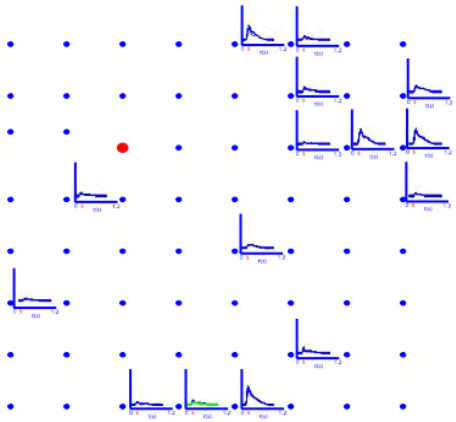

Figure 4-7 Network activity recovers after release

Since CNQX blocks AMPA transmission, which has been implicated in spike timing(Harsch and Robinson 2000), we would like to investigate whether the correlation between neurons has changed. Using the same cross correlation technique as above we find that many of the short time-scale correlations transiently disappear. Figure 4-8 plots the correlation amongst neurons as a line connecting the electrodes from whence they were recorded. By looking at the correlations graphically, the presence of spatial effects can be identified.

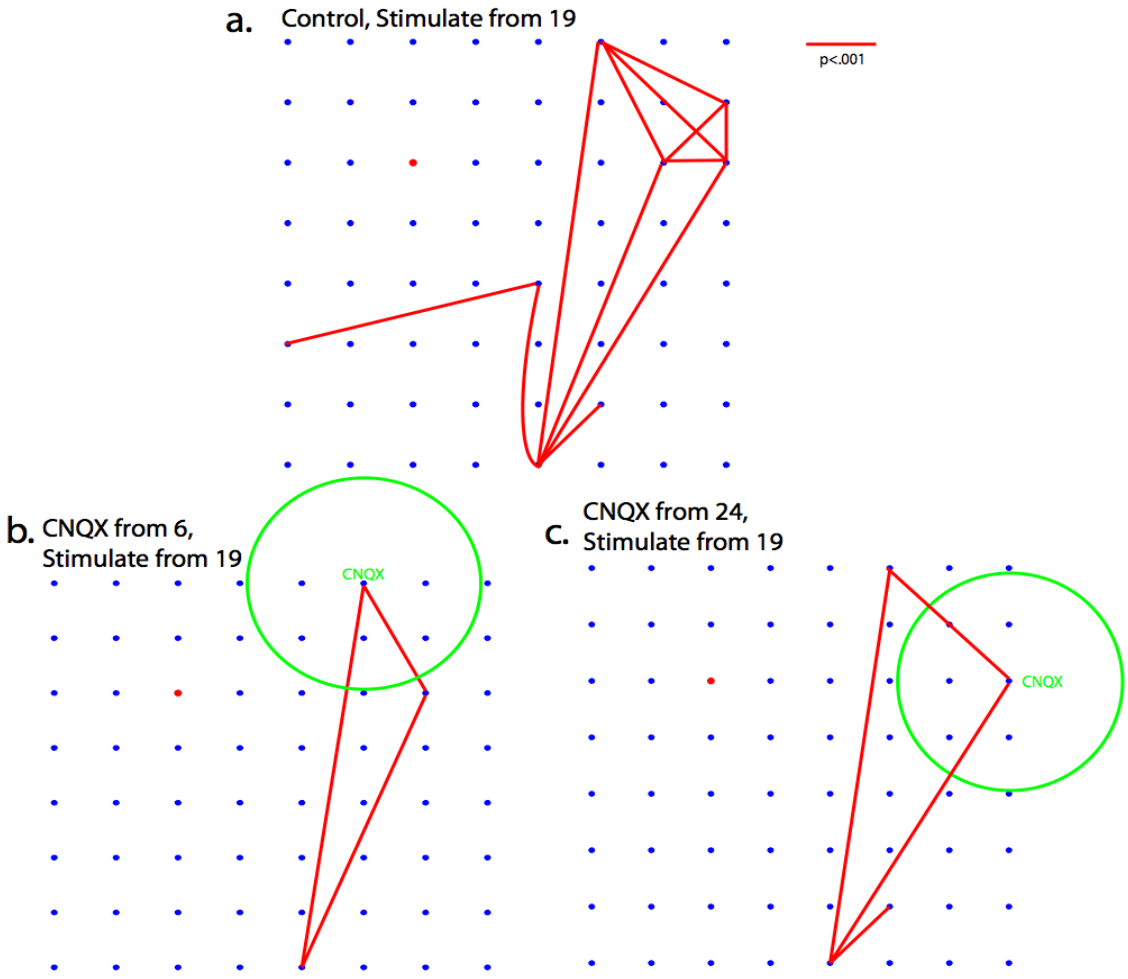

Figure 4-8 8 Effect of local CNQX release on correlation, red lines represent significant correlations (p <.001) greater than .5. a) Control correlations following 25 trials of electrical stimulation at electrode 19. b) Correlations following stimulation at 19 and release at electrode 6 and c) correlation following stimulus at electrode 19 and release from electrode 24. Green circles are the estimated effective radius of CNQX release.

These results show that release of CNQX from electrode 5 produce a different correlation pattern relative to release from electrode 24. The implication of these results is that release of CNQX from electrodes is a fundamentally different process than bath addition of CNQX. The effects of bath addition should be global and uniform. While there is currently not enough data

to identify exactly what effects are mediated directly by CNQX and which are propagated through the network, further experimentation with this system could begin to inhibit a well defined and spatially limited region.

Unlike the correlations defined in the procedure above, Figure 4-10 examine the Pearson correlation coefficients between the firing rates in the 1 s following stimulation and clusters the neurons into groups based on trial to trial variability of the firing rate. The color of the PSTH denotes cluster membership. Both before and after release there was only one correlated cluster, and many of the relationships are preserved following CNQX and the concomitant reduction in firing rate.

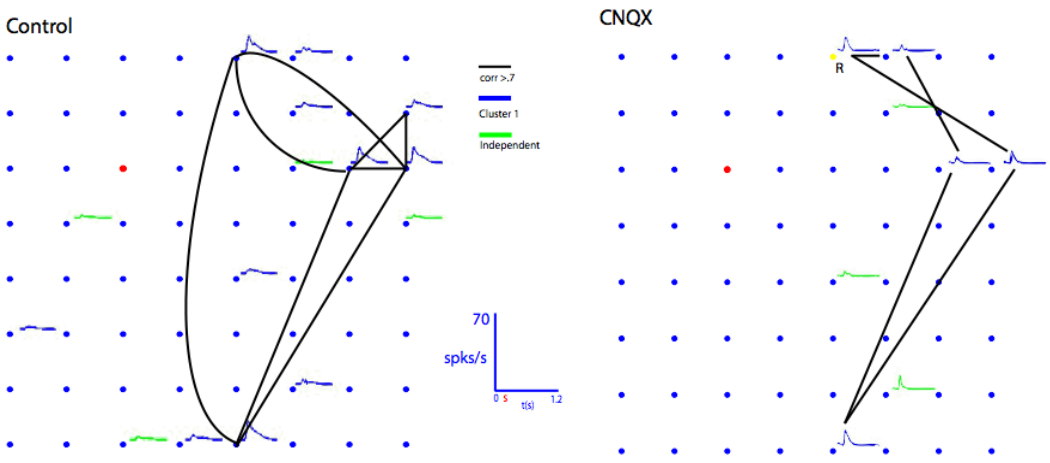

Figure 4-9 Firing rate correlations (black-lines) and cluster membership before and after CNQX release

4.4 DISCUSSION

Little is understood about the network mechanisms that lead to functional clustering that may underlie the representation of perceptual and conceptual information in the brain. D.O. Hebb postulated a mechanism for the formation and activation of functional clusters based on his 'fire together, wire together' principle. In short, his neurophysiological postulate states that groups of neurons that are excited by the same stimulus increase the strength of their physical connections, and so more easily excite each other to fire. This mechanism could explain the formation of the cell assembly as well as a method for recall where by activation of the cluster could occur through (m)any of its constituent members (Hebb 1949).

To the limited extent that CNN's have network properties similar to the intact brain, much can be learned about the activation of groups of neurons that form the substrate for higher order brain function. In CNNs, many neurons can be excited by electrical stimulation at individual electrodes. These clusters of neurons can serve as prototypical Hebbian cell assemblies. CNNs have been grown for up to two years (Potter and DeMarse 2001), and so the evolution of the cluster could be studied for a long period of time. Furthermore, patch clamp technology can be combined with MEA recording to provide direct monitoring of the connection between neuron pairs simultaneously with network recording here (Appendix A) and in Jimbo et. al. (Jimbo, Kawana et al. 2000).

Combined with pharmacological manipulation to isolate the effects of different excitatory and inhibitory channels this technique has been demonstrated to be a powerful means of studying network effects on plasticity(Jimbo, Tateno et al. 1999). The global effects of CNQX and AP5 have been previously characterized (Maeda, Robinson et al. 1995; Maeda, Kuroda et al. 1998; Jimbo, Kawana et al. 2000). Greater resolution in both space and time could be achieved by

applying these drugs at specific points in time at specific locations. The local release system for CNQX described in the previous chapter could provide a means for a more detailed study of the flow of activity through the network.

Release of CNQX from different electrodes resulted in different correlation patterns amongst neurons. This result highlights the strength of local release mechanisms and their ability to selectively perform chemical application. However the resolution of the results obtained herein are still rather far-reaching from a network perspective. In the first network that was investigated for this thesis, the effect of the local release appeared rather global when firing rate was examined. One possible reason for this is that the release parameters composed of a long release pulse (4 s, 1 V magnitude). Future studies shortening the pulse will examine the release on a more precise time scale and possible spatial scale.

Release of CNQX abolished highly significant cross correlations in the network. Previous research has implicated AMPA receptor activity as being the main component driving precise spike timing (Harsch and Robinson 2000). This would explain the results that we have observed here, specifically that some neurons are still active following release of CNQX but that millisecond scale correlations between them disappear. This would implicate some other excitatory channel, possibly NMDA currents, in providing a significant portion of the network drive; or else a dose dependent effect of the AMPA current where low levels could drive networks but are insufficient for precise spike timing. Further research using this release system, as well as the AP5 release system, could lead to a high resolution understanding of the coordination found in neuronal ensembles.

APPENDIX A

SIMULTANEOUS INTRACELLULAR AND EXTRACELLULAR RECORDING

Individual neurons could be patch clamped in a mature neuronal network so that the intracellular currents could be monitored at the same time as the network potentials were recorded (Figure A1). In the future this technique could be used to study connectivity in the dish as well as to monitor plasticity between neuron pairs in the context of network behavior. Noise posed a substantial challenge to doing this. The solution, which was to isolate the ground of the analog to digital converter (ADC), was discovered in an empirical fashion, and for any other system will probably not be applicable. The connections for the simultaneous recording are diagrammed in figure A2a. Figure A2b demonstrates the connections that were utilized to synchronize the imaging system used in chapter three.

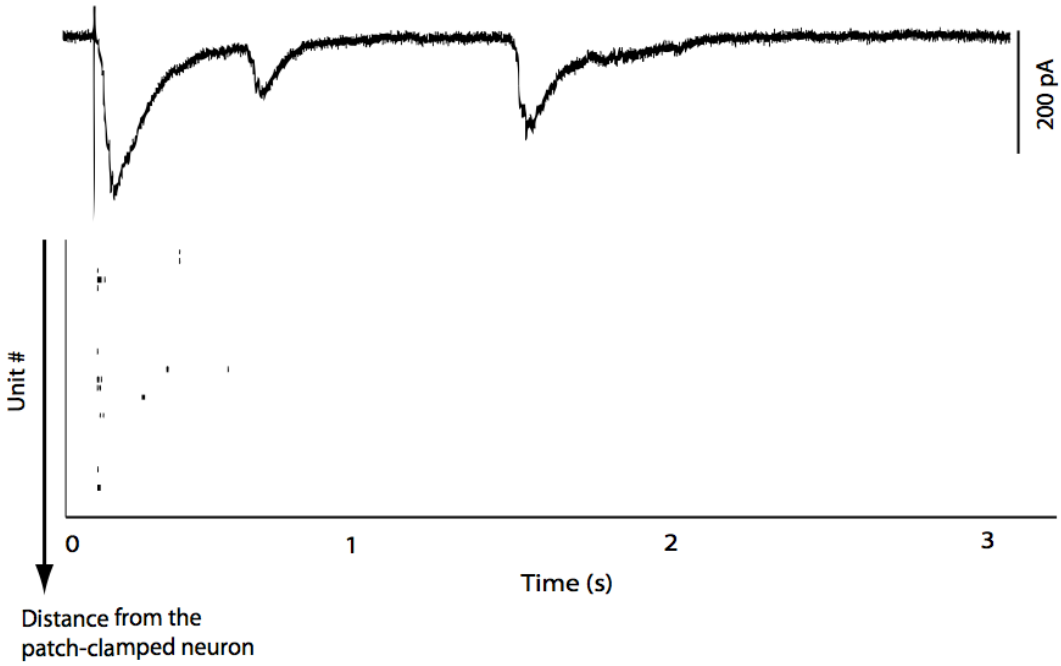

Figure A4-10 Simultaneous current recorded from a patch electrode (top) and network raster obtained from extracellular recording(bottom).

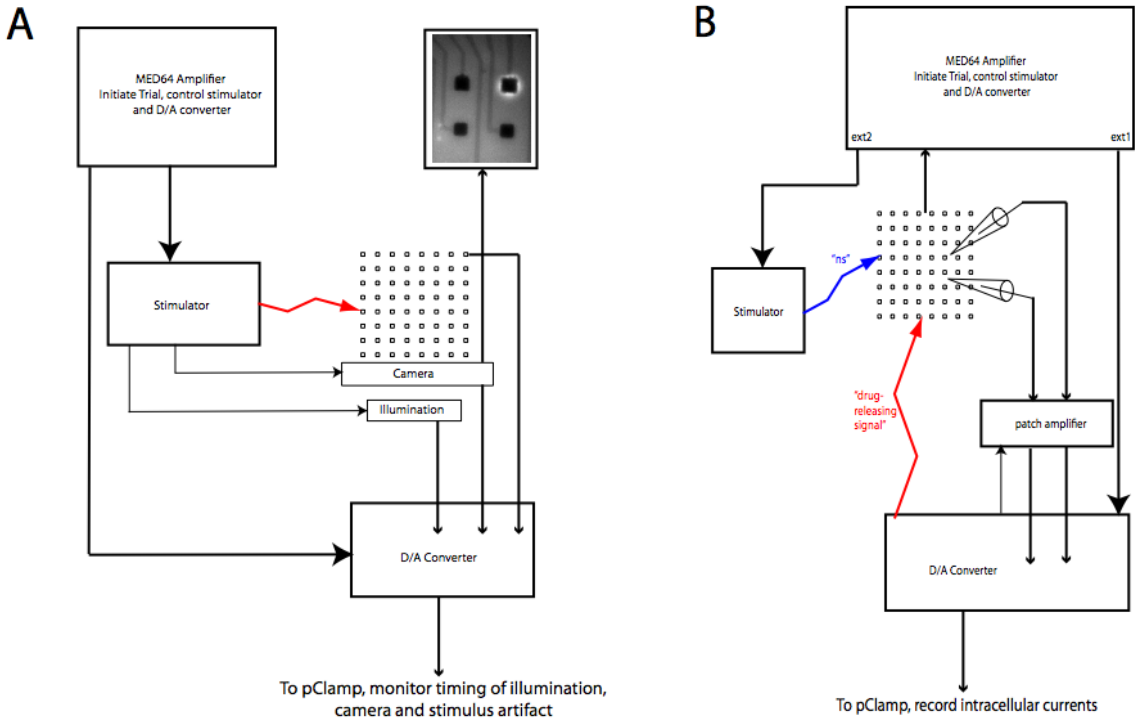

Figure A4-11 A)Experimental schematic for imaging in the MEA and B) experimental schematic for simultaneous intracellular and extracellular recording

APPENDIX B

FUNCTIONAL CLUSTERING

The functional variable clustering model utilized in this dissertation was developed by Dr. Liuxia Wang in her PhD dissertation(Wang 2005). Details of the model can be located there. In this section the essential details and procedure used in Chapter 4 will be described.

The model of clustering used is

$$y_{ij} = \mu_i + w_i \gamma_{c(i)j} + \varepsilon_{ij}$$

$$\gamma_{kj} \sim N(0,1)$$

$$\varepsilon_{ij} \sim N(0, \sigma_k^2)$$

Conjugate priors are assigned for the variables: $\mu_i \sim N(\mu_i^0, \tau_k^2)$, $w_i \sim N(w_i^0, \delta_k^2)$, $\sigma_k^2 \sim IG(\alpha_k, \beta_k)$ and a flat prior is assigned to c(i). The full conditional posterior distributions are:

$$\mu_i \mid rest \sim N\left(\left(\frac{\sum_j (y_{ij} - w_i \lambda_{k_j})}{\sigma_k^2} + \frac{\mu_i^0}{\delta_k^2}\right)\left(\frac{m}{\sigma_k^2} + \frac{1}{\delta_k^2}\right)^{-1}, \left(\frac{m}{\sigma_k^2} + \frac{1}{\delta_k^2}\right)^{-1}\right)$$

$$w_i \mid rest \sim N\left(\left(\frac{\sum_j (y_{ij}-\mu_i)\gamma_{k_j}}{\sigma_k^2}+\frac{w_i^0}{\tau^2}\right)\left(\frac{\sum_j \gamma_{k_j}}{\sigma_k^2}+\frac{1}{\tau_k^2}\right)^{-1},\left(\frac{\sum_j \gamma_{k_j}}{\sigma_k^2}+\frac{1}{\tau_k^2}\right)^{-1}\right)$$

$$\gamma_{k_j} \mid rest \sim N\left(\left(\frac{\sum_{c(i)=k}(y_{ij}-\mu_i)w_i}{\sigma_k^2}+\frac{w_i^0}{\tau^2}\right)\left(\frac{\sum_{c(i)=k} w_i^2}{\sigma_k^2}+1\right)^{-1},\left(\frac{\sum_{c(i)=k} w_i^2}{\sigma_k^2}+1\right)^{-1}\right)$$

$$\frac{1}{\sigma_k^2} \mid rest \sim \Gamma\left(\frac{mN_k}{2}+\alpha_k,\frac{1}{2}\sum\left(y_{ij}-\mu_i-w_i\gamma_{k_j}\right)^2+\beta_k\right)$$

The full posterior probability that the ith object belongs to the the kth group is

$$f\left(p_k \mid rest\right) \propto \prod_j \exp\left(-\frac{1}{2\sigma_k^2}\left(y_{ij}-\mu_i i-w_i\gamma_{k_j}\right)^2\right)$$

Data was prepared for cluster analysis by binning the spike data into appropriate bin sizes and calculating the firing rate based on the bin size. The binned data was square root normalized. Prior to cluster analysis, a BIC was calculated for each data set that provided a probability for a model with k clusters. The k with the highest probability was used as the number of cluster input into the algorithm. Initial estimation was performed accordingly. Cluster membership was estimated by running an hierarchical agglomerative algorithm on the correlation matrix of the data. In some cases a correlation matrix was used that accounted for stimulus induced correlation. Basal firing rate was estimated with the expectation from the observed firing rates. 4000 iterations of the MCMC algorithm were performed.

The component of variation due to cluster membership is scaled by a weight factor, w_i. When $w_i = 0$, the neuron will be independent of other cells as the observed firing rate function reduces to the baseline firing rate plus noise. We define a quantity:

$$T_i = \frac{w_i}{\sqrt{\sigma_k^2 + w_i^2}}$$

$\sigma_k^2 + w_i^2$ is exactly the variance of the ith variable. The data has been normalized so that the variance =1, hence the denominator falls out of the equation and we are left with $T_i \propto w_i$. It is easy to see that the posterior distribution of w_i is normal (the priors were conjugate, which means that the posterior distribution will have the same form). Under the null hypothesis, wi=0, we say that a cell is independent from the others when $w_i < 1.96 * S_{w_i}$ (where S_{w_i} is the standard deviation and w_i is the estimated mean from the output).

Prior to running the clustering algorithm, the BIC technique was employed to find the model with k clusters that best fits the data. After running the MCMC algorithm, each cell was tested for statistical independence. The mean and the standard deviation of w_i was calculated and the null hypothesis was $w_i < 1.96 * S_{w_i}$ was tested. If any independent cells were found, they were removed from the data and the a new Bayes factor was calculated, the sorting redone, and the process repeated until none of the remaining cells were found to be independent. Cluster membership was assigned when the p of cluster membership exceeded .90. An example procedure is detailed in figure B1.

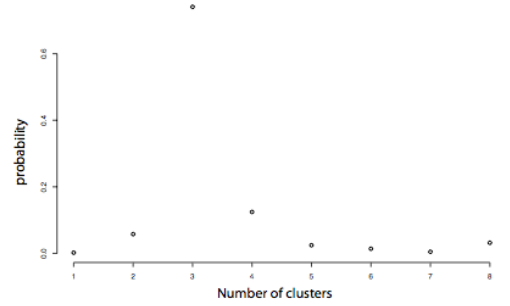

Cell	p Cluster 1	p Cluster 2	p Cluster 3	w_i	S_{w_i}	Cluster
1	0.306	0.487	0.207	-0.408	0.329	*I*
2	0.998	0.000	0.002	-2.621	0.374	1
3	0.000	0.999	0.001	-1.931	0.300	2
4	0.001	0.997	0.002	-1.825	0.301	2
5	0.005	0.994	0.000	-1.968	0.305	2
6	0.864	0.053	0.083	-0.940	0.318	uncertain
7	0.011	0.982	0.007	-1.227	0.290	2
8	0.028	0.952	0.020	-1.409	0.297	2
9	0.341	0.251	0.408	-0.058	0.382	*I*
10	0.090	0.114	0.797	0.840	0.346	uncertain
11	0.035	0.001	0.964	-2.061	0.372	3
12	0.287	0.327	0.386	-0.377	0.325	*I*
13	0.197	0.679	0.123	-0.737	0.319	uncertain
14	0.109	0.809	0.082	-0.704	0.296	uncertain
15	0.311	0.538	0.151	-0.750	0.296	uncertain
16	0.279	0.212	0.508	-0.436	0.328	*I*
17	0.005	0.989	0.006	-1.706	0.298	2

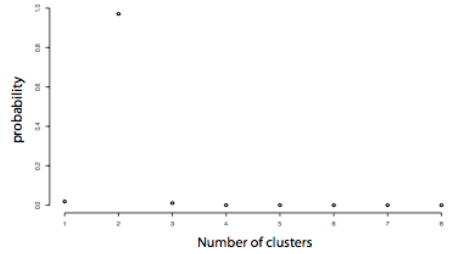

Cell	p Cluster 1	p Cluster 2	w_i	S_{w_i}	Cluster
2	1.000	0.000	2.432	0.383	1
3	0.000	1.000	-1.939	0.299	2
4	0.000	1.000	-1.839	0.297	2
5	0.000	1.000	-1.988	0.297	2
6	0.989	0.011	0.983	0.360	1
7	0.002	0.998	-1.222	0.279	1
8	0.000	1.000	-1.421	0.285	2
10	0.835	0.165	-0.368	0.380	*I*
11	1.000	0.000	1.157	0.380	1
13	0.124	0.876	-0.728	0.332	uncertain
14	0.011	0.989	-0.855	0.281	2
15	0.042	0.958	-0.740	0.305	2
17	0.000	1.000	-1.698	0.297	2

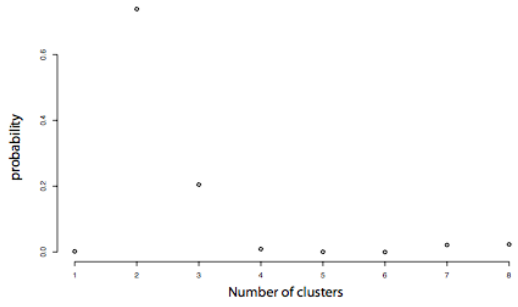

Cell	p Cluster 1	p Cluster 2	w_i	S_{w_i}	Cluster
2	1.000	0.000	2.471	0.393	1
3	0.000	1.000	-1.946	0.294	2
4	0.000	1.000	-1.846	0.304	2
5	0.000	1.000	-1.991	0.301	2
6	0.991	0.009	0.993	0.360	1
7	0.001	0.999	-1.216	0.275	2
8	0.000	1.000	-1.425	0.285	2
11	1.000	0.000	1.053	0.379	*1*
13	0.101	0.899	-0.745	0.321	2
14	0.009	0.991	-0.847	0.280	2
15	0.036	0.964	-0.741	0.297	2
17	0.000	1.000	-1.693	0.293	2

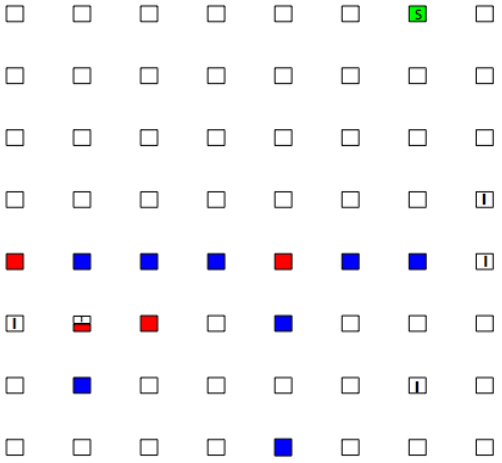

Figure B4-12 Clustering procedure Showing the multiple iterations, in this case three, to arrive at a result containing no independent cells. The three graphs represent the output of the BIC algorithm and the tables summarize the output of the clustering algorithm after every step. The MED64 schematic shows the site of stimulus (green) along with the location of electrodes recording cells belonging to cluster 1 (blue) and cluster 2 (red). Electrodes recording independent neurons are labeled with an "I"

APPENDIX C

PEDOT ELECTRODES FOR MED64 ARRAYS

A practical issue encountered in the working of this thesis was the combined cost and fragility of MED64 electrode arrays. MED array electrodes are made with indium tin oxide (ITO) leads that terminate in the 8 x 8 of electrodes. A layer of polyacrylamide is used to insulate the leads from the bath. The non-insulated electrode region is electroplated with platinum black. The function of the pt-black coating is to lower the impedance of the electrodes. It accomplishes this through an exceedingly rough surface that results in a very high surface area. For the 50 μm^2 electrodes in the MED array, the 1kHz impedance of a bare ITO electrode is ~ 250 - 280 kOhms, while a pt-black coated electrode is ~ 10 kOhms.

One drawback of pt coatings is that they are easily damaged and difficult to reuse. Furthermore, there is legitimate question asked as to whether the neurons grow easily when intimate contact between neuron and electrode occurs. A common observation during this research project has been the poor health of the cells which find themselves located in close proximity to pt electrodes. This observation was very consistent and would occur in networks that had extremely healthy cells located in other regions of the dish. The cause for this has never been elucidated, but a candidate hypothesis is that the extreme roughness of pt-black surfaces

(which endows them with ultra-low impedance) is too jagged for the smooth contours of cells. For this reason, surface modification of ITO electrodes with a PEDOT/PSS film is investigated. The EDOT monomer was mixed with PSS in solution so that the final concentration was .01 M EDOT and .1 M PSS. EDOT is difficult to get into solution so the mixture was stirred for 1 hour on a magnetic plate. In order to start with clean ITO electrodes, the MED arrays were oxygen plasma treated for 8 seconds. The EDOT solution was then flooded into the MED chamber and the array was connected to the potentiostat through a custom built interface.

We have utilized a three-electrode cell set up containing a working electrode(ITO microelectrode on the array), a counter electrode (Pt plate), and a Ag/AgCl reference electrode. The cell contains a solution mixture of monomer and dopant. Initial attempts to deposit PEDOT films onto electrodes utilized potentiostatic control. While some resulting films were indeed very low impedance, the outcome was highly variable and at least 50% had impedance similar to ITO (figure C1a).

PEDOT-PSS coatings grown under current control showed consistently low impedance. Using 100 nA for 50 s provided ideal coatings (figure C1b). Longer growing times would result in larger film deposits that easily detached.

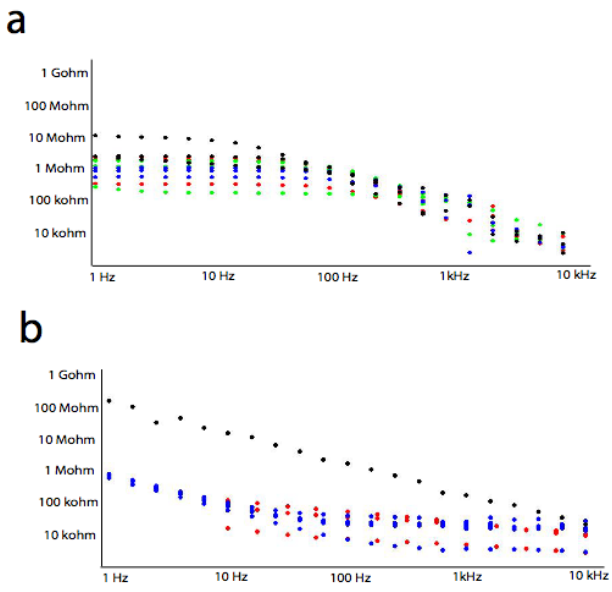

Figure C1 a) Impedance spectroscopy of PEDOT-PSS coatings grown potentiostatically and b) PEDOT-PSS coatings grown galvanostatically (blue) compared to ITO (black) and pt-black (red)

BIBLIOGRAPHY

Abeles, M. (1991). Corticotronics. Cambridge, Cambridge University Press.

Aertsen, A. M., G. L. Gerstein, et al. (1989). "Dynamics of neuronal firing correlation: modulation of "effective connectivity"." J Neurophysiol **61**(5): 900-17.

Alford, S. and S. Grillner (1990). "CNQX and DNQX block non-NMDA synaptic transmission but not NMDA-evoked locomotion in lamprey spinal cord." Brain Res **506**(2): 297-302.

Allen, N. S., K. S. Murray, et al. (1997). "Physical properties of polypyrrole films containing trisoxalatometallate anions and prepared from aqueous solution." Synthetic Metals **87**(3): 237-247.

Anderson, D. J., K. Najafi, et al. (1989). "Batch-fabricated thin-film electrodes for stimulation of the central auditory system." IEEE T Bio-med Eng **36**: 693-704.

Ard, M. D. and R. P. Bunge (1988). "Heparan sulfate proteoglycan and laminin immunoreactivity on cultured astrocytes: relationship to differentiation and neurite growth." J Neurosci **8**(8): 2844-58.

Bakkum, D. J., Z. C. Chao, et al. (2007). "Embodying cultured networks with a robotic drawing arm." Conf Proc IEEE Eng Med Biol Soc **2007**: 2996-9.

Barker, M., B. Billups, et al. (2008). "Focal macromolecule delivery in neuronal tissue using simultaneous pressure ejection and local electroporation." J Neurosci Methods.

Bi, G. Q. and M. M. Poo (1998). "Synaptic modifications in cultured hippocampal neurons: dependence on spike timing, synaptic strength, and postsynaptic cell type." J Neurosci **18**(24): 10464-72.

Biran, R., D. C. Martin, et al. (2005). "Neuronal cell loss accompanies the brain tissue response to chronically implanted silicon microelectrode arrays." Exp Neurol **195**(1): 115-26.

Biran, R., M. D. Noble, et al. (1999). "Characterization of cortical astrocytes on materials of differing surface chemistry." Journal of Biomedical Materials Research **46**(2): 150-159.

Blake, J. F., M. W. Brown, et al. (1988). "CNQX blocks acidic amino acid induced depolarizations and synaptic components mediated by non-NMDA receptors in rat hippocampal slices." Neurosci Lett **89**(2): 182-6.

Bove, M., M. Grattarola, et al. (1997). "In vitro 2-D networks of neurons characterized by processing the signals recorded with a planar microtransducer array." IEEE Trans Biomed Eng **44**(10): 964-77.

Bove, M., S. Martinoia, et al. (1998). "Analysis of the signals generated by networks of neurons coupled to planar arrays of microtransducers in simulated experiments." Biosens Bioelectron **13**(6): 601-12.

Brewer, G. J. and P. J. Price (1996). "Viable cultured neurons in ambient carbon dioxide and hibernation storage for a month." Neuroreport **7**(9): 1509-12.

Canepari, M., M. Bove, et al. (1997). "Experimental analysis of neuronal dynamics in cultured cortical networks and transitions between different patterns of activity." Biol Cybern **77**(2): 153-62.

Chambers, J. J. and R. H. Kramer (2008). "Light-activated ion channels for remote control of neural activity." Methods Cell Biol **90**: 217-32.

Chang, A. C. and L. L. Miller (1988). "Electrochemically controlled binding and release of salicylate, TCNQ•− and ferrocyanide from films of oligomeric 3-methoxythiophene." J. Electroanal. Chem **247**(1-2): 173-184.

Collier, J. H., J. P. Camp, et al. (2000). "Synthesis and characterization of polypyrrole-hyaluronic acid composite biomaterials for tissue engineering applications." J Biomed Mater Res **50**(4): 574-84.

Cosnier, S. (1999). "Biomolecule immobilization on electrode surfaces by entrapment or attachment to electrochemically polymerized films. A review." Biosens Bioelectron **14**(5): 443-56.

Cosnier, S. and A. Senillou (2003). "An electrogenerated poly(pyrrole-benzophenone) film for the photografting of proteins." Chem Commun (Camb)(3): 414-5.

Cosnier, S., M. Stoytcheva, et al. (1999). "A biotinylated conducting polypyrrole for the spatially controlled construction of an amperometric biosensor." Anal Chem **71**(17): 3692-7.

Craig, A. M. and G. Banker (1994). "Neuronal polarity." Annu Rev Neurosci **17**: 267-310.

Cui, X., J. F. Hetke, et al. (2001). "Electrochemical deposition and characterization of conducting polymer polypyrrole/PSS on multichannel neural probes." Sensors and Actuators A: Physical **93**(1): 8-18.

Cui, X., V. A. Lee, et al. (2001). "Surface modification of neural recording electrodes with conducting polymer/biomolecule blends." J Biomed Mater Res **56**(2): 261-72.

Cui, X. and D. C. Martin (2003). "Fuzzy gold electrodes for lowering impedance and improving adhesion with electrodeposited conducting polymer films." Sensors and Actuators A: Physical **103**(3): 384-394.

Cui, X., J. Wiler, et al. (2003). "In vivo studies of polypyrrole/peptide coated neural probes." Biomaterials **24**(5): 777-87.

Cui, X., J. Wiler, et al. (2003). "In vivo studies of polypyrrole/peptide coated neural probes." Biomaterials **24**(5): 777-787.

Cui, X. T. and D. D. Zhou (2007). "Poly (3,4-ethylenedioxythiophene) for chronic neural stimulation." IEEE Trans Neural Syst Rehabil Eng **15**(4): 502-8.

Cui, X. Y., J. F. Hetke, et al. (2001). "Electrochemical deposition and characterization of conducting polymer polypyrrole/PSS on multichannel neural probes." Sensors and Actuators a-Physical **93**(1): 8-18.

Cui, X. Y. and D. C. Martin (2003). "Electrochemical deposition and characterization of poly(3,4-ethylenedioxythiophene) on neural microelectrode arrays." Sensors and Actuators B-Chemical **89**(1-2): 92-102.

Cui, X. Y. and D. C. Martin (2003). "Fuzzy gold electrodes for lowering impedance and improving adhesion with electrodeposited conducting polymer films." Sensors and Actuators a-Physical **103**(3): 384-394.

deCharms, R. C. and M. M. Merzenich (1996). "Primary cortical representation of sounds by the coordination of action-potential timing." Nature **381**(6583): 610-3.

Demarse, T. B., D. A. Wagenaar, et al. (2001). "The Neurally Controlled Animat: Biological Brains Acting with Simulated Bodies." Auton Robots **11**(3): 305-310.

Diaz, A. F., J. I. Castillo, et al. (1981). "Electrochemistry of Conducting Polypyrrole Films." J. Electroanal. Chem. **128**: 115-132.

DiMatteo, I., C. R. Genovese, et al. (2001). "Bayesian curve-fitting with free-knot splines." Biometrika **88**: 1055-1071.

Ellis-Davies, G. C. (2007). "Caged compounds: photorelease technology for control of cellular chemistry and physiology." Nat Methods **4**(8): 619-28.

Evans, A. J., B. C. Thompson, et al. (2008). "Promoting neurite outgrowth from spiral ganglion neuron explants using polypyrrole/BDNF-coated electrodes." J Biomed Mater Res A.

Fisher, R. A. (1948). "Answer to Question 14 on Combining independent tests of significance." The American Statistician **2**(30).

Fukunaga, K. (1972). Introduction to Statistical Pattern Recognition, Academic Press.

George, P., D. LaVan, et al. (2006). "Electrically controlled drug delivery from biotin-doped condutive polypyrrole." Advanced Materials **18**: 577-581.

George, P. M., A. W. Lyckman, et al. (2005). "Fabrication and biocompatibility of polypyrrole implants suitable for neural prosthetics." Biomaterials **26**(17): 3511-9.

Gerhardt, G. A. and M. R. Palmer (1987). "Characterization of the techniques of pressure ejection and microiontophoresis using in vivo electrochemistry." J Neurosci Methods **22**(2): 147-59.

Gomez, N. and C. E. Schmidt (2007). "Nerve growth factor-immobilized polypyrrole: bioactive electrically conducting polymer for enhanced neurite extension." J Biomed Mater Res A **81**(1): 135-49.

Graf, J., Y. Iwamoto, et al. (1987). "Identification of an amino acid sequence in laminin mediating cell attachment, chemotaxis, and receptor binding." Cell **48**(6): 989-96.

Gross, G. W., A. Harsch, et al. (1997). "Odor, drug and toxin analysis with neuronal networks in vitro: extracellular array recording of network responses." Biosens Bioelectron **12**(5): 373-93.

Gross, G. W., B. K. Rhoades, et al. (1995). "The use of neuronal networks on multielectrode arrays as biosensors." Biosens Bioelectron **10**(6-7): 553-67.

Gross, G. W., B. K. Rhoades, et al. (1993). "Stimulation of monolayer networks in culture through thin-film indium-tin oxide recording electrodes." J Neurosci Methods **50**(2): 131-43.

Haidarliu, S., D. Shulz, et al. (1995). "A multi-electrode array for combined microiontophoresis and multiple single-unit recordings." J Neurosci Methods **56**(2): 125-31.

Harsch, A. and H. P. Robinson (2000). "Postsynaptic variability of firing in rat cortical neurons: the roles of input synchronization and synaptic NMDA receptor conductance." J Neurosci **20**(16): 6181-92.

Hebb, D. O. (1949). The Organization of Behavior : a neuropsychological theory. New York, Wiley.

Helms Tillery, S. I., D. M. Taylor, et al. (2003). "Training in cortical control of neuroprosthetic devices improves signal extraction from small neuronal ensembles." Rev Neurosci **14**(1-2): 107-19.

Hicks, T. P. (1984). "The history and development of microiontophoresis in experimental neurobiology." Prog Neurobiol **22**(3): 185-240.

Hodgkin, A. L. and A. F. Huxley (1952). "A quantitative description of membrane current and its application to conduction and excitation in nerve." J Physiol **117**(4): 500-44.

Hodgkin, A. L. and A. F. Huxley (1952). "Currents carried by sodium and potassium ions through the membrane of the giant axon of Loligo." J Physiol **116**(4): 449-72.

Hodgkin, A. L. and A. F. Huxley (1952). "The components of membrane conductance in the giant axon of Loligo." J Physiol **116**(4): 473-96.

Hodgkin, A. L. and A. F. Huxley (1952). "The dual effect of membrane potential on sodium conductance in the giant axon of Loligo." J Physiol **116**(4): 497-506.

Hodgkin, A. L., A. F. Huxley, et al. (1952). "Measurement of current-voltage relations in the membrane of the giant axon of Loligo." J Physiol **116**(4): 424-48.

Jimbo, Y., N. Kasai, et al. (2003). "A system for MEA-based multisite stimulation." IEEE Trans Biomed Eng **50**(2): 241-8.

Jimbo, Y., A. Kawana, et al. (2000). "The dynamics of a neuronal culture of dissociated cortical neurons of neonatal rats." Biol Cybern **83**(1): 1-20.

Jimbo, Y. and H. P. Robinson (2000). "Propagation of spontaneous synchronized activity in cortical slice cultures recorded by planar electrode arrays." Bioelectrochemistry **51**(2): 107-15.

Jimbo, Y., H. P. Robinson, et al. (1993). "Simultaneous measurement of intracellular calcium and electrical activity from patterned neural networks in culture." IEEE Trans Biomed Eng **40**(8): 804-10.

Jimbo, Y., H. P. Robinson, et al. (1998). "Strengthening of synchronized activity by tetanic stimulation in cortical cultures: application of planar electrode arrays." IEEE Trans Biomed Eng **45**(11): 1297-304.

Jimbo, Y., T. Tateno, et al. (1999). "Simultaneous induction of pathway-specific potentiation and depression in networks of cortical neurons." Biophys J **76**(2): 670-8.

Kaji, H., M. Nishizawa, et al. (2003). "Localized chemical stimulation to micropatterned cells using multiple laminar fluid flows." Lab Chip **3**(3): 208-11.

Kamioka, H., E. Maeda, et al. (1996). "Spontaneous periodic synchronized bursting during formation of mature patterns of connections in cortical cultures." Neurosci Lett **206**(2-3): 109-12.

Kandel, E. R., J. H. Schwartz, et al. (2000). Principles of Neural Science. New York, McGraw-Hill.

Kandler, K., L. C. Katz, et al. (1998). "Focal photolysis of caged glutamate produces long-term depression of hippocampal glutamate receptors." Nat Neurosci **1**(2): 119-23.

Khatami, D., Y. Nam, et al. (2004). "Effect of bicuculline on the spontaneous and evoked activity of patterned embryonic hippocampal neurons cultured in vitro." Conf Proc IEEE Eng Med Biol Soc **6**: 4059-62.

Kleinschmidt, A., M. F. Bear, et al. (1987). "Blockade of "NMDA" receptors disrupts experience-dependent plasticity of kitten striate cortex." Science **238**(4825): 355-8.

Kontturi, K., P. Pentti, et al. (1998). "Polypyrrole as a model membrane for drug delivery." Journal of Electroanalytical Chemistry **453**(1-2): 231-238.

Kotwal, A. and C. E. Schmidt (2001). "Electrical stimulation alters protein adsorption and nerve cell interactions with electrically conducting biomaterials." Biomaterials **22**(10): 1055-64.

Kuffler, S. W. (1976). From Neuron to Brain: A Cellular Approach to the Function of the Nervous System. Sinauer Associates, Sunerland, MA.

Lau, P. M. and G. Q. Bi (2005). "Synaptic mechanisms of persistent reverberatory activity in neuronal networks." Proc Natl Acad Sci U S A **102**(29): 10333-8.

le Feber, J., W. L. Rutten, et al. (2007). "Conditional firing probabilities in cultured neuronal networks: a stable underlying structure in widely varying spontaneous activity patterns." J Neural Eng **4**(2): 54-67.

le Feber, J., J. Stegenga, et al. (2008). "Do external stimuli, applied to train cultured cortical networks, disturb the balance between activity and connectivity?" Conf Proc IEEE Eng Med Biol Soc **2008**: 5081-4.

Lesniak, M. S., U. Upadhyay, et al. (2005). "Local delivery of doxorubicin for the treatment of malignant brain tumors in rats." Anticancer Res **25**(6B): 3825-31.

Li, X., W. Zhou, et al. (2007). "Long-term recording on multi-electrode array reveals degraded inhibitory connection in neuronal network development." Biosens Bioelectron **22**(7): 1538-43.

Liesi, P., A. Narvanen, et al. (1989). "Identification of a neurite outgrowth-promoting domain of laminin using synthetic peptides." FEBS Lett **244**(1): 141-8.

Luo, X. and X. T. Cui (2008). "Electrochemically controlled release based on nanoporous conducting polymers." Electrochemistry Communications **in press**.

Maalouf, M., R. W. Dykes, et al. (1998). "Effects of D-AP5 and NMDA microiontophoresis on associative learning in the barrel cortex of awake rats." Brain Res **793**(1-2): 149-68.

MacDonald, J. R. (1987). Impedance Spectroscopy: Emphasizing Solid Materials and Systems. New York, John Wiley & Sons.

Maeda, E., Y. Kuroda, et al. (1998). "Modification of parallel activity elicited by propagating bursts in developing networks of rat cortical neurones." Eur J Neurosci **10**(2): 488-96.

Maeda, E., H. P. Robinson, et al. (1995). "The mechanisms of generation and propagation of synchronized bursting in developing networks of cortical neurons." J Neurosci **15**(10): 6834-45.

Martinoia, S. and P. Massobrio (2004). "ISFET-neuron junction: circuit models and extracellular signal simulations." Biosens Bioelectron **19**(11): 1487-96.

Martinoia, S., P. Massobrio, et al. (2004). "Cultured neurons coupled to microelectrode arrays: circuit models, simulations and experimental data." IEEE Trans Biomed Eng **51**(5): 859-64.

Massoumi, B. and A. A. Entezami (2002). "Electrochemically stimulated 2-ethylhexylphosphate (EHP) release through Redox switching of conducting polypyrrole film and polypyrrole/poly (-methylpyrrole) or self-doped polyaniline bilayers." Polymer International **51**: 555-560.

Maynard, E. M., C. T. Nordhausen, et al. (1997). "The Utah intracortical electrode array: a recording structure for potential brain-computer interfaces." Electroencephalogr. Clin. Neurophysiol **102**: 228-239.

McBain, C. J., P. Boden, et al. (1988). "The kainate/quisqualate receptor antagonist, CNQX, blocks the fast component of spontaneous epileptiform activity in organotypic cultures of rat hippocampus." Neurosci Lett **93**(2-3): 341-5.

Miller, L. L., A. N. Lau, et al. (1983). "Electrochemical delivery of dopamine." Neurosci Lett **35**(2): 101-4.

Mourzina, Y., D. Kaliaguine, et al. (2006). "Patterning chemical stimulation of reconstructed neuronal networks." Anal Chim Acta **575**(2): 281-9.

Najafi, K. and K. D. Wise (1986). "An Implantable Multielectrode Array with On-Chip Signal Processing." IEEE Journal on Solid State Circuitry **21**: 1034-1044.

Nam, Y., J. Chang, et al. (2004). "Patterning to enhance activity of cultured neuronal networks." IEE Proc Nanobiotechnol **151**(3): 109-15.

Pernaut, L. M. and J. R. Reynolds (2000). "Use of Conducting Electroactive Polymers for Drug Delivery and Sensing of Bioactive Molecules. A Redox Chemistry Approach." Journal of Physical Chemistry B **104**(17): 4080-4090.

Pinato, G., P. Parodi, et al. (1999). "Properties of the evoked spatio-temporal electrical activity in neuronal assemblies." Rev Neurosci **10**(3-4): 279-90.

Potter, S. M. and T. B. DeMarse (2001). "A new approach to neural cell culture for long-term studies." J Neurosci Methods **110**(1-2): 17-24.

Rhoades, B. K. and G. W. Gross (1994). "Potassium and calcium channel dependence of bursting in cultured neuronal networks." Brain Res **643**(1-2): 310-8.

Richardson, R. T., B. Thompson, et al. (2007). "The effect of polypyrrole with incorporated neurotrophin-3 on the promotion of neurite outgrowth from auditory neurons." Biomaterials **28**(3): 513-23.

Robinson, H. P. and A. Harsch (2002). "Stages of spike time variability during neuronal responses to transient inputs." Phys Rev E Stat Nonlin Soft Matter Phys **66**(6 Pt 1): 061902.

Salinas, E. and T. J. Sejnowski (2001). "Correlated neuronal activity and the flow of neural information." Nat Rev Neurosci **2**(8): 539-50.

Scarlatos, A., A. J. Cadotte, et al. (2008). "Cortical networks grown on microelectrode arrays as a biosensor for botulinum toxin." J Food Sci **73**(3): E129-36.

Scheuss, V., R. Yasuda, et al. (2007). "Nonlinear [Ca2+] Signaling in Dendrites and Spines Caused by Activity-Dependent Depression of Ca2+ Extrusion." J Neurosci **26**: 8183-8194.

Schmidt, C. E., V. R. Shastri, et al. (1997). "Stimulation of neurite outgrowth using an electrically conducting polymer." Proceedings of the National Academy of Sciences of the United States of America **94**(17): 8948-8953.

Schwartz, A. B., X. Cui, et al. (2006). "Brain-Controlled Interfaces: Movement Restoration with Neural Prosthetics." Neuron **52**: 205-220.

Shahaf, G. and S. Marom (2001). "Learning in networks of cortical neurons." J Neurosci **21**(22): 8782-8.

Shein, M., V. Volman, et al. (2008). "Management of synchronized network activity by highly active neurons." Phys Biol **5**(3): 36008.

Stauffer, W. R. and X. T. Cui (2006). "Polypyrrole doped with 2 peptide sequences from laminin." Biomaterials **27**(11): 2405-13.

Stegenga, J., J. le Feber, et al. (2008). "Changes within bursts during learning in dissociated neural networks." Conf Proc IEEE Eng Med Biol Soc **2008**: 4968-71.

Szarowski, D. H., M. D. Andersen, et al. (2003). "Brain responses to micro-machined silicon devices." Brain Res **983**(1-2): 23-35.

Taketani, M. and M. Baudry, Eds. (2003). Advances in Network Electrophysiology. New York, Springer Science+Buisness Media, Inc.

Tateno, T., Y. Jimbo, et al. (2005). "Spatio-temporal cholinergic modulation in cultured networks of rat cortical neurons: evoked activity." Neuroscience **134**(2): 439-48.

Taylor, D. M., S. I. Tillery, et al. (2002). "Direct cortical control of 3D neuroprosthetic devices." Science **296**(5574): 1829-32.

Thomas, C. A., P. A. Springer, et al. (1972). "A miniature microelectrode array to monitor the bioelectric activity of cultured cells." Exp. Cell Res. **74**: 61-66.

Turner, J. N., W. Shain, et al. (1999). "Cerebral astrocyte response to micromachined silicon implants." Exp Neurol **156**(1): 33-49.

Velliste, M., S. Perel, et al. (2008). "Cortical control of a prosthetic arm for self-feeding." Nature **453**(7198): 1098-101.

Wadhwa, R., C. F. Lagenaur, et al. (2006). "Electrochemically controlled release of dexamethasone from conducting polymer polypyrrole coated electrode." J Control Release **110**(3): 531-41.

Wagenaar, D. A. (2005). Development and Control of Epileptiform Bursting in Dissociated Cortical Cultures, California Institute of Technology. **PhD**.

Wagenaar, D. A., R. Madhavan, et al. (2005). "Controlling bursting in cortical cultures with closed-loop multi-electrode stimulation." J Neurosci **25**(3): 680-8.

Wagenaar, D. A., Z. Nadasdy, et al. (2006). "Persistent dynamic attractors in activity patterns of cultured neuronal networks." Phys Rev E Stat Nonlin Soft Matter Phys **73**(5 Pt 1): 051907.

Wagenaar, D. A., J. Pine, et al. (2004). "Effective parameters for stimulation of dissociated cultures using multi-electrode arrays." J Neurosci Methods **138**(1-2): 27-37.

Wagenaar, D. A., J. Pine, et al. (2006). "An extremely rich repertoire of bursting patterns during the development of cortical cultures." BMC Neurosci **7**: 11.

Wagenaar, D. A., J. Pine, et al. (2006). "Searching for plasticity in dissociated cortical cultures on multi-electrode arrays." J Negat Results Biomed **5**: 16.

Wallace, G. G. (1997). Conductive Electroactive Polymers: Intelligent Material Systems. Lancaster, PA, Technomic Pub.

Wallace, G. G. (2003). Conductive electroactive polymers : intelligent materials systems. Boca Raton, Fla., CRC Press.

Wang, L. (2005). Model-Based Variable Clustering with Application to Neurophysiology. Statistics. Pittsburgh, Carnegie Mellon University. **PhD**.

Webb, K., V. Hlady, et al. (2000). "Relationships among cell attachment, spreading, cytoskeletal organization, and migration rate for anchorage-dependent cells on model surfaces." Journal of Biomedical Materials Research **49**(3): 362-368.

Wise, K. D. and K. Najafi (1991). "Microfabrication techniquesfor integrated sensors and microsystems." Science **254**: 1335-1342.

Wong, J. Y., R. Langer, et al. (1994). "Electrically conducting polymers can noninvasively control the shape and growth of mammalian cells." Proc Natl Acad Sci U S A **91**(8): 3201-4.

Zinger, B. and L. L. Miller (1984). "Timed Release of Chemicals from Polypyrrole Films." J. Am. Chem. Soc. **106**: 6861-6863.

Zoli, M., C. Torri, et al. (1998). "The emergence of the volume transmission concept." Brain Res Brain Res Rev **26**(2-3): 136-47.